



HAL
open science

Gel probes for Scanning Gel Electrochemical Microscopy: elaboration, functionalization, and analysis

Gustavo Echeveste

► **To cite this version:**

Gustavo Echeveste. Gel probes for Scanning Gel Electrochemical Microscopy: elaboration, functionalization, and analysis. Chemical Sciences. Université de Lorraine, 2023. English. NNT: 2023LORR0168 . tel-04612343

HAL Id: tel-04612343

<https://theses.hal.science/tel-04612343>

Submitted on 14 Jun 2024

HAL is a multi-disciplinary open access archive for the deposit and dissemination of scientific research documents, whether they are published or not. The documents may come from teaching and research institutions in France or abroad, or from public or private research centers.

L'archive ouverte pluridisciplinaire **HAL**, est destinée au dépôt et à la diffusion de documents scientifiques de niveau recherche, publiés ou non, émanant des établissements d'enseignement et de recherche français ou étrangers, des laboratoires publics ou privés.



**UNIVERSITÉ
DE LORRAINE**

**BIBLIOTHÈQUES
UNIVERSITAIRES**

AVERTISSEMENT

Ce document est le fruit d'un long travail approuvé par le jury de soutenance et mis à disposition de l'ensemble de la communauté universitaire élargie.

Il est soumis à la propriété intellectuelle de l'auteur. Ceci implique une obligation de citation et de référencement lors de l'utilisation de ce document.

D'autre part, toute contrefaçon, plagiat, reproduction illicite encourt une poursuite pénale.

Contact bibliothèque : ddoc-theses-contact@univ-lorraine.fr
(Cette adresse ne permet pas de contacter les auteurs)

LIENS

Code de la Propriété Intellectuelle. articles L 122. 4

Code de la Propriété Intellectuelle. articles L 335.2- L 335.10

http://www.cfcopies.com/V2/leg/leg_droi.php

<http://www.culture.gouv.fr/culture/infos-pratiques/droits/protection.htm>



UNIVERSITÉ
DE LORRAINE

LCPME

Laboratoire de Chimie Physique et
Microbiologie pour les Matériaux
et l'Environnement

Thèse

Présentée et soutenue publiquement pour l'obtention du titre de

DOCTEUR DE L'UNIVERSITÉ DE LORRAINE

Mention : CHIMIE

Par **Gustavo Adrián Echeveste Salazar**

Sous la direction de **Alain WALCARIUS**

**Sondes à gel pour la Microscopie Électrochimique à
Balayage : élaboration, fonctionnalisation et analyse**

25 Octobre 2023

Membres du jury :

Directeur(s) de thèse :	Dr. Alain Walcarius	Directeur de Recherche LCPME – Université de Lorraine, Nancy, France)
Président de jury :	Prof. Anne Jonquière	Professeur (ENSIC-LCPM – Université de Lorraine, Nancy, France)
Rapporteurs :	Prof. Sabine Kuss	Professeur (LBES – University of Manitoba, Canada)
	Dr. Philippe Hapiot	Directeur de Recherche (ISCR – Université de Rennes, France)
Examineurs :	Dr. Marina Inès Giannotti	Chargée de Recherche (IBEC – Universitat de Barcelona, Spain)
	Dr. Carlos Sanchez Sanchez	Chargé de Recherche (LISE – Sorbonne Université, Paris, France)
Membres invités : (coencadrant de la thèse)	Dr. Liang Liu	Chargé de Recherche (LCPME – Université de Lorraine, Nancy, France)

Laboratoire de Chimie Physique et Microbiologie pour les Matériaux et l'Environnement (LCPME)
UMR 7564, CNRS / Université de Lorraine
405 Rue de Vandoeuvre, 54600, Villers-lès-Nancy, France



Thesis

Presented and publicly defended for the title of
DOCTOR OF THE UNIVERSITY OF LORRAINE
Mention: CHEMISTRY

By **Gustavo Adrián Echeveste Salazar**
Supervised by **Alain WALCARIUS**

Gel probes for scanning electrochemical microscopy: elaboration, functionalization and analysis

25 October 2023

Jury members:

Supervisor:	Dr. Alain Walcarius	Directeur de Recherche LCPME – Université de Lorraine, Nancy, France)
Jury president:	Prof. Anne Jonquière	Professor (ENSIC-LCPM – Université de Lorraine, Nancy, France)
Reviewers:	Prof. Sabine Kuss	Professor (LBES – University of Manitoba, Canada)
	Dr. Philippe Hapiot	Directeur de Recherche (ISCR – Université de Rennes, France)
Examiners:	Dr. Marina Inès Giannotti	Chargée de Recherche (IBEC – Universitat de Barcelona, Spain)
	Dr. Carlos Sanchez Sanchez	Chargé de Recherche (LISE – Sorbonne Université, Paris, France)
Invite: (Thesis co-supervisor)	Dr. Liang Liu	Chargé de Recherche (LCPME – Université de Lorraine, Nancy, France)

Laboratoire de Chimie Physique et Microbiologie pour les Matériaux et l'Environnement (LCPME)
UMR 7564, CNRS / Université de Lorraine
405 Rue de Vandoeuvre, 54600, Villers-lès-Nancy, France

To Julio.

Acknowledgments

How do you write an acknowledgment section of a thesis that has been 40 years in the making without being unfair to some people? You cannot do it, but I still want to express my gratitude to a few people who have contributed.

First and foremost, I would like to thank my supervisors, **Alain Walcarius** and **Liang Liu**, for their unwavering support and guidance throughout my journey. I would also like to express my gratitude to **Mariela Brites-Helu**, whose knowledge and exchange of ideas were invaluable to me. To **Ning Dang**, who guided my initial steps in this project, and **Mathieu Etienne** and **Grégory Francius**, for providing me with the necessary training and assistance.

I would like to extend my most sincere appreciation to **Ranine El Hage**, **Julius Gajdar**, **Morgane Hoareau**, **Magdalena Kaliszczak**, **Rayan Kanaan**, **Qiao Liu**, **Harpreet Singh**, **Madjid Tarabet**, **Baptiste Arbez**, **Saeid Ekrami**, **Clara Richard** and **Silvia Comis** for being part of this PhD experience and all the memories that came with it.

I would also like to thank **Christophe Gantzer** -current director - and all the staff from the **LCPME**. Especially, to **Sandrine Lemoine**, **Gérard Parquot**, and **Marie Rambeau**.

To my friends, thank you for tolerating my madness, and a big thanks to my families, including the one I was born into, my political family, my UNPSJB family, my second and third families (who have “adopted” me through the years) and -most importantly- the family that I have built with my husband.

Lastly, thank you to all of you whom I ever discussed a crazy idea or an incomplete project with, in a hallway, a classroom, or a bar; because it is from the exchange with others that knowledge is built.

Table of Contents

List of abbreviations	1
Abstract.....	5
Résumé.....	7
Résumé long de la thèse en français	9
Chapter I: General introduction	21
1.1. Scanning Probe Microscopy (SPM) and Scanning Electrochemical Probe Microscopy (SEPM).....	22
1.1.1. Electrochemical scanning tunneling microscopy (EC-STM).....	24
1.1.2. Scanning electrochemical microscopy (SECM)	26
1.1.3. Scanning ion conductance microscopy (SICM).....	29
1.1.4. Scanning electrochemical cell microscopy (SECCM).....	32
1.1.5. SEPM notes and brief comparison	35
1.2. Scanning gel electrochemical microscopy (SGECM).....	35
1.2.1. Gel probes fabrication	36
1.2.2. SGECM set-up	40
1.2.3. SGECM imaging	44
1.2.4. SGECM patterning and flexible resolution.....	45
1.3. Gel probe-surface interaction	46
1.3.1. SGECM approach and retract curves	47
1.3.2. Quartz crystal microbalance.....	51
1.4. Proposition of the work.....	54
Chapter II: Preparation and functionalization of gels probe for scanning gel electrochemical microscopy (SGECM)	57
2.1. Experimental.....	58
2.1.1. Materials	58
2.1.2. Sample characterization	59
2.1.3. AFM characterization	59
2.2. Empirical shape control of chitosan electrodeposition.....	60
2.3. Chitosan-tetraethoxysilane co-electrodeposition.....	63
2.4. Chitosan-3-mercaptopropyltrimethoxysilane co-electrodeposition.	69
2.5. Other attempts to elaborate the gel probes	73

2.5.1. Chitosan + Ionic Liquid (IL) gel probe.....	73
2.5.2. Chitosan + deep eutectic solvent (Ch-DES) gel probe.	75
2.6. Summary.....	76
Chapter III: SGECM integration with QCM for studying gel probe-sample interactions.....	79
3.1. Experimental.....	80
3.1.1. Materials and chemicals.....	80
3.1.2. Fabrication of probes	81
3.1.3. QCM coupled SGECM measurements	82
3.1.4. Characterization of the samples	83
3.2. QCM coupled SGECM measurements.....	84
3.3. Gel probe stabilization.....	90
3.3. Reinforcement of the gel probe by co-electrodeposition with TEOS	93
3.4. Squeezing effect	95
3.5. Comparison among different probes	98
3.6. Summary.....	100
Chapter IV: Micro-integrated electrodes for ozone sensing.....	103
4.1. Experimental.....	106
4.1.1 Materials and chemicals.....	106
4.1.2. Micro-integrated electrode fabrication and characterization.	106
4.1.3. Electrochemical measurements.....	107
4.2. Electrochemical behavior of micro-integrated electrodes	108
4.3. Chronoamperometry using gel coated micro-integrated electrodes	116
4.4. Ozone detection by integrated electrodes.....	119
4.5. Improving the durability of integrated electrodes	123
4.5.1. MIE-GC ozone exposition with UV protection.....	123
4.5.2. MIE-GC regeneration	125
4.6. Summary.....	128
Chapter V: General conclusion and perspectives	131
References.....	137
Appendix I: Gel Probe characterization.....	163
Appendix II: Chitosan gel probe 3-MPA functionalization.....	165

List of abbreviations

Abbreviation	Definition
3-MPA	3-mercaptopropionic acid
AC	Alternating Current
ADC	Analog-to-Digital Converter
AFM	Atomic Force Microscopy
AT-cut	Cut made 35°15' from the optical axis
BMIMBF ₄	1-Butyl-3-methylimidazolium tetrafluoroborate
BTA	Benzotriazole
<i>ca.</i>	Circa, approximately
CE	Counter Electrode
Ch	Chitosan
CV	Cyclic Voltammetry
Cyt	Cytochrome
DC	Direct Current
DES	Deep Eutectic Solvent
E	Potential
<i>e.g.</i>	Exempli Gratia, for example
E_a	Approach Potential
E_{app}	Applied Potential
EBSD	Electron Backscatter Diffraction
EC-STM	Electrochemical Scanning Tunneling Microscopy
EDX	Energy-Dispersive X-Ray
EMIMBF ₄	1-Ethyl-3-methylimidazolium tetrafluoroborate
EQCM	Electrochemical Quartz Crystal Microbalance
ET	Electron Transfer
E_w	Withdrawing Potential
f	Frequency
FEM	Finite Element Method
FT-IR	Fourier Transform Infrared
Gly	Glycerol

Abbreviation	Definition
hCyt	Human Cytochrome
HER	Hydrogen Evolution Reaction
<i>i.e.</i>	Id Est, in other words
I _a	Anodic Current
IBM	International Business Machines Corporation
I _c	Cathodic Current
ID	Inner diameter
IL	Ionic Liquid
I _{L,a}	Anodic Limiting Current
I _{L,c}	Cathodic Limiting Current
IRM	Interference Reflection Microscopy
ITO	Iridium Titanium Oxide
MIE	Micro-Integrated Electrode
MIE-GC	Micro-Integrated Electrode Gel Coated
MPTMS	3-Mercaptopropyltrimethoxysilane
n	Number size
NO _x	Nitrogen Oxides
OCP	Open Circuit Potential
OD	Outer diameter
OI-SECCM	Oil Immersed Scanning Electrochemical Cell Microscopy
ORR	Oxygen Reduction Reaction
OSHA	Occupational Safety and Health Administration
Ox	Oxidized
pCyt	Plant Cytochrome
PDP	Polarization
PEG	Polyethylene Glycol
PEO	Polyethylene Oxide
QC	Quartz Crystal
QCM	Quartz Crystal Microbalance
QRCE	Quasi Reference and Counter Electrode
QRE	Quasi Reference Electrode
RE	Reference Electrode
Red	Reduced

Abbreviation	Definition
R _g	The ratio between electrode micro-disk radius and probe external radius
SAM	Self-Assembled Monolayer
SCE	Standard Calomel Electrode
SD	Standard deviation
SECCM	Scanning Electrochemical Cell Microscopy
SECM	Scanning Electrochemical Microscopy
SEM	Scanning Electron Microscopy
SEPM	Scanning Electrochemical Probe Microscopy
SGECM	Scanning Gel Electrochemical Microscopy
SICM	Scanning Ion Conductance Microscopy
SMP	Shape Memory Polymer
SPM	Scanning Probe Microscopy
STM	Scanning Tunneling Microscopy
TEM	Transmission Electron Microscopy
TEOS	Tetraethoxysilane
t _h	Holding Time
TTL-IC	Transistor–Transistor Logic Integrated Circuit
t _w	Withdrawing Time
UME	Ultra-Micro Electrode
UV	Ultraviolet
V _a	Approach Speed
VB.NET	Visual Basic .NET
V _w	Withdrawing Speed
WE	Working Electrode
XRD	X-Ray Diffraction

Abstract

Scanning gel electrochemical microscopy (SGECM) is a scanning probe technique that localizes both the electrode and the electrolyte using gel probes. The gel probe is fabricated by coating a micro-disk electrode or an etched metal wire with a controlled-shaped gel by electrodeposition. During the measurement, the gel probe scans over the sample surface in tapping, allowing simultaneous acquisition of topography and electrochemical signals. The analysis of the current response when the gel probe is in contact with the sample depends on the shape of the gel. Besides, a map with a reasonable number of pixels takes hundreds of approach-retract cycles (tapping), and the gel is deformed and restored every time due to its soft nature. Thus, the shape control and the material of the gel play a key role in SGECM development.

In **Chapter II**, chitosan was electrodeposited on micro-disk electrodes, and the deposition volume was correlated with the deposition charge. As a further step, alkoxysilanes, notably tetraethoxysilane (TEOS), were co-electrodeposited with chitosan to enhance its mechanical strength. The approach-retract behavior of the composite gel probes was discussed. The successful co-electrodeposition approach also opened the door to a wide range of possible functionalization, such as with 3-mercaptopropyltrimethoxysilane (MPTMS).

Spreading of electrolyte is a main challenge for local electrochemical measurements based on spatially localized contact between the electrolyte and the sample surface. In **Chapter III** this issue was studied through SGECM approach-retract curves of gel probes on a quartz crystal microbalance (QCM), where the resonance frequency is recorded and synchronized with the

current response. Verified by SEM observation, the frequency shift after one approach-retract cycle was taken as a measure for systematically comparing the extent of electrolyte residue on the Au-coated quartz crystal surface. The results showed that the electrolyte remaining on the sample could be reduced to negligible after a few approach-retract cycles. The incorporation of TEOS was also proven to be beneficial. The combination of QCM with SGECM offers a quality control method for gel probes before quantitative local electrochemical measurements.

A further attempt to improve the gel probe is on the configuration. In Chapter IV, the new micro-integrated electrode is composed of a micro-disk electrode and an outer ring electrode, separated by insulating material and coated with hydrogel. The redox probe is soaked in the electrode as a mediator. When the MIE-GC is exposed to an oxidative or reductive atmosphere, the redox ratio in the gel changes. This effect can be electrochemically measured by chronoamperometry, only using the two electrodes in MIE. Proof-of-concept experiments were made exposing a MIE-GC to Ozone gas in a UV ozone generator chamber. Based on the promising results, one may foresee applications of such electrodes not only in SGECM but also in explosive analysis.

Keywords: Scanning Gel Electrochemical Microscopy (SGECM), Hydrogel, Polymer Electrodeposition, Chitosan, Quartz Crystal Microbalance (QCM), Ozone Sensing

Résumé

La microscopie électrochimique à balayage à sonde à gel (SGECM) est une technique à sonde locale qui associe à la fois l'électrode et l'électrolyte au sein d'une sonde à gel. Celle-ci est fabriquée en formant un gel de forme contrôlée sur une électrode à micro-disque ou un fil métallique par électro-dépôt. Pendant la mesure, la sonde à gel balaye la surface de l'échantillon en tapotant, permettant l'acquisition simultanée de la topographie et des signaux électrochimiques. L'analyse de la réponse en courant lorsque la sonde de gel est en contact avec l'échantillon dépend de la forme du gel. De plus, une carte avec un nombre raisonnable de pixels prend des centaines de cycles d'approche-rétraction (tapotement), et le gel est déformé et restauré à chaque fois en raison de sa nature molle. Ainsi, le contrôle de la forme et la nature du gel jouent un rôle clé dans le développement de la SGECM.

Dans le **Chapitre II**, le chitosane a été électrodéposé sur des électrodes à micro-disque, et le volume de dépôt a été corrélé à la charge de dépôt. Dans une étape supplémentaire, des alcoxy-silanes, notamment du tétraéthoxysilane (TEOS), ont été co-électrodéposés avec du chitosane pour améliorer sa résistance mécanique. Le comportement d'approche-rétraction des sondes à gel composite a été discuté. L'approche réussie du co-électro-dépôt a également ouvert la porte à un large éventail de fonctionnalisations possibles, comme avec le 3-mercaptopropyltriméthoxysilane (MPTMS).

La propagation d'électrolyte est un défi majeur pour les mesures électrochimiques locales basées sur un contact spatialement défini entre la sonde et la surface de l'échantillon. Dans le **Chapitre III**, ce problème a été étudié en réalisant des courbes d'approche-rétraction de sondes de gel sur une microbalance à cristal de quartz (QCM), où la fréquence de résonance est

enregistrée et synchronisée avec la réponse SGECM. En complément d'observations par microscopie électronique, nous avons confirmé que les variations de fréquence après un cycle d'approche-rétraction constituent une bonne mesure pour comparer systématiquement l'étendue de la fuite d'électrolyte sur la surface d'un cristal de quartz revêtu d'or. Les résultats ont montré que l'électrolyte restant sur l'échantillon pouvait être réduit à négligeable après quelques cycles d'approche-rétraction. L'intégration de TEOS s'est également avérée bénéfique. La combinaison de QCM avec SGECM offre une méthode de contrôle de qualité pour les sondes à gel avant des mesures électrochimiques locales quantitatives.

Une autre tentative d'amélioration de la sonde de gel concerne sa configuration. Au **Chapitre IV**, une nouvelle électrode micro-intégrée (MIE) composée d'une électrode micro-disque et d'une électrode annulaire extérieure, séparées par un matériau isolant et recouvertes d'hydrogel. L'électrode est imbibée d'une sonde redox agissant comme médiateur. Suite à l'exposition à une atmosphère oxydante ou réductrice, les rapports de concentration Red/Ox de la sonde dans le gel changent. Cet effet peut être mesuré électrochimiquement par chronoampérométrie en utilisant uniquement les deux électrodes en MIE. Des expériences de preuve de concept ont été réalisées en exposant cette nouvelle sonde à gel à l'ozone gazeux dans une chambre de génération d'ozone par UV. Sur base des résultats prometteurs, on peut prévoir des applications de telles électrodes non seulement en SGECM mais aussi pour l'analyse d'explosifs par exemple.

Mots-clés : Microscopie électrochimique à sonde à balayage, Microscopie électrochimique à balayage à sonde à gel (SGECM), Hydrogel, Electro-dépôt de polymère, Microbalance à cristal de quartz (QCM), détection d'ozone.

Résumé long de la thèse en français

Les microscopies à sonde à balayage (« *scanning probe microscopy* », SPM) regroupent un ensemble de techniques qui ont été développées pour étudier les propriétés et les phénomènes superficiels aux échelles micro- et nanométriques. Elles constituent des outils « tout en un » qui se sont révélés puissants pour explorer des molécules uniques ou des nanostructures. Elles présentent l'avantage de pouvoir obtenir des informations fiables à de très petites tailles, les rendant extrêmement attractives pour les scientifiques dans plusieurs domaines, tels que la biologie, les études au niveau cellulaire, la corrosion, la catalyse, la caractérisation des nanostructures, la manipulation à l'échelle atomique, entre autres. Les dispositifs SPM partagent certains aspects techniques, tels que : (1) la sonde, qui dans la plupart des cas est responsable de la résolution (sa taille reflète la zone de l'échantillon en cours de numérisation), ainsi les images résolues à l'échelle nanométrique nécessitent une sonde très pointue ; (2) l'usage de matériaux piézoélectriques (l'effet piézoélectrique concerne la déformation des matériaux par application d'un champ électrique) qui permet d'analyser des échantillons avec une précision au picomètre ; (3) la nécessité d'une isolation vibratoire et des amplificateurs de signal à gain élevé et à faible bruit (les deux sont essentiels pour obtenir un rapport signal sur bruit suffisamment élevé et garantir des images de haute résolution).

Au cours des dernières décennies et plus récemment, on dénote un intérêt croissant pour une branche particulière de la famille des SPM que constituent les microscopies à sonde électrochimique à balayage (« *scanning electrochemical probe microscopy* », SEPM). Ce groupe particulier de techniques vise à étudier des échantillons dans un environnement prenant en considération la réactivité redox des surfaces analysées. Dernièrement, avec l'essor

croissant de l'électrochimie dans divers domaines de recherche, les techniques SEPM ont de plus en plus été utilisées et développées. La STM électrochimique (« *electrochemical scanning probe microscopy* », EC-STM), la microscopie électrochimique à balayage (« *scanning electrochemical microscopy* », SECM), la microscopie à conductance ionique à balayage (« *scanning ion conductance microscopy* », SICM) et, plus récemment, la microscopie cellulaire électrochimique à balayage (« *scanning electrochemical cell microscopy* », SECCM) sont parmi les techniques SEPM les plus couramment utilisées. D'autres techniques apparentées telles que l'AFM électrochimique (electrochemical « *atomic force microscopy* »), par exemple, ont également été décrites, mais en raison de l'étendue limitée de ce travail, seules les quatre nommées ci-dessus seront brièvement passées en revue dans l'introduction de la thèse (**Chapitre I**).

Conformément à EC-STM, SECM et SECCM, et dans le but d'élargir les applications possibles de SEPM, la microscopie électrochimique à balayage à sonde à gel (« *scanning gel electrochemical microscopy* », SGECM) a été proposée par notre groupe il y a quelques années sur base d'un montage classique de SECM (**Figure 1A**). Par contre, elle implique l'usage d'une électrode enduite de gel (sonde de gel) qui est utilisée pour approcher la surface de l'échantillon au lieu d'une ultramicroélectrode traditionnelle. La sonde de gel combine à la fois l'électrode et l'électrolyte. Ainsi, l'échantillon est placé dans l'air et ne nécessite pas de travailler en milieu solvant. Une fois que la sonde de gel entre en contact avec la surface de l'échantillon, les propriétés électrochimiques locales peuvent être mesurées. La nature du contact doux du gel permet également de travailler sur des surfaces de forme irrégulière. Une caractéristique particulière de l'utilisation de la SGECM réside dans la forme spécifique des courbes d'approche et de retrait de la sonde à gel (**Figure 1B**). Pour les obtenir, une tension donnée est

appliquée entre un échantillon (conducteur) et la sonde à gel. À l'approche, un contre-signal de courant de fond (proche de 0) est enregistré jusqu'à ce que la sonde touche l'échantillon. Ensuite, un pic est enregistré et ce signal est utilisé pour arrêter la sonde à gel (retour de courant). Immédiatement, le courant chute pour atteindre une valeur stable. Pendant que la sonde est rétractée, le courant est affecté par deux processus physiques consécutifs et différents: (1) l'étirement du gel, et (2) le détachement du gel de la surface. Le premier modifie la distance entre les électrodes tandis que le second modifie la zone de contact gel-échantillon. Le débit de courant est mesuré en continu tout au long du cycle d'approche et de rétraction. Les courbes d'approche et de retrait sont un outil exceptionnel pour étudier les interactions entre la sonde à gel et la surface de l'échantillon ainsi que les propriétés mécaniques du gel (les deux constituant des sujets de grand intérêt pour la SGECM). Le **Chapitre II** explore l'électro-dépôt de chitosane pour fabriquer des sondes de gel pour la SGECM. Nous considèrerons aussi son association avec d'autres polymères (co-électro-dépôt de mélanges de polymères) et les premières tentatives d'obtention d'une sonde gel fonctionnalisée. Les courbes d'approche et de retrait sont utilisées pour caractériser les différentes sondes à gel. Le **Chapitre III** présente la combinaison de la SGECM avec la microbalance à cristal de quartz (« *quartz cristal microbalance* », QCM) pour étudier les fuites d'électrolyte de la sonde gel au contact avec la surface de l'échantillon. En raison de l'interaction entre la sonde de gel et l'échantillon, une petite quantité de l'électrolyte initialement immobilisé/imprégné au sein de la sonde de gel peut rester sur l'échantillon. L'association QCM-SGECM permet de mettre en évidence ce phénomène. Enfin, le **Chapitre IV** présente une nouvelle sonde gel, une microélectrode intégrée (MIE) composée d'électrodes concentriques à micro-disques et micro-anneaux, qui est recouverte d'un gel de chitosane (MIE-GC). Cette sonde MIE-GC est trempée dans une

solution contenant une sonde redox et appliquée à l'analyse d'une molécule modèle, l'ozone. Le principe est basé sur une variation de la teneur en sonde redox au sein du gel change lorsque l'électrode à sonde à gel entre en contact avec des espèces réductrices ou oxydantes. Ce changement peut être suivi par des techniques électrochimiques et ceci a été démontré ici en tant que preuve de concept pour détecter l'ozone au moyen d'une MIE-GC dopée par le couple redox $[\text{Fe}(\text{CN})_6]^{3-/4-}$.

Les sondes à gel testées au **chapitre II** pour la SGECM sont construites en enrobant une électrode à micro-disque de 25 μm d'hydrogel de chitosane par électro-dépôt. Le chitosane est un polymère biocompatible naturel soluble à pH inférieur à 6,3. En générant un gradient de pH à la surface de l'électrode, ce polymère peut être électro-déposé. Le recouvrement des électrodes est réalisé par chronoampérométrie. Un potentiel approprié pour la réaction de dégagement d'hydrogène est appliqué, abaissant la valeur du pH de surface de l'électrode par réduction de l'eau, déclenchant ainsi la précipitation du chitosane à la surface de l'électrode. Les conditions d'électro-dépôt ont été optimisées dans le but d'obtenir un gel de forme sphérique avec un rayon égal au rayon de la sonde (électrode). En général, de bons résultats sont obtenus en appliquant un potentiel constant de -0,95V vs. Ag/AgCl (électrode de référence) pendant 300s. Les paramètres de chronoampérométrie doivent cependant être adaptés pour chaque lot de solutions de précurseur afin d'obtenir des sondes de gel de chitosane très reproductibles.

Pour générer une cartographie par SGECM, la sonde de gel doit s'approcher et se rétracter des milliers de fois des surfaces. Lorsque la sonde atteint la surface, la déformation du gel détermine la zone de contact, ce qui constitue un paramètre clé dans l'analyse des résultats. De plus, le gel subit plusieurs cycles consécutifs de compression-étirement. Éviter la déformation

du gel qui pourrait apparaître au cours de ces cycles successifs est donc important pour assurer la répétabilité des résultats. Ainsi, même si le gel de chitosane montre une performance acceptable, l'amélioration des propriétés mécaniques de la sonde de gel est fortement souhaitée. Dans le but d'améliorer les caractéristiques mécaniques du gel de chitosane, un co-électro-dépôt avec un second polymère a été proposé. On sait que des alcoxy-silanes (tels que le *tetraethoxysilane*, TEOS) hydrolysés peuvent être électro-déposés par une augmentation locale de la valeur du pH. Le mécanisme d'électro-dépôt n'est pas exactement celui du chitosane (l'augmentation de pH sert ici à catalyser la condensation du réseau silicique) mais les deux processus peuvent se produire simultanément. Des composites chitosane-tétraéthoxysilane (Ch-TEOS) et chitosan-3-mercaptopropyltriméthoxysilane (Ch-MPTMS) ont été testés pour l'élaboration de sondes à gel. Pour le premier composite, Ch-TEOS, il s'agissait de voir si l'on pouvait améliorer les propriétés mécaniques du gel. Pour le second, Ch-MPTMS, l'idée était d'introduire une fonction thiol susceptible d'interagir avec la surface de l'échantillon (dans le cas d'un substrat d'or par exemple). Les deux composites ont été électro-déposés avec succès à des taux massiques de 1:0,25, 1:0,5, 1:0,75 et 1:1 chitosane:(organo)silane. L'analyse par dispersion en énergie des rayons X (« *Energy-dispersive X-ray* », EDX) a été utilisée pour vérifier le rapport Si/C dans les gels obtenus et confirmer l'électro-dépôt du mélange. Des efforts pour caractériser les mélanges de gel par spectroscopie infrarouge à transformée de Fourier (« *Fourier transform InfraRed* », FT-IR) et par spectrométrie Raman ont été réalisés, mais les résultats obtenus avec le gel de chitosane n'étaient pas différents du gel auquel un alcoxy-silane avait été ajouté. La caractérisation électrochimique des sondes à gel de type Ch-TEOS a été réalisée en enregistrant des courbes de voltampérométrie cyclique (« *cyclic voltammetry* », CV) dans une solution contenant une sonde redox de type ferrocène diméthanol

(0,1 mM Fc(OH)₂ + 0,1 M KCl dans 1:1 glycérol:eau). Les résultats n'ont indiqués aucun changement significatif dans la réponse CV des composites Ch-TEOS par rapport aux sondes à gel formée uniquement de chitosane. L'enregistrement de courbes d'approche et de retrait par SGECM ont été exploitées pour caractériser qualitativement le comportement mécanique du chitosane et de ses composites Ch-TEOS et Ch-MPTMS. L'étirement du gel et l'adhérence gel-échantillon ont été étudiés en mesurant la distance nécessaire à la sonde à gel pour se détacher de la surface de l'échantillon (distance de détachement). La distance de détachement est obtenue à partir des courbes d'approche et de retrait en mesurant le déplacement depuis la pointe de courant en contact jusqu'au retour du courant à zéro (niveau de bruit) lors du retrait. L'utilisation des mélanges Ch-TEOS montre que cette distance diminue avec l'augmentation des proportions de TEOS, un résultat optimal atteint pour la sonde à gel de composition 1:0.5 Ch:TEOS, avec une distance de détachement réduite d'environ 54 % (**Figure 1C**). Pour le composite Ch-MPTMS de même teneur en additif silicique, une réduction d'environ 70 % de la distance de détachement a été observée. Les gels classique à base de chitosane et le composite Ch-TEOS (1:0,5) ont été également été caractérisés par AFM, résultant en l'obtention d'un module d'environ $37,4 \pm 0,45$ kPa pour le chitosane et d'environ $49,3 \pm 0,07$ kPa pour le mélange Ch-TEOS. Ces résultats, en accord avec ceux obtenus par comparaison des distances de détachement, confirment l'amélioration des propriétés mécaniques (rigidité) par le co-électro-dépôt du chitosane avec des alcoxy-silanes. Une sonde à gel fonctionnalisée au thiol a été utilisée pour explorer les possibles interactions Au-S. Les courbes d'approche et de retrait ont été réalisées à l'aide d'échantillons avec et sans revêtement d'or. Seules les distances de détachement du chitosane, du Ch-TEOS (teneurs en TEOS 1 à 0,5) et du Ch-MPTMS (teneurs de 1 à 0,5) ont été mesurées en utilisant soit une électrode d'oxyde mixte

d'indium et d'étain (« *indium-tin oxide* », ITO) nue, soit recouverte d'or (Au-ITO). Même si les sondes à gel hybrides Ch-TEOS et Ch-MPTMS montrent une amélioration globale de la rigidité du gel, il n'y a pas de tendance claire quant à un effet des interactions entre la surface d'or et les groupements thiol. Des tentatives pour améliorer les propriétés de la sonde à gel à base de chitosane en utilisant des liquides ioniques (« *ionic liquid* », IL) et un solvant eutectique profond (« *deep eutectic solvent* », DES) ont également été faites. Les résultats ne montrent pas une nette augmentation de la distance de détachement des sondes de gel Ch-IL et Ch-DES, mais pas non plus d'amélioration de la conductivité du gel.

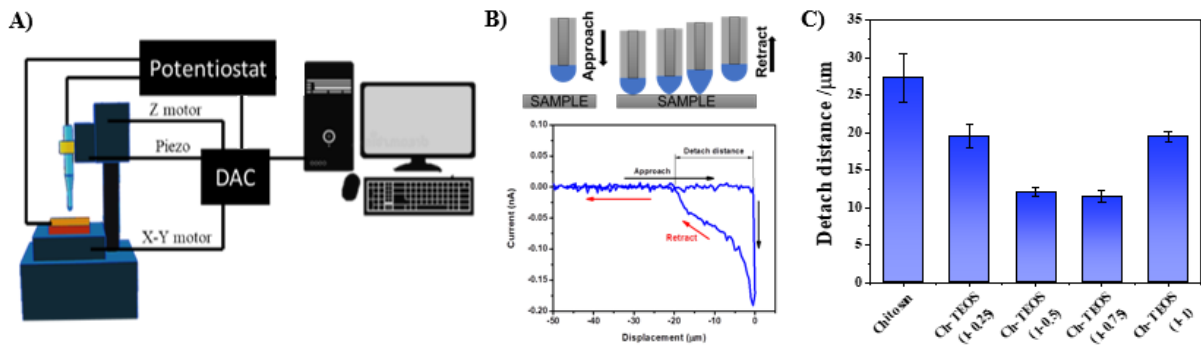


Figure 1 Schéma de configuration de la microscopie électrochimique à balayage (A). Schéma représentant l'approche et le retrait d'une sonde à gel rétractable et réponse de courant typique (B). Comparaison de distances de détachement observées pour les sondes à gel à base de chitosane seul ou en mélange avec différents teneurs de TEOS en utilisant une plaque de Pt comme substrat (C).

Les courbes d'approche et de retrait se sont révélées être un outil très pratique. Mais l'absence d'une quantification appropriée de la réponse actuelle nous a conduit à explorer des méthodes alternatives pour étudier l'interaction entre la sonde à gel et l'échantillon. Dans le **Chapitre III**, la combinaison SGECM avec QCM est proposée (**Figure 2A**). Pour y parvenir, nous nous sommes concentrés sur le substrat de l'échantillon qui a donc été remplacé dans le système par un cristal de quartz revêtu, nous permettant de construire un dispositif associant SGECM et QCM. Une fréquence est appliquée au cristal de quartz (CQ) et sa variation est enregistrée

pendant le cycle d'approche et de retrait. En cas de modification de la surface du CQ à la suite de l'approche de la sonde de gel (comme un dépôt d'électrolyte, par exemple), la fréquence de résonance changera (**Figure 2B**). Cette configuration a été proposée pour étudier de possibles fuites d'électrolyte lors du contact entre la sonde à gel e la surface de l'échantillon analysé. SGECEM suppose qu'en confinant l'électrolyte sous forme de gel, les fuites d'électrolyte sur l'échantillon peuvent être évitées. Pour étudier cela, une méthode analytique basée sur la mesure des courbes d'approche-rétraction des sondes à gel sur une microbalance à cristal de quartz (QCM) a été proposée, tout en s'assurant de synchroniser l'enregistrement de la fréquence de résonance QC avec la réponse du SGECEM. La sonde à gel a été approchée vers le QC revêtu d'or et immédiatement rétractée, tout en appliquant une tension constantan de 0,4 V (E_{sample} vs. E_{probe}). La fréquence de résonance QC et le courant de la sonde ont été enregistrés au cours de chaque cycle d'approche et de retrait. Le décalage de fréquence après un cycle d'approche-rétraction est pris comme mesure pour comparer systématiquement l'étendue de la fuite d'électrolyte sur la surface du cristal de quartz revêtue d'or. Pour relier la fuite d'électrolyte au décalage de fréquence QC, des observations complémentaires par microscopie électronique à balayage (« *scanning electron microscopy* », SEM) ont été effectuées dans le but d'observer la surface QC revêtue d'or avant et après les opérations d'approche-retrait et ainsi tenter d'observer les éventuels dépôts d'électrolyte et de les relier au décalage de fréquence. La fuite d'électrolyte au niveau des sondes à gel de chitosane et des composites à base de chitosane déposées sur microdisque à différents états de vieillissement a été testée à l'aide de la configuration SGECEM-QCM. Chaque sonde a été approchée et rétractée séquentiellement, mesurant le décalage de fréquence par rapport au premier cycle d'approche et de rétraction. Pour toutes les sondes à gel étudiées ici, une fuite initiale est observée mais elle diminue ensuite

drastiquement après quelques cycles d'approche et de rétraction. Les résultats montrent que la fuite d'électrolyte des sondes à gel fraîchement préparées, en particulier après imprégnation par des sondes redox, peut être réduite à un niveau négligeable après quelques cycles d'approche-rétraction (**Figure 2C**). Ces fuites peuvent également être inhibées par co-électro-dépôt de chitosane avec le TEOS, probablement parce que le TEOS améliore les propriétés mécaniques de la sonde à gel (gel Ch-TEOS moins compressible et fuites d'électrolyte après compression réduites). Elles sont par contre plus importantes lorsque la sonde de gel est trop pressée contre l'échantillon (un phénomène analysé en compressant les sondes de 2 à 10 μm après avoir touché l'échantillon). L'effet de fuite de deux types de sondes de gel et de microcapillaires a également été comparé. Tous ces résultats indiquent que la configuration SGECM-QCM est un outil bien adapté pour évaluer l'effet du contact des sondes à gel avec l'échantillon, les éventuelles fuites d'électrolytes, et une estimation des zones de contact sonde-échantillon. De plus, l'approche-rétraction sur une surface QC peut être envisagée comme un protocole standard pour assurer une bonne stabilisation et une fuite négligeable des sondes à gel avant des mesures quantitatives par SGECM.

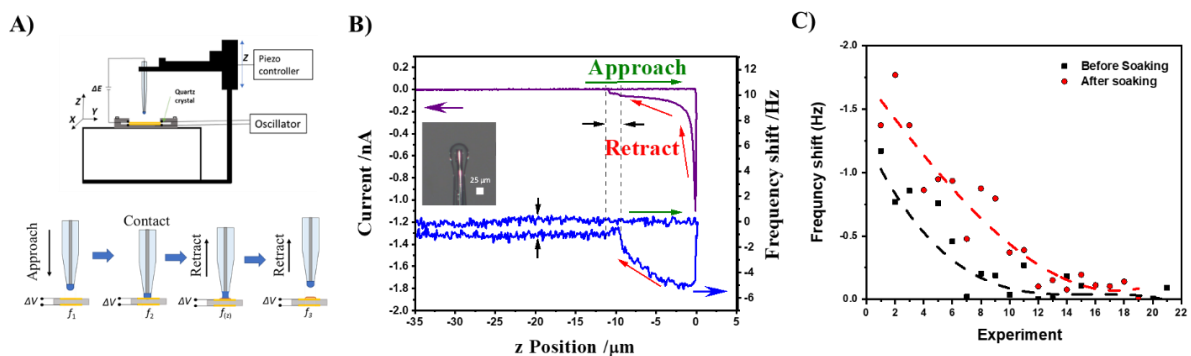


Figure 2. Schéma de configuration QCM-SGECM et schéma d'approche-rétraction d'une sonde à gel sur la surface QC avec fuite d'électrolyte (A). Courbe d'approche et de retrait typiques de la sonde à gel de chitosane par QCM-SGECM avec fuite d'électrolyte sur la surface QC (B). Décalage de fréquence de l'or QC après approche-rétraction de la sonde à gel de chitosane avant et après trempage dans une solution de ferrocène diméthanol (1 mM $\text{Fc}(\text{MeOH})_2$ + 0,05 M KCl dans 1:1 vol. glycérol:eau) (C).

Dans le but d'évaluer les possibilités d'application de la SGECM et d'étendre nos connaissances sur l'interaction entre la sonde à gel et l'échantillon, une nouvelle configuration de sonde à gel est explorée au **Chapitre IV**. Une électrode à micro-anneau est intégrée à l'électrode à micro-disque. Cette seconde électrode peut être réalisée en plusieurs matériaux, pouvant jouer le rôle d'électrode de référence (« *reference electrode* », RE) ou de contre-électrode (« *counter-electrode* », CE). Une électrode à micro-disque de Pt est recouverte dans ses parties latérales d'une couche de Pt. La couche de Pt peut être connectée par un fil de Cu pour être utilisée comme seconde électrode. En conséquence, une sonde avec deux électrodes concentriques séparées par un matériau insolant est obtenue, et nous l'avons nommée électrode micro-intégrée (« *micro-integrated electrode* », MIE). La pointe MIE a été recouverte d'un gel de chitosane (MIE-GC) pour construire une cellule électrochimique à 2 électrodes où la couche de Pt externe agit comme une électrode micro-anneau (**Figure 3A**). Sur base d'une telle configuration MIE-GC, on peut prévoir des applications potentielles dans la mesure des résidus d'oxydants ou de réducteurs (par exemple, des explosifs) sur des surfaces. Pour ce faire, une sonde redox est imprégnée dans le MIC-GC, agissant comme intermédiaire, et suite à l'exposition du MIC-GC à un agent oxydant ou réducteur, les concentrations relatives des espèces oxydées et réduites de la sonde redox dans le gel changent. Cet effet peut être mesuré électrochimiquement par chronoampérométrie. Des expériences de preuve de concept ont été réalisées en exposant un MIC-GC imprégné par une solution 1:1 $[\text{Fe}(\text{CN})_6]^{3-}:[\text{Fe}(\text{CN})_6]^{4-}$ à une atmosphère oxydante constituée d'ozone (O_3), en plaçant l'électrode à l'intérieur d'une chambre de génération de O_3 (où O_3 est produit par rayonnement UV) (**Figure 3B**). Lorsque MIE-GE imbibée de la sonde redox est exposée à une atmosphère d' O_3 , le rapport entre les états oxydé et réduit de la sonde redox change. En appliquant une tension constante positive

suffisante à la partie oxydée de la sonde redox (+0,5 V E_{disk} vs. E_{ring}), un courant constant est atteint (courant d'oxydation). Ce courant est proportionnel à la partie réduite de la sonde redox (**Figure 3C**). De même, si la tension appliquée est négative (-0,5 V E_{disk} vs. E_{ring}), le courant cathodique est proportionnel à la partie oxydée de la sonde redox (**Figure 3D**). Ainsi, le rapport entre le courant d'oxydation et de réduction est analogue au rapport de concentration entre les espèces réduite et oxydée de la sonde redox dans le gel. Les résultats montrent que le rapport entre les courants d'oxydation et de réduction change avec le temps d'exposition du MIE-GC dans un environnement d'ozone généré par les UV. Les expériences de chronoampérométrie montrent une bonne relation entre le temps d'exposition à l' O_3 et la diminution de $[Fe(CN)_6]^{4-}$ dans le MIC-GC. L'exposition à l'impact de la lampe UV dans les courants obtenus a également été explorée. Un dispositif pour protéger le MIE-GC du rayonnement UV a été construit et placé à l'intérieur de la chambre O_3 . La protection interfère avec le flux d' O_3 à l'intérieur de la chambre, mais une relation entre le temps d'exposition et le taux de sonde redox peut être obtenue. L'intégrité du gel au cours d'expériences successives a également été explorée, plus précisément au travers de l'impact de la ré-imprégnation du MIE-GC sur la stabilité de la sonde redox. Le MIC-GC imbibé d'une sonde redox a été placé 60 secondes à l'intérieur de la chambre O_3 , les courants anodique et cathodique ont été immédiatement mesurés. L'électrode MIC-GC a été replongée dans une solution de sonde redox et exposée à nouveau 60s à O_3 . Après quelques-uns de ces cycles, le courant MIE-GC réimprégné avant l'exposition ne correspond pas à l'initial, indiquant que le MIE-GC ne peut pas résister à plus de 4 cycles de ré-imprégnation. Dans l'ensemble, nous avons démontré qu'il existe bien une dépendance entre l'exposition à l'ozone et la réponse chronoampérométrique. Ainsi, il a été montré que le MIE-GC est capable d'identifier la présence de cette substance, indiquant de surcroît que cette

configuration disque-anneau peut être prometteuse pour faire avancer la SGECM.

Au travers des différents chapitres de ce travail de thèse, plusieurs aspects des sondes à gel pour SGECM ont été explorés. Des tentatives pour améliorer les propriétés générales de la sonde à gel par l'utilisation d'additifs ont montré une amélioration significative des propriétés mécaniques du gel. Le couplage SECGM avec QCM a précisé les interactions entre la sonde à gel et l'échantillon, permettant une meilleure compréhension de la réponse de la sonde (via les courbes d'approche et de retrait). Bien qu'une interprétation plus approfondie de ces courbes soit nécessaire, des informations importantes peuvent en être extraites. Enfin, MIE-GC a montré une capacité manifeste à étendre les applications SGECM.

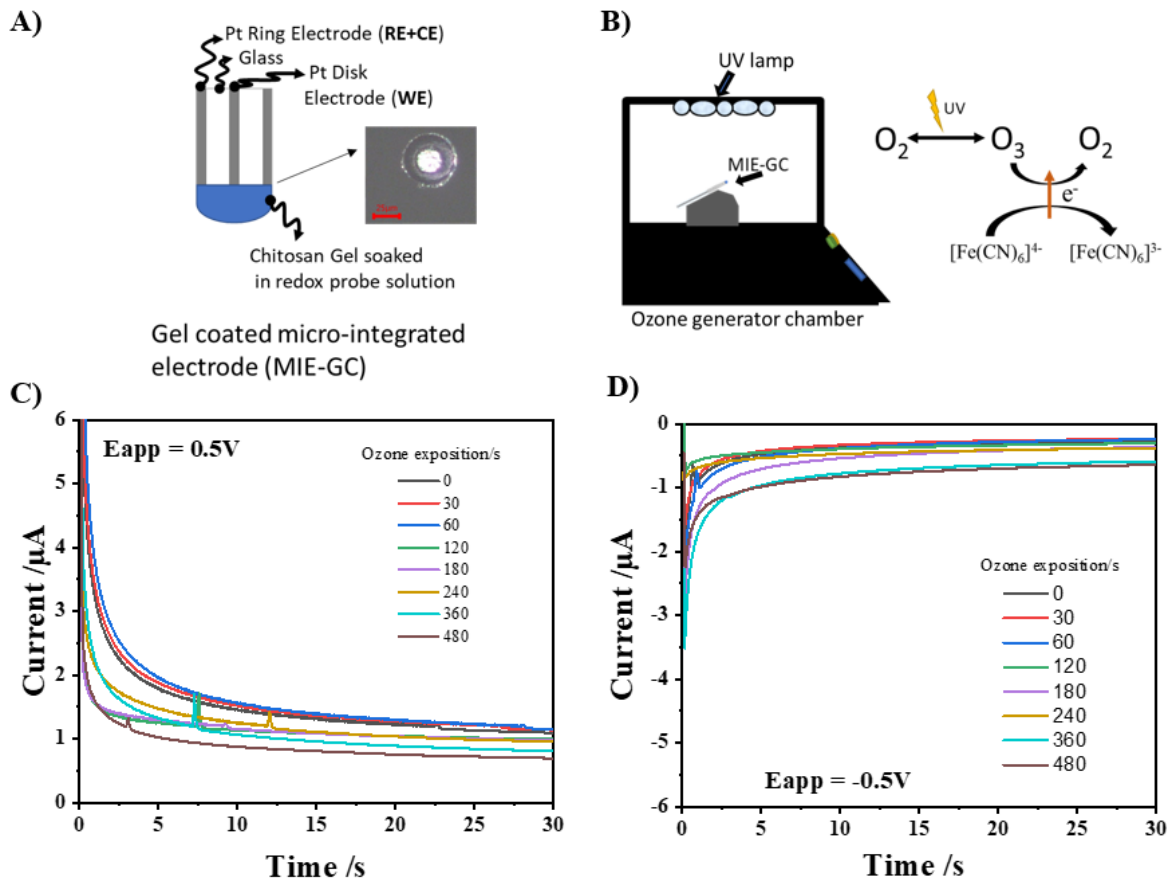


Figure 3 Schéma MIE-GC et image SEM de la pointe disque-anneau (A). Schéma de la chambre de génération d'ozone et sa détection via le couple $[Fe(CN)_6]^{3-/4-}$ (B). Chronoampérométries enregistrées au moyen d'une électrode MIE-GC imbibée de $[Fe(CN)_6]^{3-/4-}$ à différentes périodes d'exposition à l'ozone, respectivement à des potentiels appliqués de +0,5V (C) et -0,5V (D).

Chapter I

General introduction

In today's context, where one invests -at least- 10% of the day charging the phone battery, discussing the importance of electrochemical reactions in our daily life is beyond necessity. Nowadays, electrochemistry science has become a regular companion of our everyday lives, to the point of constantly carrying a lithium battery [1] (Nobel Prize 2019) with us. Solar cells [2], fuel cells [3] and water electrolysis [4], only to mention some examples, are more present than ever in our lives. Material science advances and the need for new energy sources pushed electrochemistry science forward to never-before-seen levels. This is the reason why, the study of electrochemical reaction mechanisms has become indispensable, not only for understanding and developing new materials, but for investigating degradation mechanisms. Thus, tools to characterize materials and study their electrochemical properties at the micro and nanometric levels were and are being developed. Recently, to push the boundaries of materials development and fulfill modern world requirements, researchers are in the need to study a novel material at micro and nanometer size ranges or even atomic and single entity levels. Thus, improving electrochemical characterization techniques is a need and highly desirable. In this context, scanning gel electrochemistry microscopy has been proposed (SGECM). It is based on a gel-coated micro-disk electrode which is in soft contact with the sample. During measurements, the sample is placed in ambient conditions, and the small quantity of gel serves as electrolyte (able to conduct electricity through the movement of free ions contained in it) for performing local electrochemical analysis. SGECM belongs to a family of characterization

techniques: scanning probe microscopy (SPM) and, in particular, scanning electrochemical probe microscopy (SEPM). So, to properly understand SGECM, we must go, first, through SPM.

1.1. Scanning Probe Microscopy (SPM) and Scanning Electrochemical Probe Microscopy (SEPM)

SPM gathers a group of techniques that were born to study surface properties and phenomena at micro and nanometric scales. In general, single molecules or nanostructures are explored using these tools. The advantage of obtaining reliable information at such small sizes is extremely attractive for scientists from several fields (biology, cell studies, corrosion, catalysis, nanostructures, and atomic manipulation, among others). SPM techniques share the following technical aspects: (1) The probe. In most cases, is responsible for the spatial resolution. Thus, getting images with nanometric resolution requires, generally, a highly sharp probe. (2) Precise positioning of the probe. Stepper motors are used for micrometer resolution, while piezoelectric effect (deformation of materials by applying an electric field) allows scanning samples with picometer precision. (3) Vibrational isolation and high-gain, low-noise signal amplifiers. Both are critical to achieving a sufficiently high signal-to-noise ratio, ensuring highly resolved images.

From the SPM family, it is fair to say that Scanning Tunneling microscopy (STM) and Atomic Force Microscopy (AFM) are the two most well-developed tools, and also the oldest ones. STM was presented by Binnig and Rohrer from IBM Zürich in 1981 [5]. The device is based on the current tunneling current principle. When two atoms are too close to each other, electrons can ‘tunnel’ through the empty space between them. If a voltage is applied in between, the tunneling effect results in a net electron current. STM is based on a very sharp

conductive tip that is used to approach the sample surface until the tip stops when a tunneling current is recorded. The surface is scanned using a feedback loop to keep the tunneling current constant, obtaining highly localized images with atomic resolution. Gerd Binnig and Heinrich Rohrer won the 1986 Nobel Prize for STM invention.

Shortly, after the STM invention, AFM was born [6], mainly to overcome some STM issues. AFM uses a cantilever with a very sharp tip as probe. While it approaches, the cantilever deflects as a result of tip-surface interaction forces. A laser beam is used to record the magnitude of the deflection. Because the deflection is caused by interaction forces, conductive and non-conductive samples and tips can be used. This also gives the users freedom in selecting the tip, allowing them to scan the surface for topographical information as well as measuring material properties. For example, in the nano-indentation mode, the tip contacts the sample at a known distance, and, by the deflection of the cantilever, mathematical models can be used to quantify sample surface mechanical properties. In recent years, the number of commercially available AFM (mostly) and STM devices has increased. As a result, SPM-based publications have grown through the years (**Figure 1.1**).

Figure 1.1 highlights the increasing interest in a particular branch of the SPM family: Scanning Electrochemical Probe Microscopy (SEPM). This particular group of techniques aims to study samples in a more realistic environment. Lately, with the uprising of electrochemistry as a research topic, SEPM techniques are increasingly used and developed. Electrochemical STM (EC-STM), Scanning Electrochemical Microscopy (SECM), Scanning Ion Conductance Microscopy (SICM), and, more recently, Scanning Electrochemical Cell Microscopy (SECCM) are the most common SEPM techniques in use. Other SEPM techniques can be found in existence and use, such as Electrochemical AFM [7], but due to the limited extent of

this work, only the four named before will be shortly reviewed.

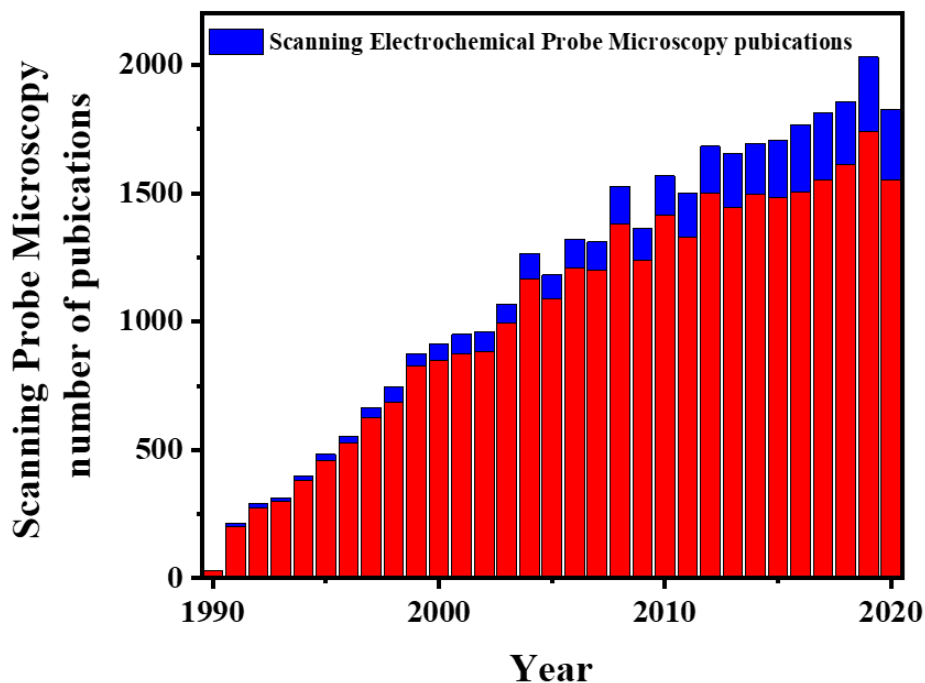


Figure 1.1 Yearly number of Scanning Probe Microscopy publications from 1990 to 2020. Source: *webofscience.com*. 06/20/23. Criteria search: “Scanning Probe Microscopy” and “Scanning Electrochemical Probe Microscopy”

1.1.1. Electrochemical scanning tunneling microscopy (EC-STM)

To study samples in more realistic environments, as well as following redox processes on surfaces, an adaptation of STM was developed: EC-STM [8]. The technique, with atomic-scale resolution, results in a helpful way to study surface structure and reactivity by electrochemistry.

For EC-STM, a 4-electrode configuration is used (**Figure 1.2A**), including a Tip (WE1) and a sample (WE2) immersed in an electrolyte solution, along with a reference (RE) and a counter (CE) electrode. In this configuration, sample and tip potentials can be set independently. Also, electrochemical reactions can be carried out on the tip or the sample. EC-STM, as STM, uses tunneling current to scan the surface. Therefore, electrochemical currents must be reduced as much as possible. For this, the tip is coated with non-conductive material leaving only its sharp

end exposed. So, faradic currents are minimized concerning the tunneling current.

Sample mapping can be carried out by adjusting the tip position in the vertical direction to reach the same set point value, or keeping the vertical distance constant and recording tunneling current. The former reduces the acquisition time, but the tip could be at risk if the sample has a high roughness.

Examples of EC-STM applications go from fundamental studies of metal single-crystal surfaces [9], ordered adsorption of anions [10] and organic molecules [11,12], initial stages of metal deposition [13], up to applications in electrocatalysis [14,15], passivation [16], and corrosion [17] of surfaces.

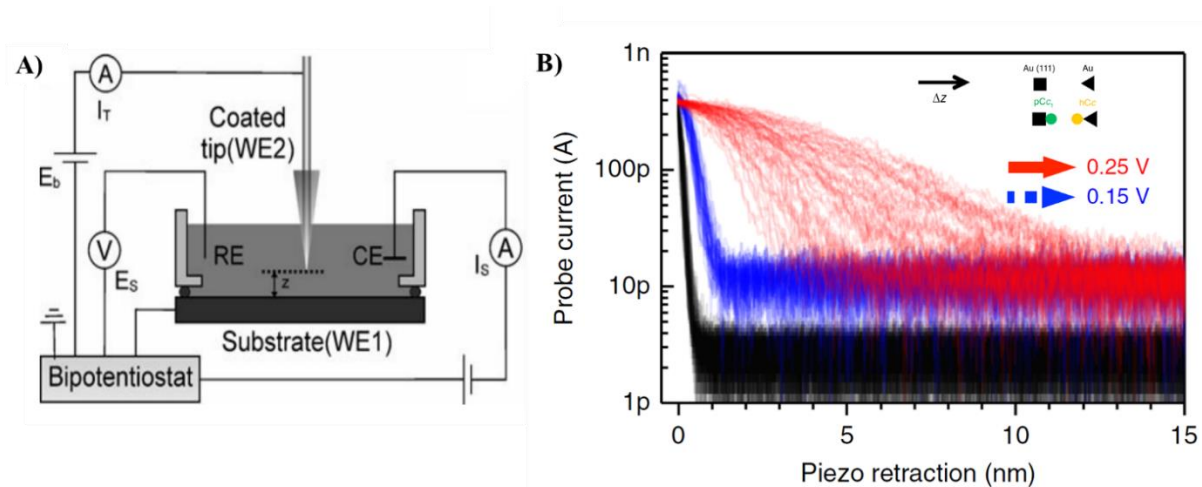


Figure 1.2 EC-STM scheme [18] (A). Electrochemical gating of long-distance electron transfer between pCc1 and hCyt c. I - z plots at 200 mV constant bias for pCc1–hCyt c at UP = 0.45 V and US = 0.25 V (red), and at UP = 0.35 V and US = 0.15 V for pCc1–hCyt c (blue) and for bare gold (black). Red curves ($\beta = 0.5 \pm 0.3 \text{ nm}^{-1}$) show long-distance ET beyond 10 nm (B) [19].

Let's discuss one example from the bioelectrochemistry field. Electron transfer (ET) studies in proteins have mostly focused on intramolecular transfer because of its relative simplicity.

Gorostiza *et al.* used EC-STM to study the electron transfer rate between redox partner proteins [19]. They studied the ET process between cytochrome c (Cyt c) and the mitochondrial complex III (CIII), or cytochrome bc1, a representative step of the mitochondrial respiratory

chain. The interaction can be conveniently studied using (mutant) human cytochrome c (hCyt c) and the soluble domain of plant cytochrome Cyt c1 (pCyt c1). Redox partner proteins were studied under physiological conditions using EC-STM. Also, near biological membrane potentials were explored. The latter experiments were performed at different probe and sample potentials that keep a constant moderate bias of 200 mV (**Figure 1.2B**). In this case, ET was observed for a more than 10 nm distance between the coated hCyt c-tip and pCyt c1-sample. In general, it is presumed that the studied redox partner proteins needed to be in contact for the ET process. Further simulation studies, showed that water solvation layer helps to shield the ET process.

1.1.2. Scanning electrochemical microscopy (SECM)

Bard *et al.* reported SECM in 1989 [20], arguably one of the most popular SEPM techniques. In essence, the setup is similar to the one used in EC-STM, but in this case, the STM sharp tip is replaced by an ultra-micro electrode (UME). Sample and UME are immersed in an electrolyte solution and with them RE and CE (**Figure 1.3**). UME is used to record the current in the vicinity of the sample, imaging sample surface electrochemical properties. SECM's principal advantage over EC-STM resides in the use of UMEs. They can be easily fabricated from a few nm up to μm size, depending on the desired resolution and application. The fabrication process is, normally, carried out by pulling a glass capillary with a conductive material wire (or etched wire) placed inside. Then the tip is polished, and the wire is exposed, resulting in a micro-disk electrode sealed by glass. The ratio between electrode radius (a) and UME total radius, is known as R_g . In SECM, the UME is approached to the sample by current feedback. UME current is perturbed by the substrate proximity by blockage of the diffusion of solution species to the tip (negative feedback) and by regeneration of the redox species at the

substrate (positive feedback).

SECM has been extensively used to study surface processes [21], such as local charge transfer kinetics [22], species adsorption [23] or self-healing mechanism of polymer coating [24], imaging of living cells [25], studying biological systems [26] and, even, oxygen evolution on leaf surfaces [27]. Performing localized surface modifications like electrodeposition [28,29] and etching [30] is also possible.

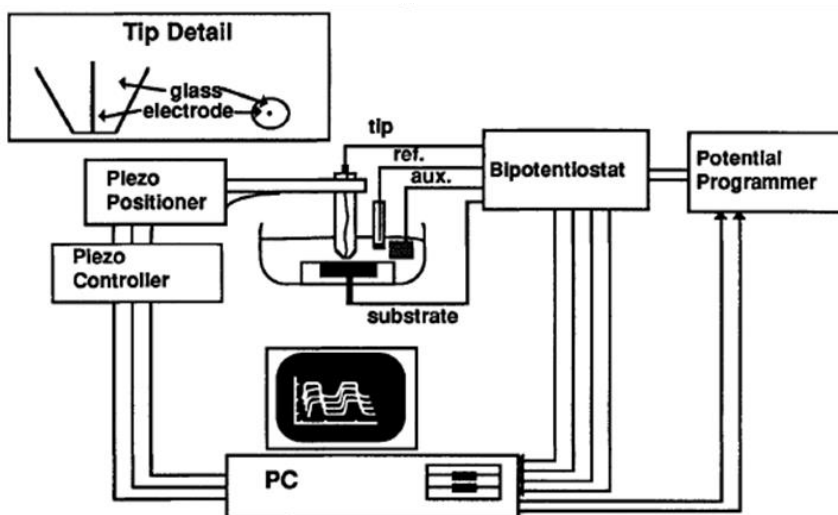
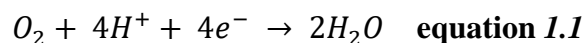


Figure 1.3 Scanning Electrochemical Microscopy setup scheme [31]

Terryn *et al.* include SECM in the analysis of their self-healing polymers, with possible application in corrosion protection [24]. The coating is based on the dual effect of corrosion inhibitor benzotriazole (BTA) and an epoxy-based shape memory polymer (SMP). Healing process is carried out by thermal treatment. Scratched polymer was evaluated with SGECM before and several days after the self-healing process. Sample was immersed in electrolyte solution (3.5 wt.% NaCl) and SECM was used for monitoring the oxygen reduction reaction (ORR) over the scratch. Hydrogen is a common by-product of corrosion processes and can be followed by the ORR according to **equation 1.1**



A four-electrode system was used for the SECM measurements, with a coated panel as the working electrode, scanning the scratched region with a 10 μm diameter Pt electrode at a tip potential of 0.75 V (vs. the SCE). As the damaged area decreased, the sample recovered its protection, and the current decayed. The scratch was monitored for 3 days to ensure the corrosion protection properties of the polymer (**Figure 1.4**). Although SECM is not the main protagonist of this work, its power as a tool to determine the self-healing anti-corrosion properties is clearly demonstrated.

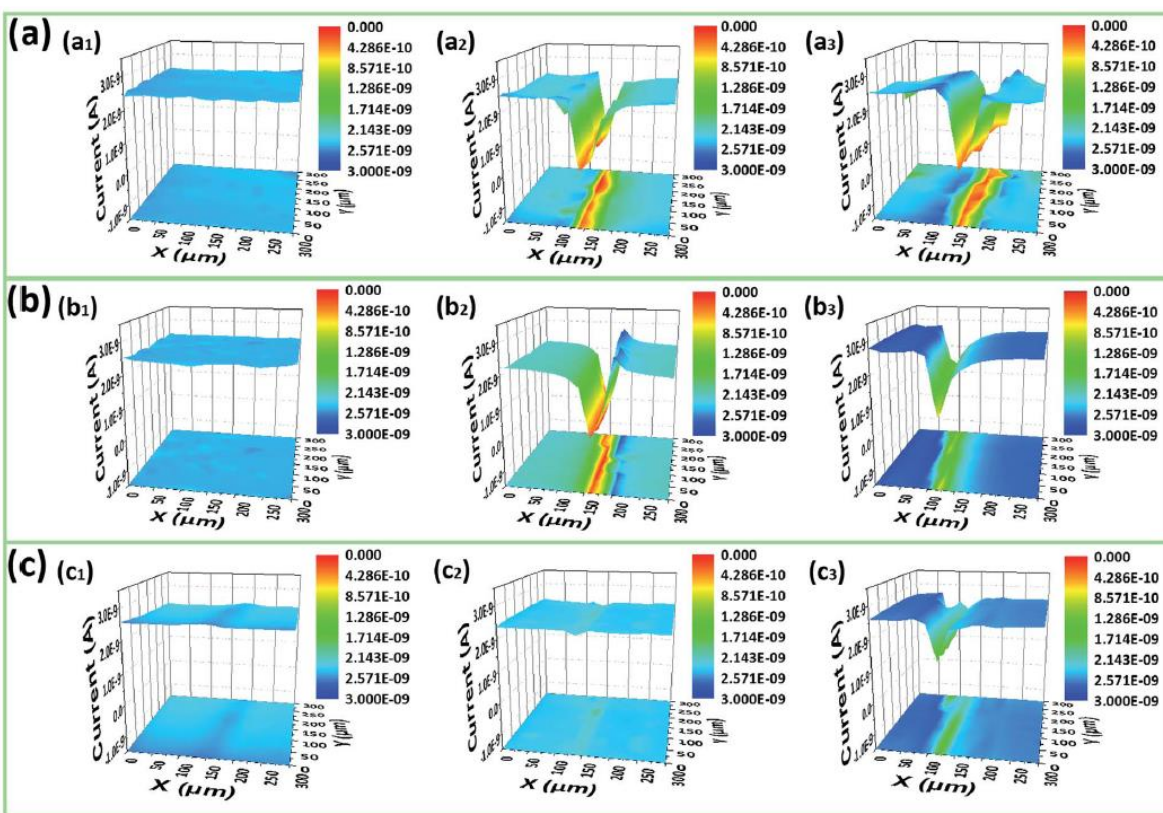


Figure 1.4 SECM maps of the original BTA-free coating surfaces(a1) and the scratched BTA-free coating surfaces immersed in a 3.5 wt.% NaCl solution for 1 day (a2) and 3 days (a3). SECM maps of the original BTA-5% coating surfaces (b1) and the scratched BTA-5% coating surfaces immersed in a 3.5 wt.% NaCl solution for 1 day (b2) and 3 days (b3). SECM maps of the healed BTA-5% coating surfaces immersed in a 3.5% NaCl solution for 0 days (c1), 1 day (c2) and 3 days (c3) [24].

1.1.3. Scanning ion conductance microscopy (SICM)

Hansma *et al.* introduced SICM in 1989, as a high-resolution and noncontact imaging SEPM technique [32]. Here, pulled microcapillaries with nanometer scale openings (nanopipette) filled with an electrolyte solution are used as probes. The technique relies on the flow of ionic current between an electrode inside the nanopipette and a second electrode immersed in the bulk solution. Normally, a DC or AC voltage is applied between the two electrodes, both usually Ag/AgCl quasi-reference electrodes (QRE). Current is caused by the ionic flux through the nanopipette opening. When the probe is close to the surface, the flow of ionic species is restricted (**Figure 1.5**), providing a feedback signal for accurately mapping the sample topography without physical contact. Therefore, the ionic current decreases due to the physical flow restriction. Pulled microcapillaries can be reproducibly fabricated with nanometer-sized openings at the tip, giving SICM a truly high resolution. Besides topography measurements [33], SCIM is also widely used to map activities of soft organic samples [34,35] thanks to its good operability when working with non-conductive samples.

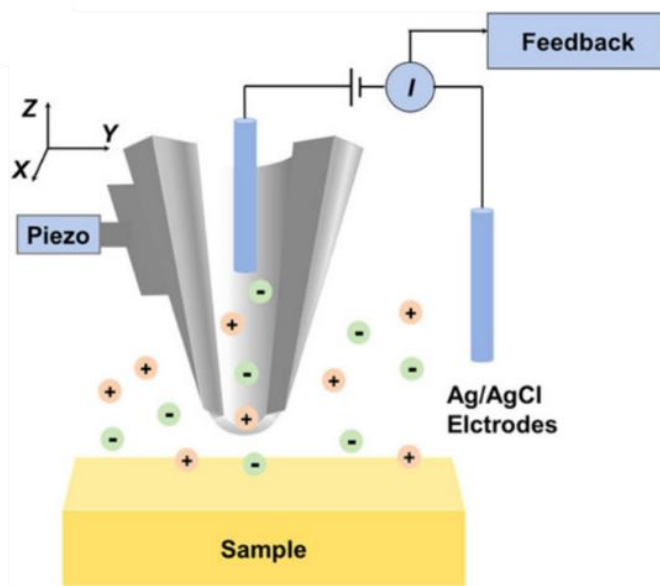


Figure 1.5 Scheme of the scanning ion conductance microscopy (SICM) [36].

Beyond topography, the SICM probe was also extended to perform electrochemical measurements. Using a double-barrel nanopipette, Unwin *et al.* were able to measure sample topography and pH simultaneously [37]. To build the pH-SICM probe one of the barrels was sealed (SICM barrel) while the other was coated with carbon in its interior (Figure 1.6A to C). The carbon layer is connected to a copper wire and used to obtain a hydrated iridium oxide film by electrodeposition (pH electrode barrel). Iridium oxide potentiometric electrodes are known to exhibit a super-Nernstian pH response. This has been attributed to a rather complex redox process governing the potentiometric response (equation 1.2)

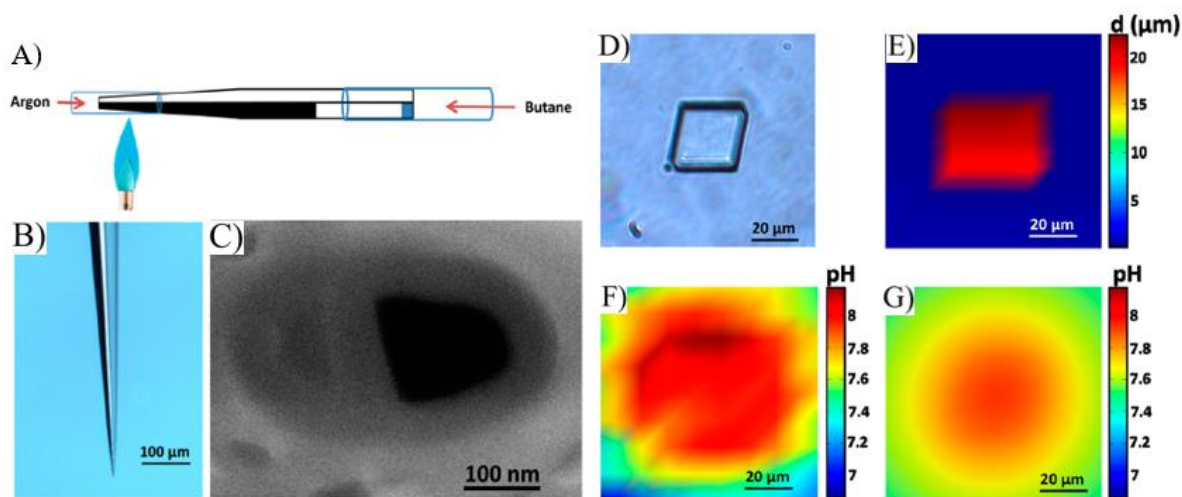
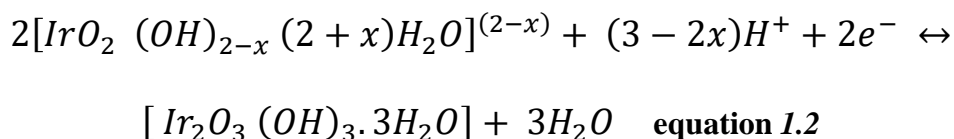


Figure 1.6 Scheme of the carbon deposition step for the fabrication of pH-SICM (A). Optical micrograph (side view) of a typical nanoscale pH-SICM probe after carbon deposition in the left barrel (B). SEM micrograph (end view) of the tip of a typical nanoscale SICM-pH probe before electrodeposition of iridium oxide (C). Optical micrograph of the calcite microcrystal (D). SICM topography image of calcite microcrystal (E). pH map close to (100 nm from) the calcite microcrystal and glass surface recorded simultaneously with topography (bulk pH 6.85) (F). FEM model of the pH distribution close to (100 nm from) the calcite microcrystal and supporting glass substrate for a dissolution flux of $1.6 \times 10^{-9} \text{ mol cm}^{-2} \text{ s}^{-1}$ (G) [37].

Dissolution of calcite is strongly pH-dependent, and this process increases the local pH at the calcite–water interface. After pH calibration, a pH-SICM probe was used for mapping an entire calcite microcrystal during dissolution. **Figure 1.6E** shows the topography recorded by the SICM barrel and **Figure 1.6F** pH values 100 nm away from the surface in the perpendicular direction. The first is compared to a SEM image (**Figure 1.6D**) and the latter to the results of pH values obtained by the use of finite element method (FEM) modeling (**Figure 1.6G**). Under dissolution conditions, a *ca.*13% pH increment (compared to bulk solution) near the microcrystal was observed. Through the comparison with SEM images and data obtained from the FEM model, is clear the ability of pH-SICM probes to generate spatially resolved pH maps of surfaces and interfaces.

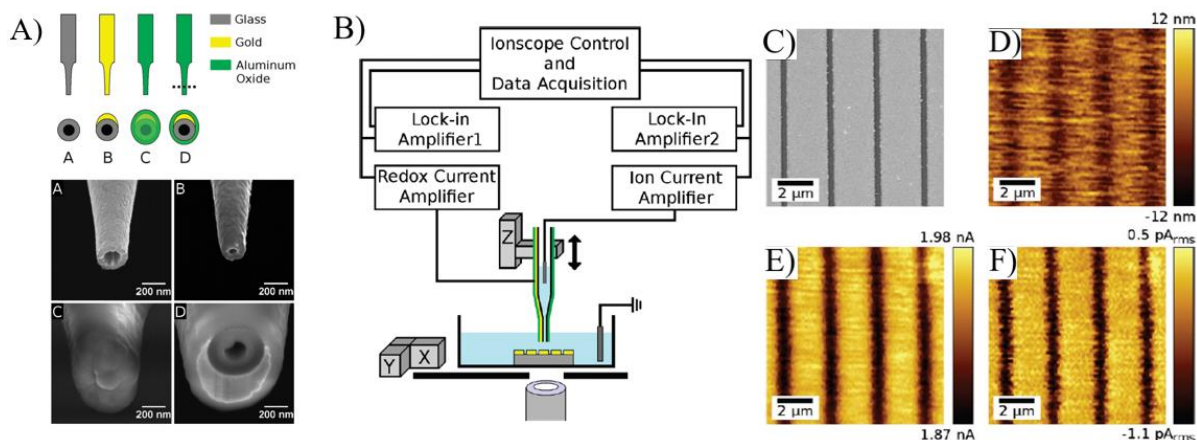


Figure 1.7 Schematic and SEM of integrated SECM-SICM nanopipette throughout the fabrication process: as pulled borosilicate nanopipette, (AA), after evaporation of the Au electrode film with titanium adhesion layer (AB), after ALD of 100 nm thick Al_2O_3 with occluded nanopipette tip (AC), and after FIB milling to expose the gold and open the nanopipette tip (AD). Schematic of the SECM-SICM imaging instrumentation (B). SEM and feedback-mode SECM-SICM images of 400 nm wide trenches FIB-milled into a gold film on a glass substrate; SECM-SICM images were acquired in 10 mM $\text{Ru}(\text{NH}_3)_6\text{Cl}_3$, 100 mM KNO_3 solution: SEM (C), SECM-SICM topography (D), SECM-SICM DC redox current (E), and SECM-SICM ac redox current (F) [38].

Successful SECM mapping requires a very high control of tip-sample distance, normally at a few times the electrode radius. Distance control is one of the major advantages of SICM, but

on the other hand, it misses a method to evaluate electrochemical sample surface properties. Hersam *et al* [38] introduced SECM-SICM aiming to combine both technique advantages. SECM-SICM probe (**Figure 1.7A**) is built by coating a nanopipette with Au. Then, an insulating layer of Al₂O₃ is added, giving a total diameter of 500 nm. Lastly, the tip probe is milled using Focused Ion Beam, and the Au film is exposed as an UME. SECM-SICM setup scheme is presented in **Figure 1.7B**. A gold-on-glass substrate, where 400 nm wide tranches were removed, served as sample. **Figure 1.7C** shows the results obtained using current (AC and DC) feedback. Even if the probe diameter is bigger than the tranches, they are still detected in the topography image, allowing the correlation between the current information with the topography.

1.1.4. Scanning electrochemical cell microscopy (SECCM).

SECCM uses, as probe, a pulled glass capillary filled with an electrolyte solution and a small opening at its end. Introduced by Unwin *et al.* in 2009 [39], this technique is capable of imaging surfaces with a lateral resolution in the nanometer range. The electrolyte is confined inside the capillary, while only a drop is exposed in the opening at the end. When a single capillary is used (**Figure 1.8A**), an electrode is placed inside acting as quasi-reference and counter electrode. It is more elegant to use double or multiple barrel capillaries (**Figure 1.8B**), where a true reference electrode can be implemented. The sample is placed in ambient conditions during SECCM scanning. The probe approach is made by applying a voltage between the conductive or semi-conductive sample and the probe. When the droplet gets in contact a non-faradic current is produced, this current being used as a feedback signal to stop the probe. The pulled capillary never touches the surface and the electrolyte solution droplet is confined in the area between the capillary and the sample (localizing the electrolyte).

As in previous methods, mapping can be carried out by keeping a constant capillary-sample distance by adjusting the magnitude of the ion current signal with the SECCM tip position, or in a hopping scanning mode where the tip is withdrawn far away from the surface and re-approached at each sampling point.

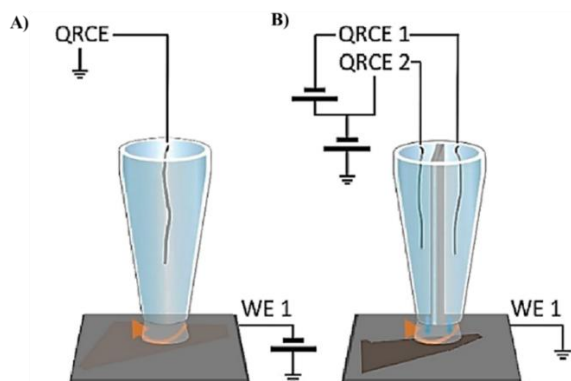


Figure 1.8 SECCM scheme (A) single and (B) double barrel [40].

So far, SECCM has been used for studying grain boundaries [41], 2D nanomaterials[42–46], surface inhomogeneities [47–50], thin films [51–54] and electrochemical behavior of single entities[55–63], as well as locally deposited catalyst particles [64]. It can be even combined with EBSD [65] and IRM [66] to expand the applications of the technique.

An interesting variation of SECCM was presented in 2020, for example, the oil-immersed SECCM (OI-SECCM) [67]. Here, the droplet is immersed under a thin layer of hydrophobic and inert oil that covers the substrate surface, thus preventing the droplet from evaporation and spreading, and increasing the droplet's stability. Using OI-SECCM, recently, the group of Mauzeroll explored the effects of grain orientations on cathodic and anodic corrosion processes and pitting of a polycrystalline Al alloy sample [68]. The setup consisted of a micropipette connected (by a tube) to a more open syringe, where RE and CE were immersed in the electrolyte solution. Micropipette was approached to the sample (WE) under the mineral oil applying a constant potential. Once the droplet made contact with the sample, the circuit was

closed. A current spike was detected, stopping the probe. After OCP stabilization, PDP measurements (from -1.35 to -0.3 V at 100 mV/s) were performed. Surface mapping was performed in hopping mode with a separation of 5 μm between locations. From PDP curves, cathodic and anodic currents, as well as pitting potentials, were extracted to be analyzed in function of the grain orientation. Although cathodic currents exhibited a strong grain orientation dependence (where larger currents were found in grain boundary regions, proving the enhanced cathodic reactions at grain boundaries), anodic currents and pitting did not show clear grain dependence (likely because anodic corrosion processes are more dependent on the properties of the oxide film). This work highlights the powerful capability of OI-SECCM in identifying microstructure-induced differences in corrosion processes and will facilitate the electrochemical study of grains of polycrystalline samples.

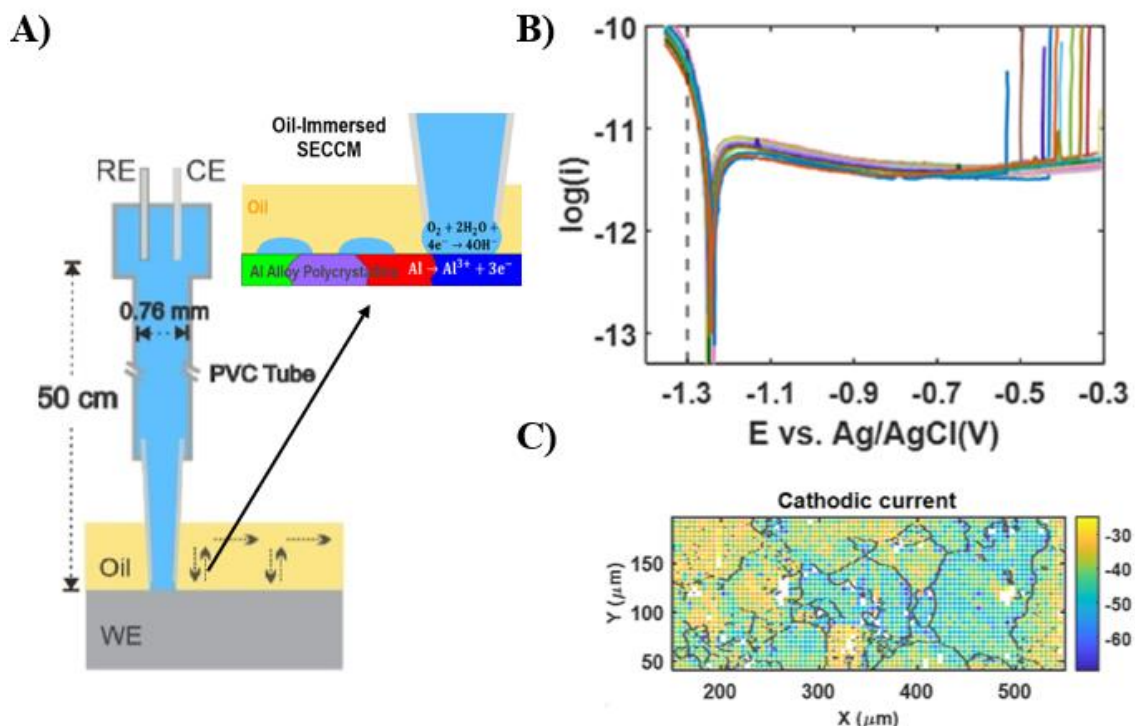


Figure 1.9 Schematic of the OI-SECCM setup (A). 26 PDP curves (randomly selected) from the 2511 locations on OI-SECCM maps (B). Cathodic current map superimposed on the grain boundary map, in which the cathodic currents were extracted from PDP curves at -1.3 V vs Ag/AgCl QRE (C) [68]

1.1.5. SEPM, notes and brief comparison

As it was shown in previous sections, the SECM field has had constant growth for the past 30 years. Aiming always to overcome new challenges, EC-STM is an incredible technique likely to perform studies at the atomic level. Although EC-STM has a very high resolution, the tunneling current is highly sensible to faradic processes interfering in the measurements. A very sharp tip is necessary to map the surface, having a big probability of contamination or deformation. SECCM uses an UME as probe to address some EC-STM drawbacks. By measuring faradic currents, SECCM is useful to quantitatively detect reaction products and to study reaction kinetics or to map surface reactivity. Its resolution depends on the electrode diameter. SICM is a technique based on the use of nanopipettes as probes, ensuring the resolution of the technique. The aforementioned SECM and SICM share a common condition, the sample must remain immersed in the electrolyte for the whole experiment. This can take several minutes, possibly affecting surface initial conditions. SECCM avoids localizing the electrolyte in the probe. To achieve this, a common strategy is to use micro or nano-capillary for containing the electrolyte. The capillary, with a droplet hanging at its opening, is approached to the sample surface. When the droplet touches the sample, a local electrochemical interface is formed and electrochemical measurements can be carried out. After probe retraction, a portion of the electrolyte remains in the measured point. As an effort to overcome electrolyte remains, scanning gel electrochemical microscopy (SGECM) was proposed. SGECM will be discussed in the next section.

1.2. Scanning gel electrochemical microscopy (SGECM)

In line with EC-STM, SECM and SECCM, and to expand possible applications of the SEPM, Scanning Gel Electrochemical Microscopy (SGECM) was proposed [69]. A gel-coated

electrode (gel probe) is used to approach the sample surface. The gel probe localized both the electrode and the electrolyte. So, the sample is placed in air. Once the gel probe enters in contact with the sample surface, its local electrochemical properties can be measured. The soft nature of gel contact allows, also, to work on irregularly shaped surfaces. Confining the electrolyte in a gel form also prevents its leakage over the sample, a subject that is explored in more detail in **Chapter III** of this work.

Due to their similarities, a comparison between SECCM and SGECM is inevitable. Both techniques aim to localize the electrolyte at the probe's tip. In SECCM, the electrolyte droplet, used to contact the sample, hangs from the opening at the end of the pulled glass micropipette. So, for samples with high roughness or tilt compared to droplet height, micropipette walls could pose a risk for the sample. On the other hand, SGECM uses a gel probe with the tip entirely coated, making the probability of the sample entering into contact with a non-coated zone of the probe negligible. SECCM faces major challenges in meniscus control and electrolyte wetting [70,71]. These challenges become difficult to overcome when dealing with complex-surfaced samples such as porous materials. The electrolyte solution can percolate through the pores, changing the contact area with the sample. In contrast, SGECM offers better control of the physical interaction between the electrolyte and the sample by confining the electrolyte in gel form. Presenting a clear advantage over SECCM in the analysis of complex surfaces.

1.2.1. Gel probes fabrication

As in previous work [72], chitosan was chosen to build gel probes for SGECM because of its many advantages. Chitosan is a natural, biocompatible, biodegradable, low-toxicity polymer. Chitosan Hydrogel can be obtained by Electrodeposition, further discussed in Chapter II,

which is the preferred method to fabricate gel probes. On the other hand, SGECM is a growing technique. So, chitosan offers flexibility to work with different systems. For example, exploring biological systems either (1) confined in the gel and analyzing their response to the surface sample or (2) in the sample while the gel is soaked in a redox probe or mediator solution.

Two kinds of gel probes were developed, until now, for SGECM: micro-disk gel probe and “electrodeposition + pulling” gel probe. Variations of these probes can be obtained by changing the electrode material or by using a different polymer to coat the electrode surface, but preparation is, in essence, the same. Their preparation is described hereafter.

Micro-disk gel probe (named type I gel probe) is fabricated by coating micro-disk electrodes with hydrogel. Electrodes are prepared by sealing Pt wire (25 μm diameter usually) in glass capillaries using epoxy resin, targeting an R_g (diameter ratio of the insulating shield to the Pt wire) of 2. These electrodes are used to perform polymer electrodeposition, considering as good gel coating the semispherical geometries of a radius not bigger than the total electrode radius (**Figure 1.10**). Other coating methods exist, and electrodeposition is the one that allows good control of the gel shape. Nevertheless, any method requires close control to avoid difficulties. For example, if R_g is bigger than 3, obtaining a round gel shape by electrodeposition can be difficult. Gel electrodeposition to build micro-disk gel probes is further explored in **Chapter II**.

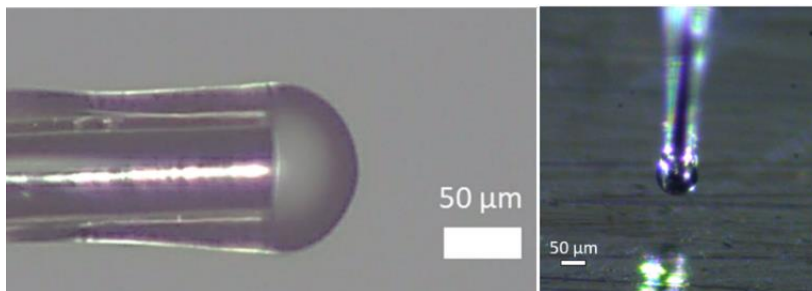


Figure 1.10 Chitosan gel probe obtained using a Pt micro-disk electrode.

After electrodeposition, the probe can be used as it is, or soaked in various electrolytes according to the need. The gel could also be removed by mechanical polishing after experiments and the Pt micro-disk electrode could be regenerated for electrodeposition again. As was mentioned before, SGECM resolution is limited by gel probe size. That makes the micro-disk gel probe reliable, easy to fabricate and versatile, but with less resolution than the probes used in the other techniques mentioned in this chapter.

The **electrodeposition + pulling gel probe**, also named Type II gel probe, is fabricated by pulling the electrode out of the precursor solution while performing the electrodeposition. Very sharpened metal wires (W, Pt, Ag or Au) are used as electrodes. To shape the gel, the method takes advantage of the formation of a precursor solution thin meniscus. The meniscus is a transient state, and therefore its shape needs additional physical or chemical processes to be kept. In most cases, carrying precursor electrodeposition out (jellifying the meniscus) and slowly pulling the electrode out (giving time for partial local solvent evaporation) result in a stable and continuous meniscus formation. Three steps are involved in the preparation of gel probes by electrodeposition + pulling (**Figure 1.11**). (1) Approaching: the electrode is approached toward the precursor solution at V_a speed applying a potential E_a . The electrode is stopped using current feedback. After reaching the surface, the electrode is slightly pulled out to ensure the meniscus creation. (2) Holding: a potential E_h is applied for a time t_h to jellify the first precursor layer over the electrode. This step must be closely controlled to avoid gel overgrowth and ensure a good attachment of the electrodeposited gel onto the surface. (3) Pulling: the electrode is pulled out from the solution while applying a potential E_w at a V_{w1} speed during a time t_{w1} . After t_{w1} speed can be switched to V_{w2} to control the final gel length.

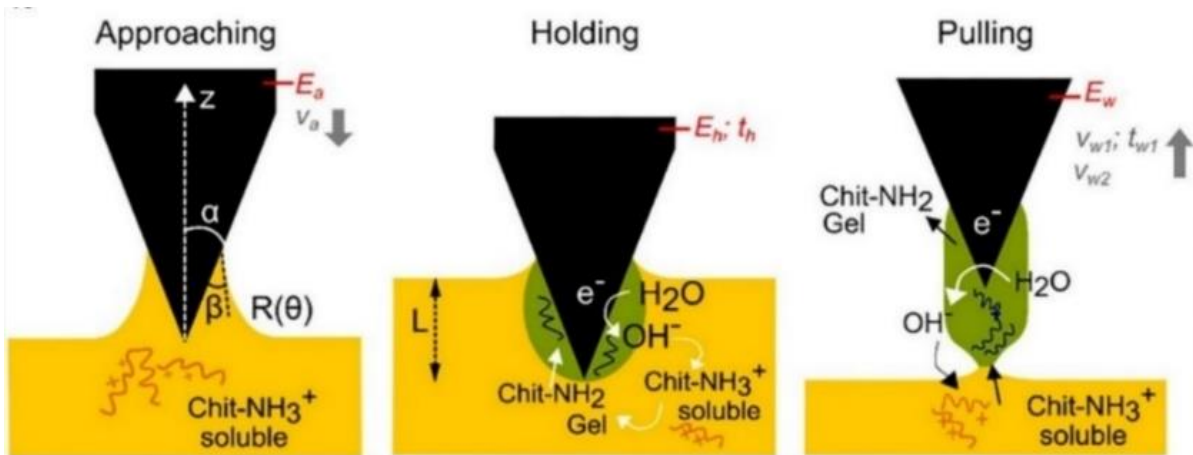


Figure 1.11 Scheme of the fabrication of sharpened hydrogel by “electrodeposition + pulling” [73].

To successfully obtain a gel probe by “electrodeposition + pulling” is necessary to match the kinetics of electrodeposition with the dynamics of meniscus evolution. Precursor gelation affects meniscus shape and vice versa. This dynamic process forces us to tune the deposition parameters integrally for every system. **Figure 1.12** shows how the values of some parameters impact the gel formation.

Gel probes prepared by “electrodeposition + pulling” offer a reliable lateral resolution of $<10 \mu\text{m}$, up to *ca.* $1\text{--}2 \mu\text{m}$. Also, the resolution is tuneable by pressing or stretching the gel probe against the surface. The contact area remains unchanged when the sample is tilted up to 45° . Finally, it is important to highlight that “electrodeposition + pulling” gel probes are prepared by a fully automated process.

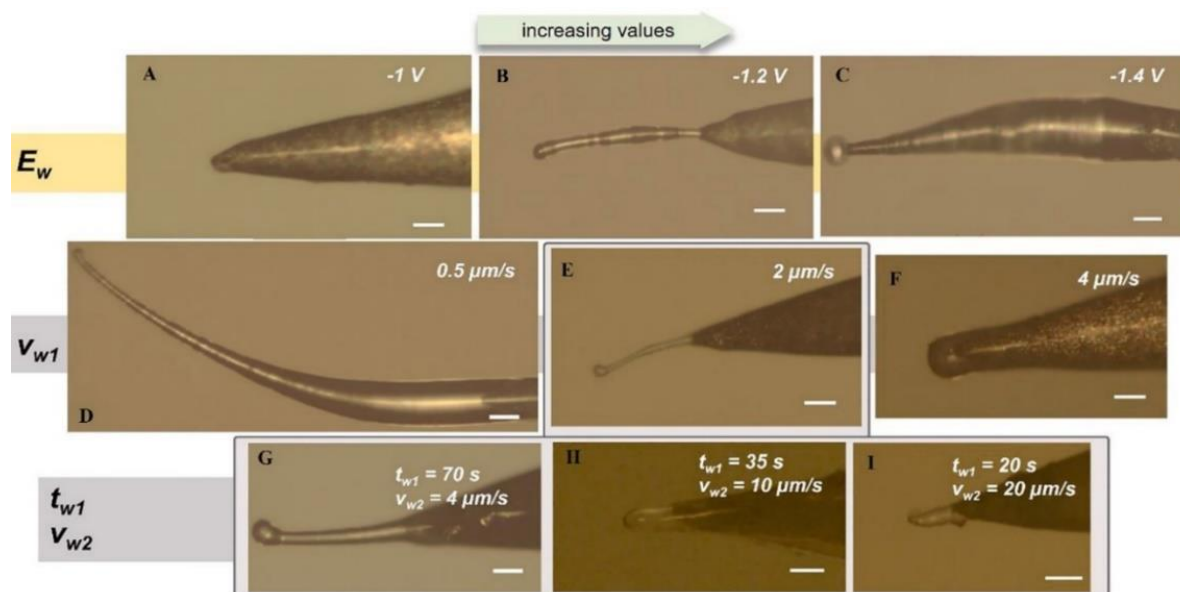


Figure 1.12 Influence of “Electrodeposition + Pulling” parameters during the pulling step using a 250 μm electroetched Pt wire. Conditions of deposition: $E_a = -0.7\text{ V}$; $L = 20\ \mu\text{m}$; $E_h = -1.2\text{ V}$; $t_h = 5\text{ s}$. Scale bars: 25 μm [73].

1.2.2. SGECM set-up

For this work, a homemade SGECM setup was used (**Figure 1.13**). A software developed in our group controls the z motor probe position as well as the x and y positions of the sample. A piezo is used to accurately control the probe-sample distance. Normally, the probe approach is carried out in two steps. First, z motor moves toward the sample, stopping once the surface is reached. Then, the piezo is used to precisely control the probe z position. While scanning, piezo is normally used to control probe-sample distance, and x and y motor to move the sample in the plane perpendicular to the gel probe.

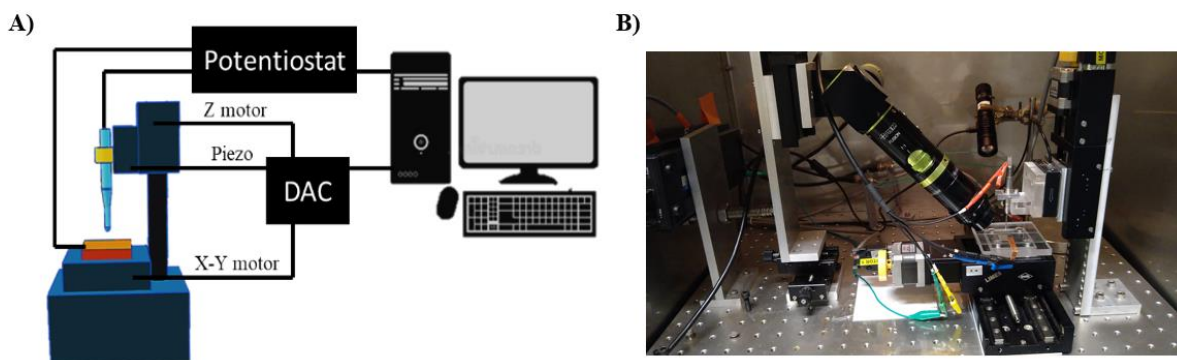


Figure 1.13 Scheme of Scanning Electrochemical Microscopy setup (A). Picture of the SGECM setup used in the current work (B).

The gel probe can be approached by two methods: shear force and current feedback. For the first one, two piezoelectric plates connected with a lock-in amplifier are mechanically attached to the probe using a custom-design homemade holder. While an AC excitation is applied to one plate, the second is used to record the amplitude and phase of the tip oscillation [74]. As the electrode reaches the sample surface, the second plate signal is altered and the approach is stopped. The signals are frequency-dependent in the hundreds of kHz range, and usually, the frequency that offers the highest signal-to-noise ratio is selected for approaching the probe. The second approach method is by current feedback. A voltage is constantly applied while the gel probe approaches. Before the gel probe touches the sample, the WE is disconnected, thus the measured current is zero (in practice with noise and eventually also offset). Once the probe touches the sample, the electrical circuit is closed and current starts flowing. Depending on the gel content (ions and electroactive species) the current response will be composed of (1) non-faradic and (2) faradic processes. The former corresponds to the charging of double-layer at gel/sample and gel/probe interfaces upon contact. This is usually described as capacitors and can be expressed by **equation 1.3** if ignoring the charge transfer reaction at the electrode surface.

$$i = \frac{E_{app}}{R_s} e^{-t/R_s C_d} \quad \text{equation 1.3.}$$

where E_{app} is the applied potential, R_s is the electrolyte resistance and C_{dl} is the total (series) capacitance of the gel/sample and gel/probe interfaces.

When the gel is soaked in redox active species, Faradic processes may occur at the electrode interfaces. Faradic current can be obtained from the Butler Volmer formulation (**equation 1.4**) and the concentration of the redox species at the electrode surface can be obtained from Fick's law (**equation 1.5**) considering only diffusion for mass transfer of species.

$$i = nFAk^0 [C_{Red}^s e^{\frac{(1-\alpha)zF}{RT}\eta} - C_{Ox}^s e^{\frac{-\alpha zF}{RT}\eta}] \quad \text{equation 1.4}$$

$$\frac{\partial C}{\partial t} = -D \nabla C \dots \text{equation 1.5}$$

where i is the current, C the concentration, C_{Red}^s the concentration of the reduced species at the electrode surface, C_{Ox}^s the concentration of the oxidized species at the electrode surface, t the time, α is the charge transfer coefficient, z the number of exchanged electrons, T the temperature, F the Faraday's constant, R the universal gas constant and η the overpotential.

Solving these equations presents a particular challenge in SGECM. Diffusion plays an important role in the faradic current response of the system, thus the distance between the sample and the microdisk-electrode in the gel probe as well as the physical boundary of the gel shall be considered. This requires the mechanical properties of the gel to treat its deformation. Also, to calculate the current, the potential of each electrode is not that easy to obtain due to the two-electrode system. The potential difference is applied between the two electrodes (sample and probe), but the potential at each electrode will depend on the area and material, as well as the electrochemical potential of the electrolyte. As difficult as it seems, solving the system is not impossible, and it is a work that is currently ongoing.

Despite it only works with conductive samples, current feedback is the preferred method for approaching the gel probe due to its proven accuracy compared to the shear force approach

[75]. A Cu TEM grid glued to a flat Fe plate was used to test both approach methods (**Figure 1.14A**). In all cases, topography was measured using a profilometer and compared to that obtained from current (**Figure 1.14B**) and shear force (**Figure 1.14C**) feedback. Although both approach signals are fairly accurate for determinate sample highs, the lateral resolution is noticeably better using current feedback.

In any case, the final resolution depends on the gel probe diameter and, consequently, the contact area. So, normally, surface mapping is carried out with at least 1 gel probe diameter width separation resolution.

A potentiostat is part of the SGECM setup, recording the current at any time regardless of the gel probe approach method and, of course, performing the electrochemical measurements when desired. Surface mapping is carried out by approach-retract cycles (the gel probe is approached toward the sample, reaches the surfaces, and is retracted immediately or after performing an electrochemical measurement). Current is recorded during the entire cycle and presented as a function of the probe-sample distance (Z displacement). The approach and retract curve, as it was named, is an exceptional tool to study probe-sample interaction. More will be discussed in this chapter later on.

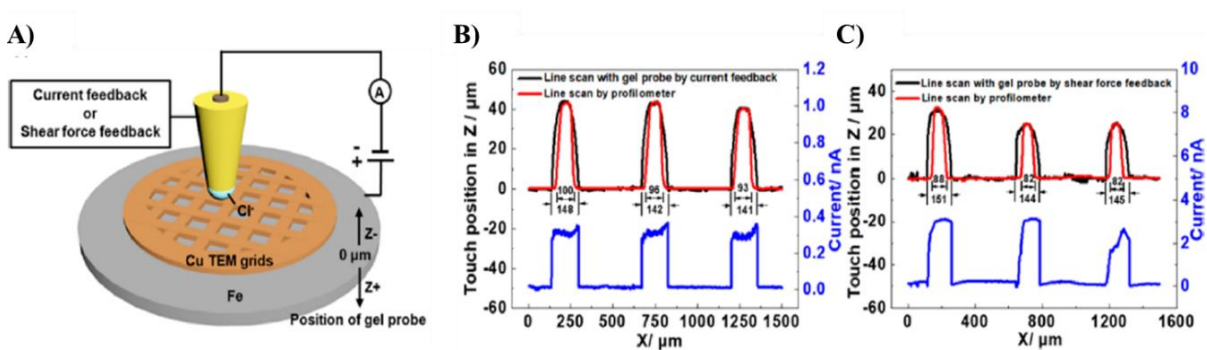


Figure 1.14. Scheme of line scan on Cu TEM grid/Fe plate by current and shear force feedback SGECM (A); line scan of profile and steady state current by current (B) and shear force (C) feedback. The data were recorded at touching position with E_{sample} vs $E_{probe} = 0.5$ V after waiting for 3s [75].

1.2.3. SGECM imaging

SGECM can be used to get information simultaneously on topography and electrochemical properties based on sample images. As an example, **Figure 1.16** depicts the topographical response (**Figure 1.16A**) and current imaging (at a constant potential E) (**Figure 1.16B**) of a sample made of an Al plate intentionally scratched, using a Pt micro-disk gel probe. Similar data on topography (**Figure 1.16C**) and electrochemical potential mapping (**Figure 1.16D**) are depicted for an Al plate with a two Cu strip, using a Ag/AgCl gel probe.

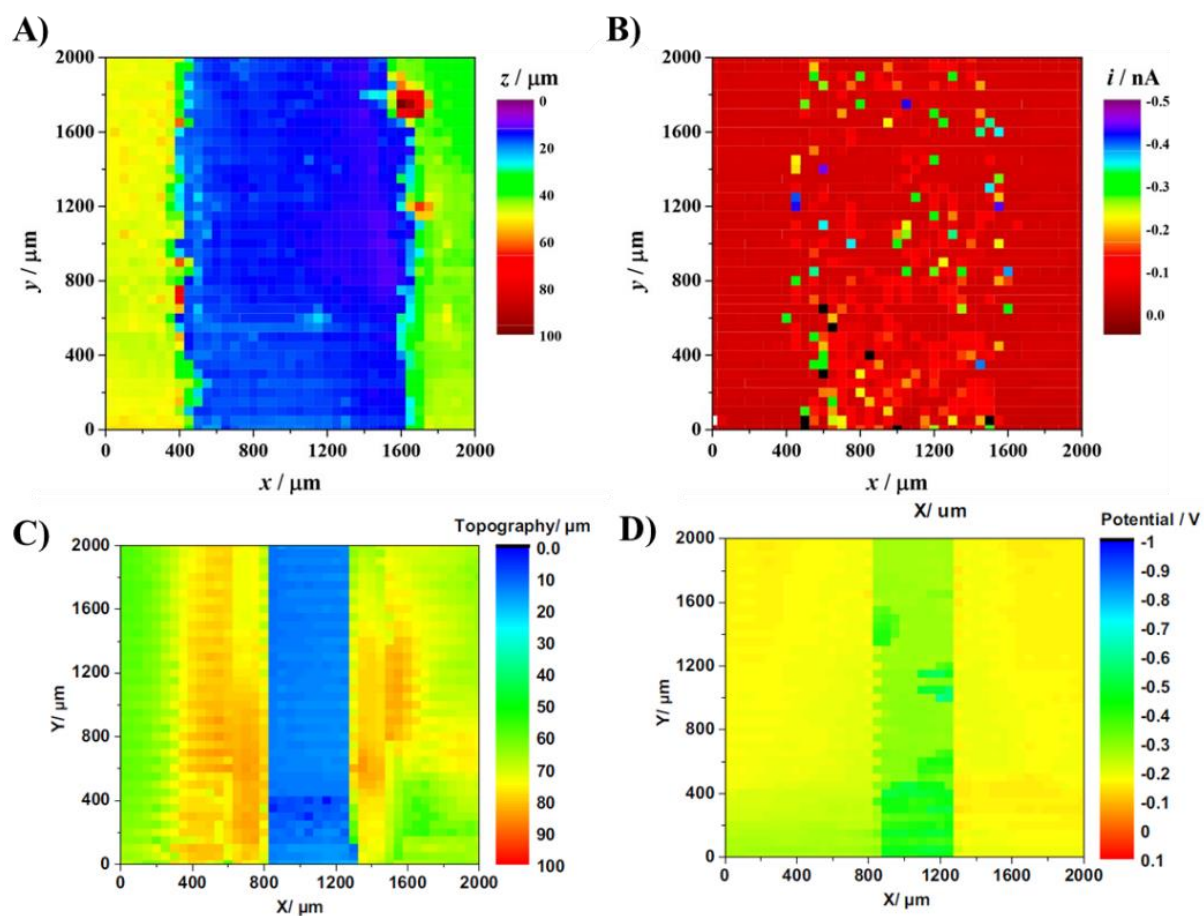


Figure 1.16 SGECM topography (A) and current (B) image of scratched Al plate [69] and Cu tapes on Al substrate topography (C) and potential (D) imaging [76].

Topographical images (**Figure 1.16A** and C) from the studied sample, were achieved with a resolution close to the gel probe diameter ($50 \mu\text{m}$). As it was discussed before, gel probe size

restricts the technique resolution. This applies in general to all SPM techniques. A key factor must be considered to obtain a good reliable image with SGECM, gel stiffness. The soft nature of the gel probe is desired for the application of SGECM, but its deformation must be supervised. Approaching and retracting the gel probe several hundred times from the surface using a gel that can be deformed easily, remains an issue for the reliability of the technique. In principle, the gel probe shall be elastic and not plastic. Besides, it shall well immobilize the electrolyte, avoiding any spreading and remaining on the sample surface.

1.2.4. SGECM patterning and flexible resolution

The gel located on top of the tip probe acts as an electrolyte recipient. As long as the selected electrolyte solution is compatible with the gel used to coat the tip, the probe can be soaked in it and, if needed, re-soaked to refresh the solution in the gel. Such gel probe versatility, in principle, allows us to introduce different chemical species into the gel. For example, a AgCl patterning can be achieved by locally oxidizing Ag while the gel probe contains Cl^- . The gel probe is approached to an Ag plate, by current or shear force feedback, and a voltage is applied to locally oxidize Ag into Ag^+ which reacts with Cl^- to form AgCl. This leaves spots with permanent color change on the sample (**Figure 1.17A**). Due to the soft nature of the gel, the contact area can be tuned by approaching or retracting the gel probe from the surface. In **Figure 1.17B** and **C** are examples of this. Again, a gel probe containing Cl^- is used to locally oxidize an Ag plate. But in this case, after the gel probe contacts the surface, the sample surface in contact with the gel is modified.

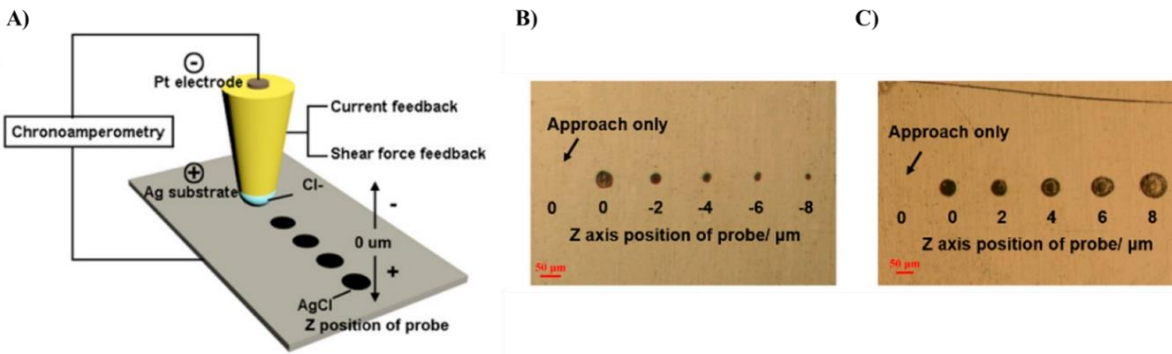


Figure 1.17 Scheme of AgCl deposition using SGECM (A). AgCl depositions on Ag substrate ($E_{\text{sample}} \text{ vs } E_{\text{probe}} = 1.2 \text{ V}$) with the gel probe positioned at negative (B), positive (C) z after touching the sample [75].

When the probe is moved toward (+ z) the surface, gel is compressed. Thus, the contact area is bigger. On the contrary, when the gel probe is retracted from the surface (- z), the contact area is smaller. Contact area diminution using this mechanism is possible, but it may not be stable enough. When the gel is retracted, a balance between surface adhesion and starching forces is responsible for maintaining the gel in contact with the surface. Thus, one must be careful if the chosen method to reduce the contact area is by retracting the probe.

1.3. Gel probe-surface interaction

Interfacial interactions of the gel probe with the sample are a subject of great interest for SGECM application. Mainly, three questions are of interest to study: (1) contact area, (2) gel mechanics (elasticity and adhesion) and (3) possible remains of electrolyte over the sample. Gel-sample contact area has been addressed before, using AgCl electrodeposition to identify it. The second, as it is going to be discussed in the next subsection, can be inferred from the approach and retract curves. The latter is the most challenging to verify using the original SGECM setup [69]. The gel volume in the probe is *ca.* $3,27 \times 10^{-8}$ mL. If we -roughly- consider the density of the gel as 1 g/mL, the total gel mass in the electrode is 32.72 ng. Now, to determine if even a slight portion of this mass is left over the sample, a tool of incredible

precision is needed. With this in mind, Quartz Crystal Microbalance (QCM) is proposed to be coupled with SGECM.

1.3.1. SGECM approach and retract curves

Like in classical SEPM techniques, the first step of the experiment is to bring the probe close or in contact with the sample. This is achieved mostly by measuring the current while moving the probe in the vertical direction (z -axis), although other signals such as optical focus or shear force were also used. In SGECM, approaching the gel probe is also preferred to be carried out by current feedback, if the sample is conductive. Moreover, once the gel probe touches the sample, it can be withdrawn until it detaches, and the current variation can also be measured. These constitute the approach-retract curve, which is highly informative and will be used as a main tool for evaluating gel probes in the later chapters.

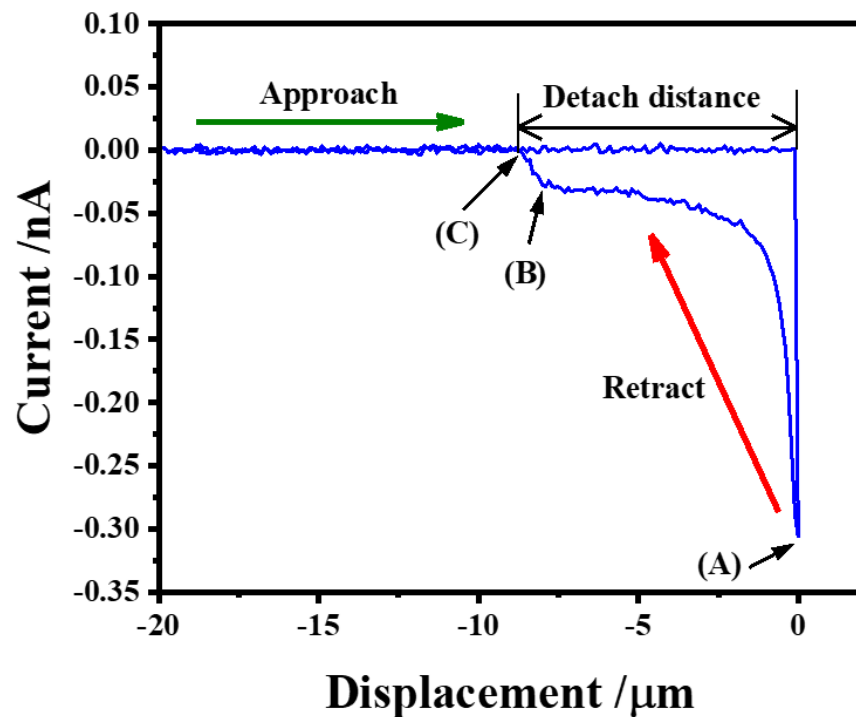


Figure 1.18. Example of approach and retract curve marking most important points.

Experimentally, the approach-retract curve is measured by applying a voltage between the sample and the gel probe. As the gel probe approaches, the current is initially zero (with noise) before the probe touches the sample. When the gel probe reaches the sample, a current spike is recorded. This signal is used to stop the approaching, known as current feedback. The touching position is normalized to $z = 0$. Then, depending on the experiment, the probe can be further pressed, or retracted away from the sample. The retraction is stopped when the current returns to zero (with noise).

The SGECM approach-retract curve not only indicates the positioning of the gel probe referred to the sample, but it is also helpful for studying gel probe-sample interaction. One can identify in the curve the following typical features: (1) Contact point (A). The contact point is clearly marked by a current spike, which reflects the initial current response of the system. It is quickly noticeable in the graphic, a sudden change in the current that indicates a physical gel-sample interaction. (2) Detaching current (A to B). Immediately after contacting the surface, the current drops to a plateau. The current value at the plateau is acceptably stable. Now, this is the hardest zone to interpret. Neither gel shape nor electrode distance are constant. (3) Deadhesion slope (B to C). When the gel-sample adhesion is strong enough to slowly detach the gel from the surface, a change in the current slope can be seen. Here the contact area is physically changing and therefore the current decreases faster. In many cases, this zone is easy to identify, but not always. In cases no adhesion cases, the current drops suddenly. When adhesion forces are high, the current slowly decays to its initial value. In this case, identifying the zone is difficult because one cannot separate it from the detaching current or have security from where the process started. Especially if the general current levels are low. (4) Detaching point (C). It is the distance where the current returns to its original value. The gel probe is

considered fully detached from the surface. Though its full interpretation lacks a strong mathematical theory, some results and interpretations can be extracted from it.

The gel probe is approached and retracted at the same speed of 2 $\mu\text{m/s}$ in this work. Selection of the speed was determined by an empirical process, considering the following factors: (1) risk of probe crashing versus approach-retraction cycle time, (2) detach distance (discussed below) and (3) mechanical properties of the gel. The former impacts mainly during the retraction of the gel probe from the sample. Hydrogels present in general a viscoelastic behavior, so strain does not depend only on the stress but also the time. So, two things enter into conflict at the moment of choosing the speed taking into account the mechanical properties: (1) if the gel is retracted too slowly, on one hand, is advantageous because stress increments are small (avoiding the risk of failure). On the other hand, if it is too slow, we could have a deformation due to the viscoelastic behavior. (2) a high gel probe retract speed, may cause a failure of the material due to the fast stretching of the gel. After all these considerations, we selected a speed where the detach process of all the gel probes tested in this work can be observed and compared while minimizing the risk of gel mechanical failure and probe crashing.

In early works [72], approach and retract curves obtained by shear force were studied. As well as the impact approaching voltage (E_{sample} vs. E_{probe}) in them using current feedback (**Figure 1.19**).

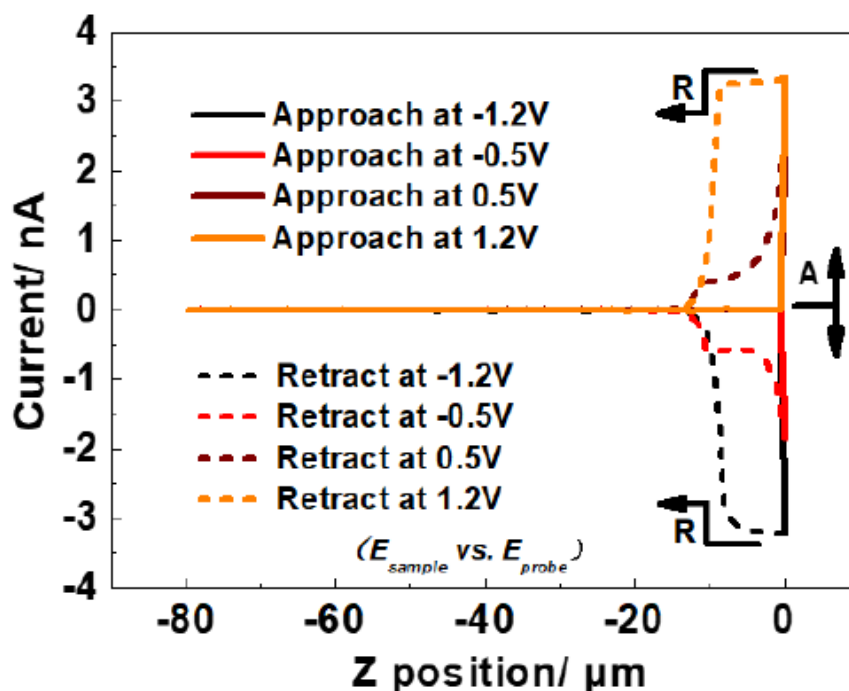


Figure 1.19 Approach and retract curves of current feedback at ± 1.2 V and ± 0.5 V (E_{sample} vs. E_{probe}) [72].

Experiments were carried out using a chitosan gel probe and a Ag plate as sample. In all the voltages (E_{sample} vs. E_{probe}) tested, the current spike can be clearly identified. As the current upon gel probe-sample contact mainly reflects a non-faradic process, the current recorded during the retraction of the probe depends on the applied voltage. These experiments demonstrated that SGECM is suitable to work with a wide range of applied voltages. Moreover, approach and retract curve characteristics (named early) remain despite the voltage applied during the measurement.

In this work, we have relied on the detach distance as a parameter to compare the general behavior of the gel probe. Although it englobes several properties of the gel, evaluating detach distance gives a vision of the kind of mechanical stress is the gel probe under. So, by measuring and following this simple parameter, one can have an overview of the gel modifications' impact on the general gel probe enhancement. But even if this is incredibly helpful information, much

more data is yet to be extracted and understood from the approach and retract curve. Great efforts have been made in this direction, and although a qualitative explanation of the curve can be given, to achieve a quantitative level more analysis is needed.

1.3.2. Quartz crystal microbalance

Crystalline materials with acentric crystallography (no symmetry centers) are known as piezoelectric materials [77]. They have a particular characteristic, when mechanical stress is applied to these materials an electric current is generated as response (piezoelectric effect). Pierre and Jacques Curie demonstrated this effect in 1880 [78] and proved that the inverse effect is also possible. When a voltage is applied to a piezoelectric material, it will deform. If an alternating voltage is applied, then the piezoelectric will mechanically oscillate with the resonance frequency proportional to its mass (**Figure 1.20**) [79,80]. Taking advantage of this proportionality, piezoelectric materials, such as quartz, are widely used to follow mass changes. Quartz crystal microbalance (QCM) has been applied for a long time to determine small masses, thanks to its precision. Sauerbrey *et. al* [81] proposed in 1959 the relation (**equation 1.6**) between the mass variation (Δm) and crystal oscillation frequency change (Δf).

$$\Delta f = - \frac{2f_0^2 \Delta m}{A_0(\mu_q \rho_q)^{1/2}} \quad \text{equation 1.6}$$

Where f_0 is the fundamental frequency, A_0 the area, μ_q the shear modulus of quartz and ρ_q the density of the quartz resonator.

This analysis is limited to thin homogeneous films with a rigidity similar to quartz. Despite these boundary conditions restricting the application of Sauerbrey's equation, QCM applications have spread over the years.

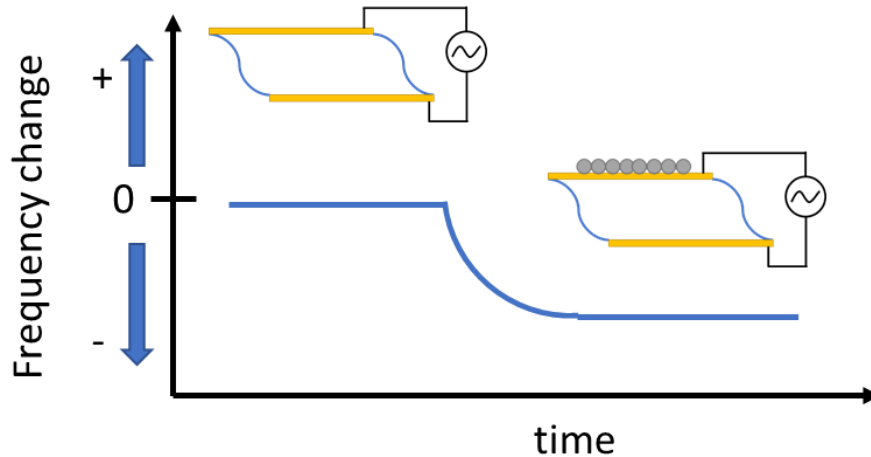


Figure 1.20 Scheme of Au-coated quartz crystal frequency change with mass.

Kanazawa [82] studied QCM behavior when the quartz is in contact with a liquid. By measuring how QCM response is affected by it, a correction of Sauerbrey's equation was proposed (**equation 1.7**).

$$\Delta f = -f_0^{3/2} \left(\frac{\eta_g \rho_g}{\pi \mu_q \rho_q} \right)^{1/2} \quad \text{equation 1.7}$$

Where η_g is the viscosity and ρ_g the density of the fluid

His work opened the door to a vast group of applications, including QCM's most characteristic one: the study of electrochemical processes. It is known as Electrochemical Quartz Crystal Microbalance (EQCM). In this technique adaptation, one of the electrical contacts used to apply an alternative voltage to the quartz crystal becomes also an electrode for the electrochemical cell.

EQCM has been used to study copper corrosion inhibition [83], ion adsorption [84] and film formation [85].

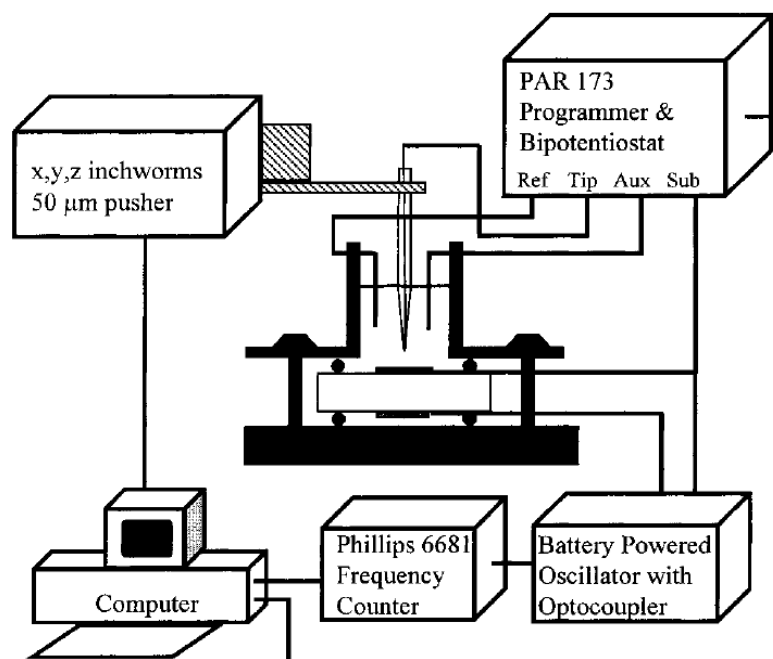


Figure 1.21 Combined scanning electrochemical microscopy-quartz crystal microbalance [86].

Bard *et al.* reported in 1998 the coupling of QCM with SECM (**Figure 1.21**) [86]. Initially, they studied the effect of lateral and vertical tip movement on QCM Frequency. Due to the small amount of mass changes involved in the microelectrode electrochemistry process, both movements showed a frequency response comparable with mass changes that can be achieved by using SECM. However, if the tip is held stationary at a given location above the sample surface, frequency changes reflecting mass changes can be monitored. Later, Tip-Induced Metal Layer Etching was studied with a SECM-QCM setup. The setup was used to study fullerene (C_{60}) film in MeCN with $K^+ CF_3SO_3^-$ electrolyte. The tip is held over the sample at a potential where C_{60}^- anions are oxidized. C_{60} films are soluble in MeCN in presence of K^+ . So, as the film starts dissolving, an anodic current is observed at the tip that results from the diffusion of C_{60}^- anions from the substrate surface, confirming the collection of C_{60} at the tip. This work indicated that SECM-QCM is a useful tool to *in-situ* follow the sample mass loss

during local electrochemical processes.

As mentioned at the beginning of this section, when using SGECM, there is a risk of leaving a small amount of material over the sample surface (electrolyte leakage). Lower detection limit, capability to work in different environments, and possibility to custom quartz crystal coating material, make QCM one of the most appealing techniques to follow mass changes. So, the combination SGECM-QCM could be very advantageous to study the effect of possible electrolyte wetting.

1.4. Proposition of the work

The objective of the present work is the further development of SGECM, putting major effort into the improvement of the chitosan gel probe. As complex as it can be, micro-disk electrode fabrication is more or less standard. There are even commercial brands where these electrodes can be purchased. So, initially, the focus was pushed forward in the analysis and enhancement of hydrogel electrodeposition. Chitosan polymer was selected to be used in this work. Controlling its electrodeposition accurately is a key factor in ensuring gel probe reproducibility. **Chapter II** explores chitosan electrodeposition, its improvement through the combination with other polymer (co-electrodeposition polymer blends), and the first attempts to obtain a functionalized gel probe.

Chapter III addresses a long-lasting question about the results of gel-sample interaction: the electrolyte wetting. With a chitosan gel probe fabrication process well established, we are ready to analyze the behavior of the gel when it reaches the surface. In **Chapter III** the focus is put on possible electrolyte leakage of the gel probe over the sample. To analyze this, SGECM is coupled with QCM. A highly sensitive response from the QCM allows us to “see” as we were on the sample. Adding new precious information, not only to identify electrolyte remains

but also to follow the approach, retraction and detachment from the probe.

As it was mainly shown in SICM applications (**subsection 1.1.3**), probe modifications would help to extend the information that a SEPM technique can collect as well as its applications. So, a novel gel probe configuration for SGECEM is explored in **Chapter IV**. A second electrode is integrated with the micro-disk electrode. Aiming to reach quantitative information from the sample. Here, the first concept of this gel coated micro-integrated electrode (MIE-GC) is tested. Furthermore, a possible application as ozone detector is also explored.

Chapter II

Preparation and functionalization of gel probes for scanning gel electrochemical microscopy (SGECM)

From **Chapter I**, we have learned that the heart of SGECM is the gel probe. As the gel serves as electrolyte, it should have reasonable ionic conductivity. For obtaining reliable and reproducible results of measurement, the shape of the gel probe has to be well controlled. Moreover, as the gel probe needs to repeatedly touch and detach from the sample surface, it is preferred not to be susceptible to permanent deformations after stretching. As discussed in **Chapter I**, accurate and reproducible measurements were achieved when using a chitosan gel probe [75,76]. Yet, there is a clear need to control gel shape as well as improve key gel properties: elasticity, stability and conductivity.

Various approaches have been used to enhance the mechanical strength of gel in literature. Several attempts to enhance its properties have been made. The addition of stabilization agents such as mannitol [87], sorbitol [88] or glycerol [89] has proven to be a promising way to protect chitosan from degradation. Chemical cross-linking is considered the most effective due to the stability that brings the covalent bonds, this process is irreversible. The most common chemical crosslinkers of chitosan are dialdehydes, such as glutaraldehyde or glyoxal [90,91]. However, chemical cross-linking also changes chitosan physicochemical properties. In the physical cross-linking process, a network of ionic bridges between negatively charged components and the positively charged chitosan chains is formed. Tripolyphosphate is commonly used [92]. In some cases, chitosan can be cross-linked by cations, such as Fe(III) [93]. Co-electrodeposition with other natural polymers (cellulose [94], starch [95]) or synthetic ones (polyvinyl alcohol

[96], polyethylene oxide [97], polyvinyl pyrrolidone [98]) is also possible. These hybrids, in general, show improved physicochemical properties in comparison to the pure polymer. Functionalization of the gel probe can also be achieved by this method. Selecting a co-polymer with the desired functional group.

In this chapter, the shape control of chitosan gel by electrodeposition is studied, aiming to correlate the deposition volume with the deposition charge. Several electrodeposition parameters are tested. The obtained gel volume is calculated using optical microscopy. From the electrodeposition conditions, the charge can be obtained and an empirical relation with the charge can be obtained. Furthermore, co-electrodeposition of chitosan with silanes was achieved, enhancing gel properties. The probes were characterized by cyclic voltammetry (CV), FTIR, Raman spectroscopy and AFM. Moreover, the approach-retract behavior of gel probes was systematically studied. Information about the mechanical behavior of the gel probe was qualitatively obtained from the approach and retract curves. Detach distance was primarily used to compare gel probes. Approach and retract curves were also used to study gel-surface interaction, especially with attempts to discuss the Au-S interactions between the gel probe and the sample surface. Lastly, in attempting to improve chitosan gel probe conductivity, gel probes were made by electrodepositing chitosan with ionic liquids and deep eutectic solvents. They were characterized by their approach and retract curves.

2.1. Experimental

2.1.1. Materials

Chitosan and chitosan blend gel probes were prepared by electrodeposition. Using as WE a 25 μm diameter Pt micro-disk electrode with R_g (ratio between the diameter of the insulating shield and the micro-disk electrode) between 2 and 3. Electrode preparation was described in

previous works [75,76]. Gel electrodeposition was made from a 1:1 (vol. ratio) glycerol/H₂O solution containing 0.8 wt.% chitosan and 0.1 M NaNO₃ at a pH between 5.5 and 6. Chitosan concentration was chosen based on its solubility in water-based solutions when the pH is adjusted between 5 and 6 using HCl [99]. For the co-electrodeposition of chitosan with tetraethoxysilane (TEOS), 21.3 μ L of TEOS was added to 5 mL of the solution above, reaching a TEOS concentration of 19 mM. The electrodeposition was carried out by applying -0.95V vs. Ag/AgCl quasi-reference electrode (QRE) for 300 seconds. Co-electrodeposition of chitosan with 3-mercaptopropyltrimethoxysilane (MPTMS) was made applying the same method; here, the electrodeposition solution contains 20 mM of MPTMS instead of TEOS.

2.1.2. Sample characterization

Gel probes were observed under optical microscope (Nikon, Japan). Gel composition (after evaporation of solvent) was analyzed and mapped by EDX (Oxford Instruments, UK) at a working distance of 10 mm and a voltage of 10 kV. Electrochemical characterization was carried out in a 1 mM ferrocenedimethanol, 0.1 M KCl, 1:1 (vol. ratio) glycerol/H₂O solution, using a Pt wire as counter electrode (CE), and Ag/AgCl QRE as reference electrode (RE), all connected to a potentiostat (PalmSens3, The Netherlands).

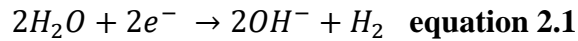
2.1.3. AFM characterization

AFM (Atomic Force Microscopy) images were recorded using a Bioscope Resolve (Bruker France SAS, Palaiseau, France) operating in PeakForce-Quantitative Nano-Mechanical (PeakForce QNM) imaging mode in ambient conditions. Silicon nitride probes with a nominal spring constant of 0.12 N/m and a nominal tip radius of 5 nm were purchased from Bruker (PeakForce-QNM tips, Bruker France SAS). Data was collected with a resolution of 256 \times 256 pixels, a scan rate of 1 Hz, and a maximal applied force of 0.5 nN. For gel mechanical modulus,

data analysis was made using Sneddon's model [100] in NanoScope Analysis (version 1.19) software.

2.2. Empirical shape control of chitosan electrodeposition

Chitosan is a natural polymer that may reversibly switch between soluble and gel in aqueous media. The protonation of amino groups at pH below 6.3 makes chitosan soluble, while at pH above 6.3, the deprotonation turns chitosan into gel form. The pH trigger can be achieved by electrochemical reactions, such as cathodic reduction of water [101]. For example, the hydrogen evolution reaction (HER) can be expressed as follows: (**equation 2.1**).



The charge can be directly linked to the amount of OH^- production by Faraday's law (**equation 2.2**).

$$\int I_{(t)} dt = z n F \quad \text{equation 2.2}$$

Where I is the current, t the time, n number of moles, z number of exchange electrons and F is Faraday's constant (96500 C/mol).

Precise control of electrodeposition is needed for gel microelectrode fabrication. Unlike direct electrodeposition processes where the quantity of deposit can be directly linked to the deposition charge by Faraday's Law, the electrodeposition of chitosan is made by an indirect process that depends on the pH gradient. Thus, the problem is more complex, meaning that not all the OH^- ions turn into deposition. Instead, the deposition is determined by the pH gradient, where gelation is triggered at $pH > 6.3$. The scheme is illustrated in **Figure 2.1**.

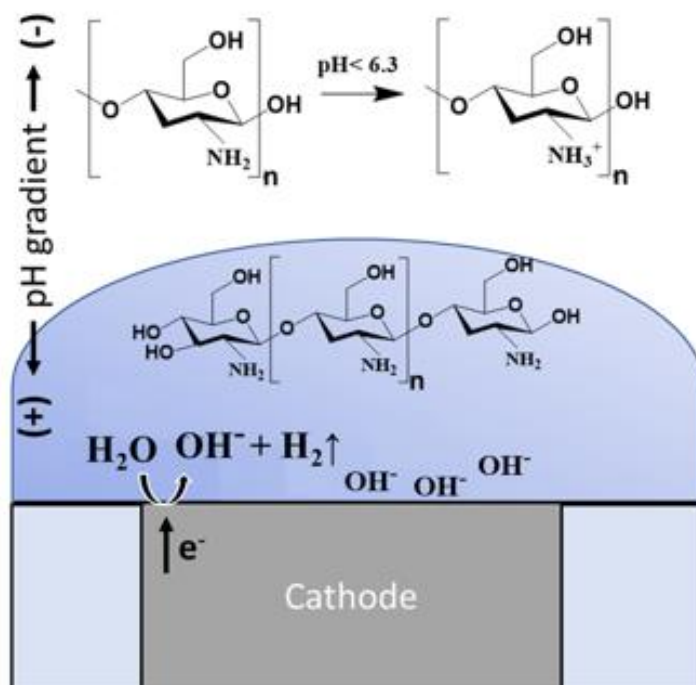


Figure 2.1 Schematic representation of the electrodeposition of chitosan by cathodic modulation of pH at the electrode/solution interface.

Gel probes are fabricated by chronoamperometry using a Pt micro-disk electrode as WE at a potential of -0.95V vs Ag/AgCl QRE. This potential was applied for 50, 100, 150, 200, 250 and 300 seconds to obtain gel probes with different gel volumes (**Figure 2.2A**). After every electrodeposition, optical images were taken (**Figure 2.2B**) and gel volume was approximately calculated using **equation 2.3**.

$$V = \frac{2}{3} \pi h R^2 \quad \text{equation 2.3}$$

where V is the gel volume, h is the gel height and R is the probe diameter.

Electrodeposition potential was established by experience and works made in the past. Its value is determined for inducing HER, but not allowing intensive H_2 evolution. The H_2 bubbles were found to be problematic especially when trapped in the gel matrix, which would affect the gel properties making it unusable for SGECM measurements. $NaNO_3$ is also added to inhibit bubble formation inside the gel [72].

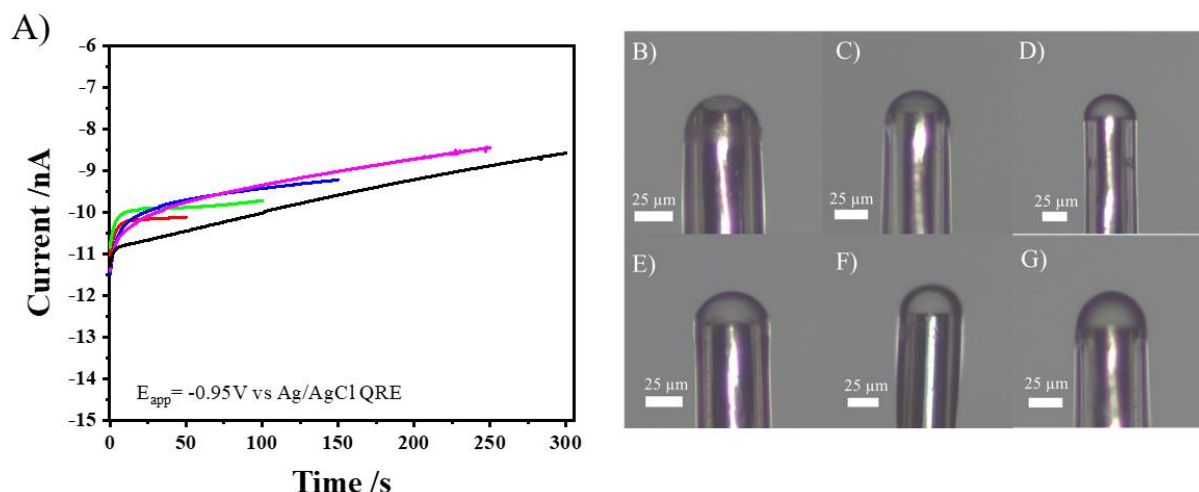
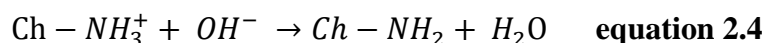


Figure 2.2 Chitosan electrodeposition by chronoamperometry at -0.95 V vs. Ag/AgCl QRE from a 0.8% , (m/v) chitosan, 0.1 M NaNO_3 , 1:1 glycerol/ H_2O solution and different electrodeposition times. Images of gel probes obtained at an applied potential (E_{app}) of -0.95 V vs Ag/AgCl QRE (A) and 50 (B), 100 (C), 150 (D), 200 (E), 250 (F) and 300 (G) seconds.

It is straightforward to see from **Figure 2.2** that the gel grows bigger with time. **Figure 2.3** shows the calculated volume of chitosan gel as a function of electrodeposition time. As the electrodeposition is driven by the reaction of OH^- with dissolved chitosan as in **equation 2.4**, the gelation follows the gradient of OH^- ions.



This indirect electrodeposition could well explain the evolution of the gel shape with time, considering the evolution of the diffusion layer. It may also explain the non-linear relationship between the gel volume and the deposition charge in **Figure 2.3**. Note that it is also possible to deposit gel laterally to the side of the microelectrode, but this shall be avoided for SGECM due to the poor spatial resolution. This empirical study points out a way of fine-tuning the shape of the gel. Future work could be on the quantification of the deposition process by modeling that considers the kinetics of OH^- production (**equation 2.1**), diffusion of OH^- (in the solution and the gel) and the chitosan gelation (**equation 2.3**).

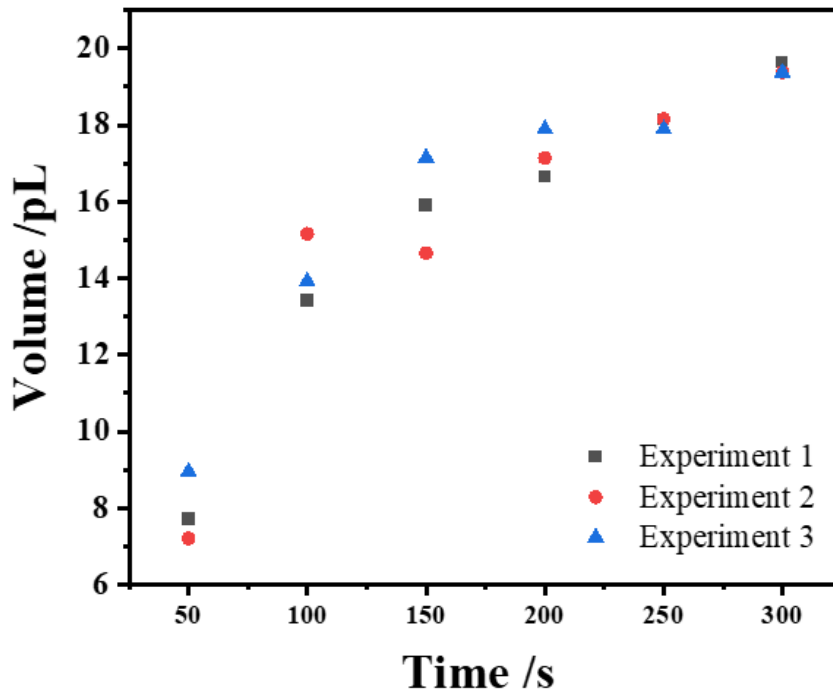


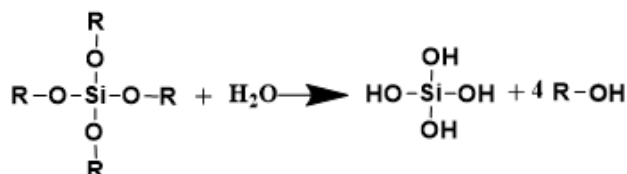
Figure 2.3 Chitosan gel volume obtained by chronoamperometry at -0.95 V (vs. Ag/AgCl QRE) from a 0.8% , (m/v) chitosan, 0.1 M NaNO_3 , 1:1 glycerol/ H_2O solution, using different electrodeposition times.

2.3. Chitosan-tetraethoxysilane co-electrodeposition

The silica sol-gel process is a well-known method that is composed mainly of two steps: the hydrolysis and condensation of silica precursors. Taking alkoxy silanes as example and R as methyl or ethyl groups, the hydrolysis occurs as in **Figure 2.4A** to produce silanol and unlabeled alcohol. The hydrolyzed alkoxy silane then condenses to form Si-O-Si bonds by either alcohol or (more common) water elimination. The condensation reaction can also occur between silanol and hydroxyl groups of a surface, leading to the covalent bonding of silane to the surface. Hydrolysis and condensation reactions are pH-dependent. In acidic medium, a low rate of condensation and a high rate of hydrolysis. Applying cathodic potentials to a conductive substrate, a pH gradient is created, increasing the pH on the electrode surface. This rise of the pH incites the condensation of the hydrolyzed precursor (**Figure 2.4B**). A similar phenomenon

occurs with the chitosan, which also polymerizes by the local increase of the pH on the subtract surface. Thus, a chitosan–silica copolymer can be obtained by electrodeposition from the blend of both [102,103].

A)



B)

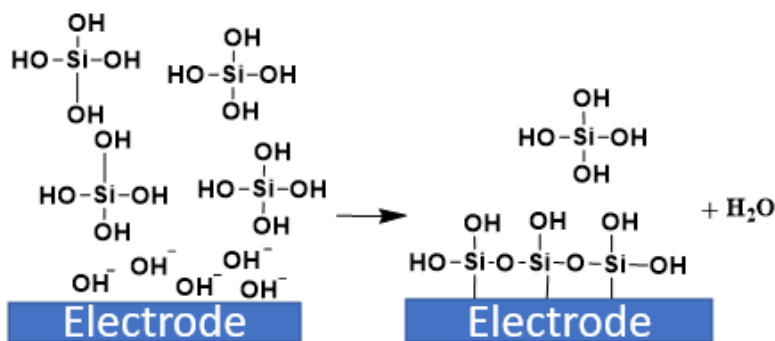


Figure 2.4. Alkoxysilane hydrolysis (A) and condensation (B) schemes.

TEOS is a promising precursor for this purpose. It has been intensively reported that TEOS-based sol-gel-derived silica could co-deposit with chitosan, improving the mechanical properties of the obtained composite gel [104]. More importantly, TEOS could also be electrodeposited under similar conditions as chitosan. In the mild acidic precursor solution, TEOS is in hydrolyzed form (e.g. Si(OH)₄ if fully hydrolyzed), and by applying a suitable cathodic potential the local pH at the electrode increases yielding the condensation of silanol [103,105]. This could perfectly match the electrodeposition of chitosan, which is also based on the local modulation of pH near the cathode.

Here, TEOS was added to the chitosan deposition solution and co-electrodeposition was realized, as verified by the Si/C ratio from EDX (**Figure 2.5B**). Hydrogel chemical characterization is challenging, mainly because most used characterization techniques do not perform well when water is present in the sample. EDX has been established as a good tool to identify Si in samples, it must be dried though. After gel electrodeposition and before drying, it is important to mention that the gel was immersed for a few seconds in 1-1 glycerol/H₂O. The goal is to remove the remains of electrodeposition solution from the gel. Guaranteeing that all Si detected comes from the electrodeposited gel. A drop of the electrodeposition solution was also dried and analyzed to compare the results. After EDX analysis, Si/C ratios obtained confirm the presence of Si in the final sample, showing also that the Si/C ratio in dried electrodeposited gel remains similar to the dried solution drop.

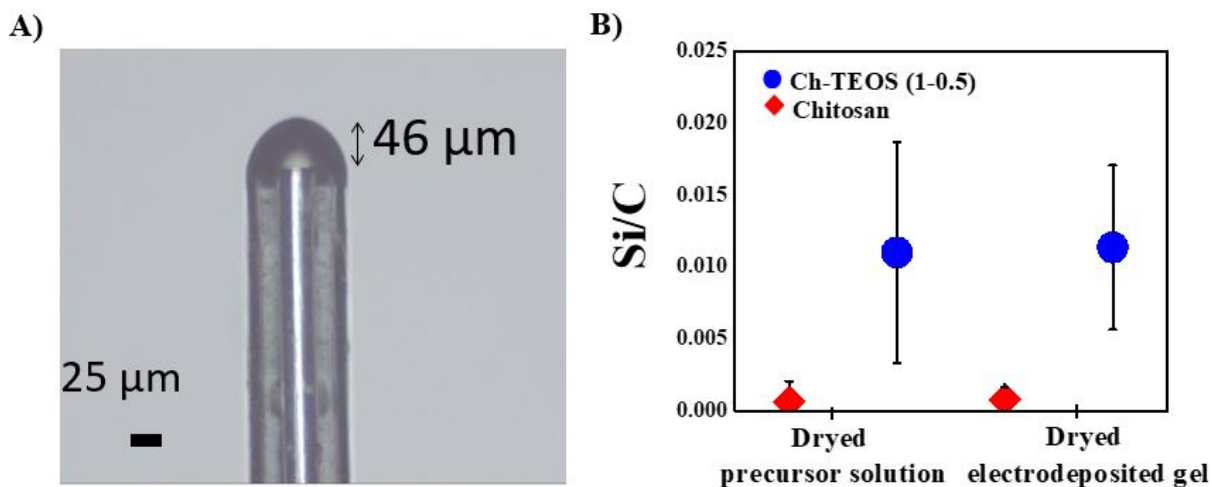


Figure 2.5 Ch-TEOS gel probe obtained by chronoamperometry applying $-0.95V$ during 300s (A) Mean Si/C ratio \pm SD obtained by EDX analysis of chitosan ($n=5$) and Ch-TEOS ($n=7$) gel precursor solutions and obtained gel by electrodeposition (B).

Gel probe's main targeted use, whatever its size, configuration or particular application, is to perform electrochemical measurements. So, gel-electrolyte matrix stability and properties play a major role in finding a successful gel probe suitable for SGECM. Cyclic voltammetry (CV) in a 3-electrode setup (**Figure 2.6A**) was used to characterize chitosan and chitosan-TEOS gel

probes. **Figure 2.6B** shows the results of performing CV in 0.1mM Fc(OH)₂, 0.1M KCl, 1-1 glycerol/H₂O solution using chitosan and chitosan-TEOS blends gel probes. Although the chitosan to TEOS mass ratio reaches 1 to 1, there are no significant changes in the CV response. Current values and redox potential remain unchanged. One can assume that adding TEOS to the gel matrix up to a 1-1 mass ratio neither diminishes nor enhances its electrochemical properties.

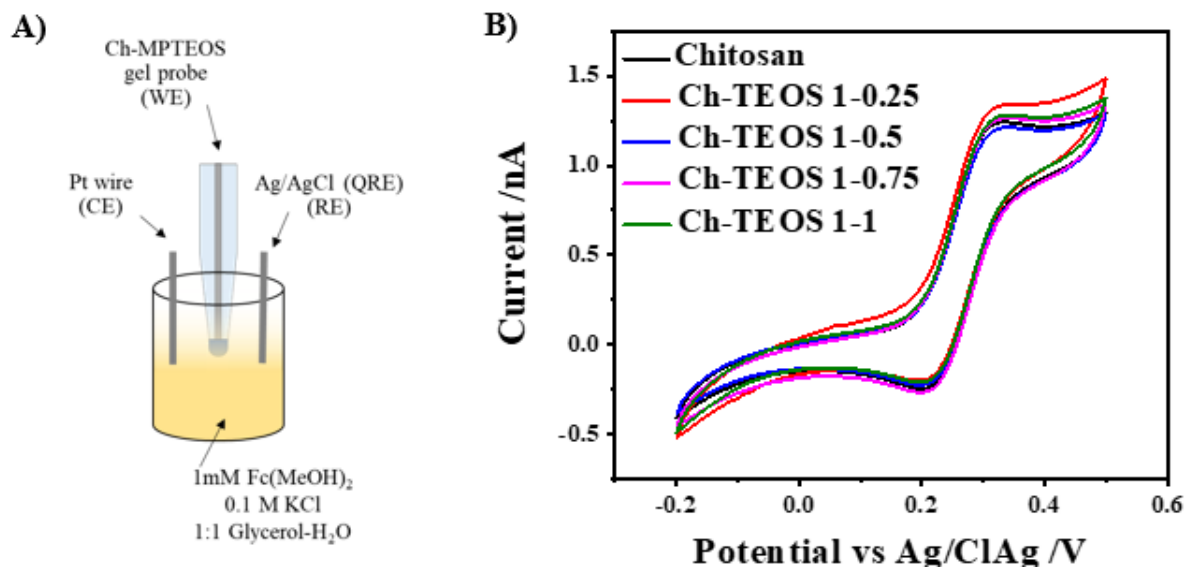


Figure 2.6 Scheme of electrochemical setup (A) used to obtain CV of chitosan and Ch-TEOS blends at 50 mV/s in 1mM Fc(MeOH)₂, 0.1M KCl, 1:1 glycerol-H₂O solution (B).

Mechanically, we were able to characterize the Chitosan-TEOS sample using SGECM approach and retract curve and non-contact AFM. The latest, a well-developed technology, is used as a comparative measurement to corroborate or deny SGECM mechanical results.

Retract and approach curves are an accurate tool to determine gel detach distance. Current is recorded during the gel probe approaching and retracting (after reaching the sample) from the surface. The distance travelled by the gel probe between points of touching (marked by a clear current spike), and detaching (distance from the surface where the current returns to its initial value), is called detach distance. It is related, mainly, to two factors: mechanical properties of

the gel and adhesion forces. For SGECEM, it is important to minimize this distance. To scan a surface using SGECEM, gel probe must approach and retract the surface hundreds of times. Constant stretching can be prejudicial to the mechanical integrity of the gel. **Figure 2.7B** shows the mean detach distance $\pm SD$ of chitosan and chitosan-TEOS blends using the same blend ratios as **Fig 6B**. With the biggest Chitosan to TEOS mass ratio (*i.e.*, 1-0.25) tested, the detach distance is reduced between *ca.* 20 to 25%. Reaching an optimal at 1-0.5 Ch-TEOS mass ratio. It is clear that TEOS incorporation into the gel matrix reduces gel deformation. These results are in concordance with similar studies [104,106], where an enhancement of mechanical properties of chitosan gel is reached by the incorporation of TEOS as a co-polymer.

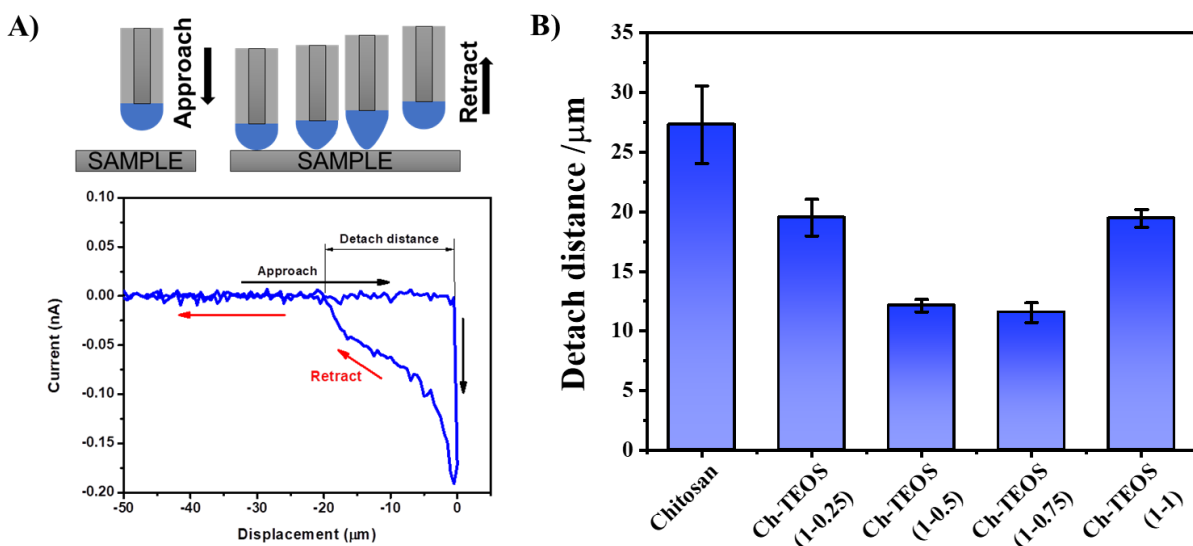


Figure 2.7 Approach - retract gel probe scheme and typical current response (A). Mean detach distances $\pm SD$ of Chitosan ($n=9$) and Chitosan-TEOS (Ch-TEOS) 1-0.25 ($n=8$), 1-0.5 ($n=9$), 1-0.75 ($n=9$) and 1-1 ($n=8$) mass ratio blends using ITO as substrate, applying a E_{probe} vs $E_{\text{sample}} = 0.4\text{V}$ and approach speed of $2\mu\text{m/s}$ (B).

Mechanical behavior was also explored through AFM. Although both techniques are different, AFM has been widely used in the study of soft material mechanical properties at nanometric sizes. 0.5 to 1 mm high chitosan and Ch-TEOS 1-0.5 (mass ratio) films were electrodeposited on the Pt electrode. Samples were analyzed as soon as polymers were produced, avoiding an

excess of solvent evaporation. **Figure 2.8A** and **B** shows the mean modulus \pm SD value obtained using AFM as described before, *ca.* 37.4 ± 0.45 kPa for chitosan and *ca.* 49.3 ± 0.07 kPa for Ch-TEOS 1-0.5 blend. Once again, the polymer blend gel probe shows advantages over just chitosan ones. The gel modulus reflects the applied force and the displacement of the stretched or compressed body. Ch-TEOS Modulus is bigger than chitosan gel. This means that it is less compressible. So, Ch-TEOS detach distance is expected to be smaller than chitosan gel probe, as proven using SGECM.

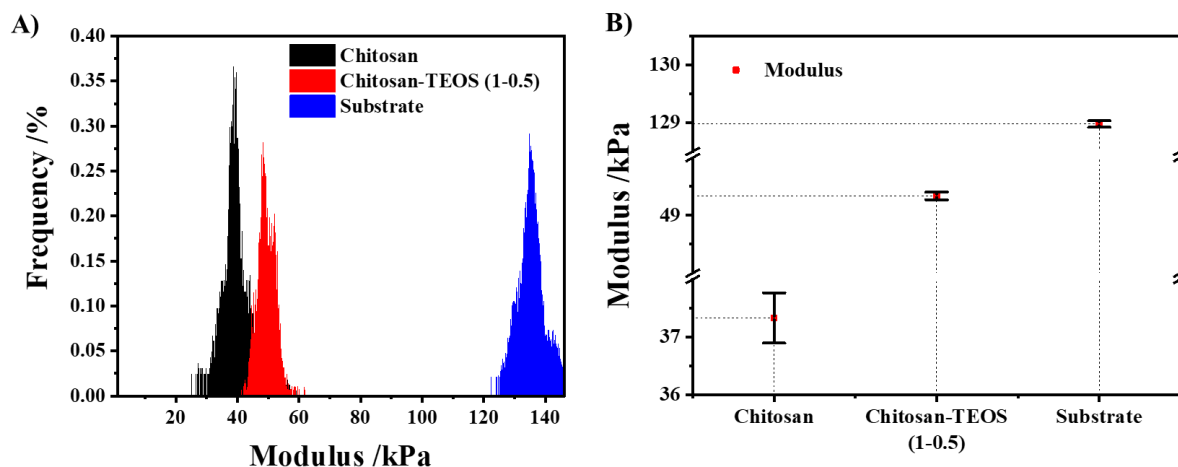


Figure 2.8. Modulus histogram (A) and mean Modulus \pm SD from chitosan ($n=1193$), Ch-TEOS (1-0.5) ($n=1246$) and Pt on glass substrate ($n=1086$) (B) obtained from AFM Peak Force QNM force volume analysis. Data was collected with silicon nitride probes with a nominal spring constant of 0.12 N/m and a nominal tip radius of 5 nm, a resolution of 256×256 pixels, a scan rate of 1 Hz, and a maximal applied force of 0.5 nN. For gel mechanical modulus, data analysis was made using Sneddon's model in NanoScope Analysis (version 1.19) software.

No quantitative model has explained the relation between detach distance and gel elastic modulus in SGECM yet. Nevertheless, the results obtained by AFM and SGECM can be compared qualitatively. Both results indicate the same behavior, TEOS enhances the mechanical properties of chitosan. Even further, approach and retract curves have been demonstrated as an accurate tool to evaluate, at least qualitative, micrometer-sized

electrodeposited polymers. Currently, polymer mechanical properties are studied either at the macro or (thanks to recent developments of AFM) nanometer level, leaving an underexplored size breach, micrometer size. The accurate results obtained by approach and retract curves turn them into a potential tool to evaluate mechanical properties of micrometer-sized electrodeposited polymers, expanding our knowledge of polymers' mechanical behavior from this size.

2.4. Chitosan-3-mercaptopropyltrimethoxysilane co-electrodeposition.

Exploring alkoxy silane-chitosan co-electrodeposition has a second purpose: obtaining a functionalized gel probe. A long-term target application for SGECM is to reach quantitative results from gel-surface interactions. To further explore this interaction, here, a thiol-functionalized gel was proposed as a first example. We expect that if Au (in any form) is present on the sample surface, it will be able to interact with the functional groups in the gel, and this interaction may be reflected by the approach and retract curve. The Au-S bond has been a subject of wide study during the past years [107]. This interaction is also extensively used to obtain self-assembled monolayers (SAMs) [108–110] on gold and, in the STM field, to investigate electrode functionalization or protein properties with techniques such as STM [111] or AFM [112]. Sulfur atoms can link a hydrocarbon chain of variable length to a metal surface through a covalent bond, while van der Waals forces between neighboring chains contribute to stabilizing the structure. Chitosan functionalization with thiol groups was studied before [113,114]. In this work, the goal is to study the functionalization of the gel probe and its electrochemical response.

Chitosan can be functionalized by the use of functional groups already existing in the molecule [115]. An important concept, in the study of polymers, is the number of death ends. This

concept is related to the number of sites in a polymer molecule that are not able to form a network. Mechanical properties depend greatly on how strong are the bonds between polymer units. Thus, when the number of death ends is high, the polymer's mechanical properties diminish. So, one must take into account that a direct functionalization of the polymer not always is the best path. For example, a first chitosan functionalization attempt was made using 3-mercaptopropionic acid (3-MPA). As a result, gel mechanical properties were not appropriate for SGECM (**Appendix I**). Thus, direct chitosan functionalization was discarded. Also, direct functionalization included the post-treatment of the electrodeposited gel. Due to the small gel volume, post-treatment frequently affects gel size, which must be avoided.

After confirming Ch-TEOS's successful co-electrodeposition. A chitosan (Ch) with 3-mercaptopropyltrimethoxysilane (MPTMS) blend was proposed to achieve our goal of introducing thiol groups in the gel matrix of the SGECM probe. MPTMS was chosen following two main guidelines: (1) possess a thiol functional group, (2) electrodeposition mechanism. The former is similar to chitosan and, of course, TEOS. The presence of MPTMS thiol functional groups allows us to explore Au-S interaction, approaching the gel probe to Au samples. Ch-MPTMS gel probes were obtained using the same conditions for electrodepositing Ch-TEOS gel. Solutions using Ch-MPTMS 1-0.25, 1-0.5, 1-0.75 and 1-1 mass ratios were stable as well. Polymer characterization will be discussed below.

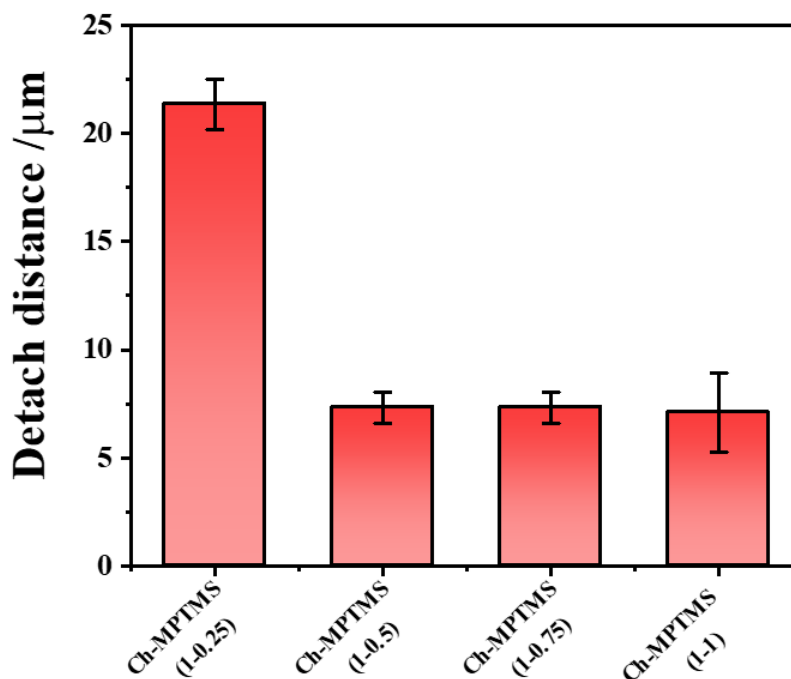


Figure 2.9. Mean detach distances \pm SD of Chitosan-MPTMS (Ch-MPTEOS) 1-0.25 ($n=12$), 1-0.5 ($n=13$), 1-0.75 ($n=11$) and 1-1 ($n=12$) mass ratio blends using ITO coated with 30 nm of Au as substrate, applying a E_{probe} vs $E_{sample} = 0.4V$ and approach speed of $2\mu m/s$.

As for Ch-TEOS blends, **Figure 2.9** shows that a mass ratio of 1 to 0.5 Ch-MPTMS reaches the smallest detach distance, which remains unchanged with higher MPTMS ratios. Even if detach distances are different, our goal is to compare chitosan, Ch-TEOS and Ch-MPTMS responses when samples with and without gold coating are used.

Figure 2.10 resumes the mean detach distance \pm SD from the ITO surface of Ch-TEOS and Ch-MPTMS gel probes. A platinum plate, sputtered gold on glass, and a gold foil, are used as substrates to evaluate the mechanical properties of the gel probes.

Even if Ch-TEOS and Ch-MPTMS hybrid gel probes show an overall improvement of the gel stiffness, there is no really clear tendency. Also, the analysis of the use of the Ch-TMEOS in the gold samples required further investigation.

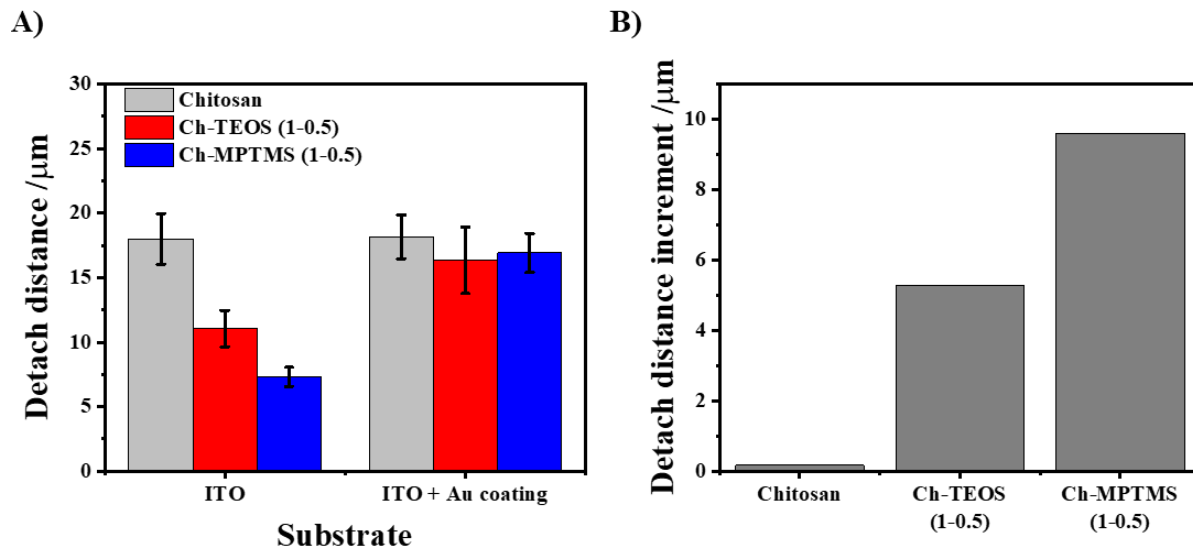


Figure 2.10. Mean detach distances \pm SD of Chitosan ($n=17$), Chitosan-TEOS (Ch-TEOS) 1-0.5 mass ratio ($n=15$) and Chitosan-MPTMS (Ch-MPTMS) 1-0.5 mass ratio ($n=16$) applying a E_{probe} vs $E_{sample} = 0.4V$ and approach speed of $2\mu m/s$ (A). Detach distance increment ratio (B) from ITO and ITO+ Au 30 nm obtained from (A).

It is common knowledge, that to analyze a material, the used technique must be as less invasive as possible, trying always not to distort the physicochemical properties of the substance. In general, for gel analysis, methods carried out in specific environmental (vacuum, freezing) conditions may modify the gel morphology to an unknown degree. Sample preparation as cut after freezing, coating or addition of probe particles, could lead to inaccurate results. Conventional X-ray diffraction (XRD) generally gives broad, amorphous patterns for gels meaning that analysis is difficult. However, it can be a useful technique to identify fabricated crystalline structures within an amorphous gel such as chitosan self-assembly into crystals [116]. Scanning Electron Microscopy (SEM) and Transmission Electron Microscopy (TEM) are useful tools to obtain images of dried gel surfaces, and study their morphology [117]. If the gel can be frozen, even three-dimensional images can be obtained after cutting the gel and revealing its cross-section [118]. However, SEM and TEM use vacuum technology, therefore gel must be dried as a precondition to perform the analysis. So, the gel is no longer in the condition it was obtained or pretended to be used. Never mind how powerful SEM and TEM

techniques are for material characterization, the result corresponds to a sample that no longer is in its original condition. A similar problem is faced when Fourier Transform Infrared (FT-IR) and Raman spectroscopy, another two well-known characterization techniques, are used. Although there are no particular temperature or pressure conditions, the sample must be dried to avoid water interference. Raman spectroscopy and FT-IR of chitosan, Ch-TEOS and Ch-MPTMS were performed without much success (**Appendix II**), leading us to explore new methodologies to analyze our gel probes.

2.5. Other attempts to elaborate the gel probes

The gel probes in our group are generally prepared from 1:1 glycerol/H₂O solvent. The addition of glycerol purpose is to reduce the evaporation of solvent during SGECM measurements. However, it may also inevitably affect the electrochemistry, notably on the ionic conductivity and the diffusion coefficient of species. Aiming at enhancing the conductivity while keeping a relatively low evaporation rate, we attempted to use ionic liquids (IL) and deep eutectic solvents (DES) for partially replacing glycerol in the precursor for the electrodeposition of chitosan.

2.5.1. Chitosan + Ionic Liquid (IL) gel probe

1-Ethyl-3-methylimidazolium tetrafluoroborate (EMIMBF₄, **Figure 2.11A**) and 1-Butyl-3-methylimidazolium tetrafluoroborate (BMIMBF₄, **Figure 2.11B**) were tested to be incorporated to the chitosan gel matrix due to its high solubility in water[119]. Both are purchased from Sigma Aldrich (purity $\geq 99.0\%$). To be able to compare with previous experiments, Ch-IL solutions were prepared with the same formulation as just chitosan gel solution, 0.8 wt.% chitosan and 0.1 M NaNO₃, pH adjusted to 5.5 and 6 using 1 M HCl. As solvent, different mixtures of H₂O, glycerol and IL were used: 50%H₂O-50%Gly-0%IL,

50%H₂O-40%Gly-10%IL, 50%H₂O-30%Gly-20%IL, 50%H₂O-20%Gly-30%IL, 50%H₂O-10%Gly-40%IL and 50%H₂O-40%Gly-10%IL. Solution stability was followed for 1 week. Only Ch-IL prepared with 50%H₂O-40%Gly-10%IL, EMIMBF₄ and BMIMBF₄, showed no visible alteration (precipitate, turbidity). From the two stable formulations, we were able to obtain a Ch-IL gel probe by electrodeposition using just the solution with 10% EMIMBF₄. Ch-IL electrodeposition was carried out applying -0.95V vs Ag/AgCl QRE for 300 s.

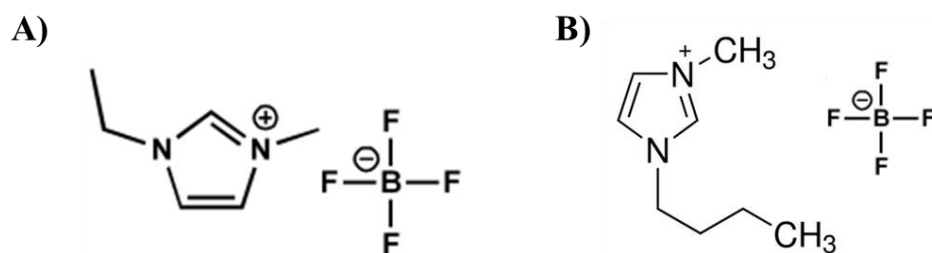


Figure 2.11 Structure of EMIMBF₄ (A) and BMIMBF₄ (B).

Figure 2.12 compares the approach-retract behavior of chitosan gel probes electrodeposited from 1:1 glycerol/H₂O with and without the addition of EMIMBF₄. Both probes show reproducible approach-retract behavior in multiple cycles, indicating that they can be used as gel probes for SGECM. However, there is no evidence of improvement in the conductivity of the probes, as the current response at touch position and during retract is similar for both probes. Further increasing the content of ionic liquid, either EMIMBF₄ or BMIMBF₄, caused the solution to precipitate. This is probably due to the cross-linking effect of ionic liquids [120,121]. Considering these limitations, we did not further develop the chitosan-based gel probes with ionic liquids.

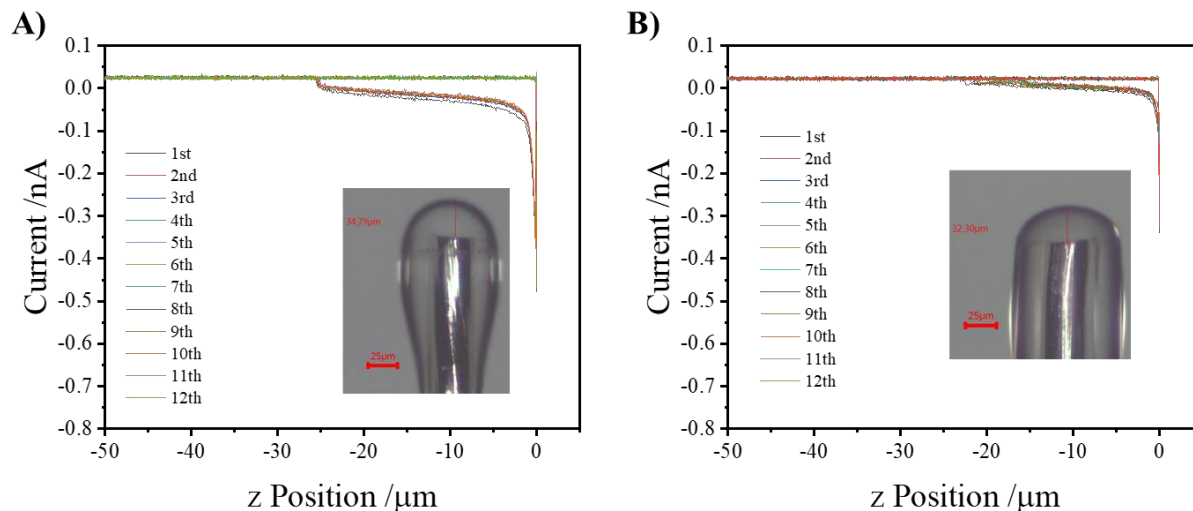


Figure 2.12 Detach and retract curves at an approach speed of $2\mu\text{m/s}$ applying a E_{probe} vs $E_{\text{sample}} = 0.5\text{V}$ and using a Pt substrate from Chitosan with 0% (A), 10% (B) in volume of EMIMBF₄. Inlet: gel probe used in each case optical image.

2.5.2. Chitosan + deep eutectic solvent (Ch-DES) gel probe.

Still aiming to improve gel probe conductivity, a second attempt to completely replace the glycerol in the original chitosan electrodeposition solution was made. Here, to prepare the chitosan solution, a deep eutectic solvent (DES) was used. DES was prepared by dissolving choline chloride (Sigma Aldrich purity $\geq 99.0\%$.) in water as reported before in the literature [122,123]. Unlike Ch-IL solutions, glycerol was excluded completely from the formulation. Ch-DES solution contains 0.8 wt.% chitosan and 0.1 M NaNO₃, and pH was adjusted to 5.5 and 6 using 1 M HCl. As solvent 10, 20 and 30 % (M/V) choline chloride water base solutions were used. All Ch-DES solutions remained stable after a week. Ch-DES gel electrodeposition was carried out by applying -0.95V vs. Ag/AgCl QRE for 300 s.

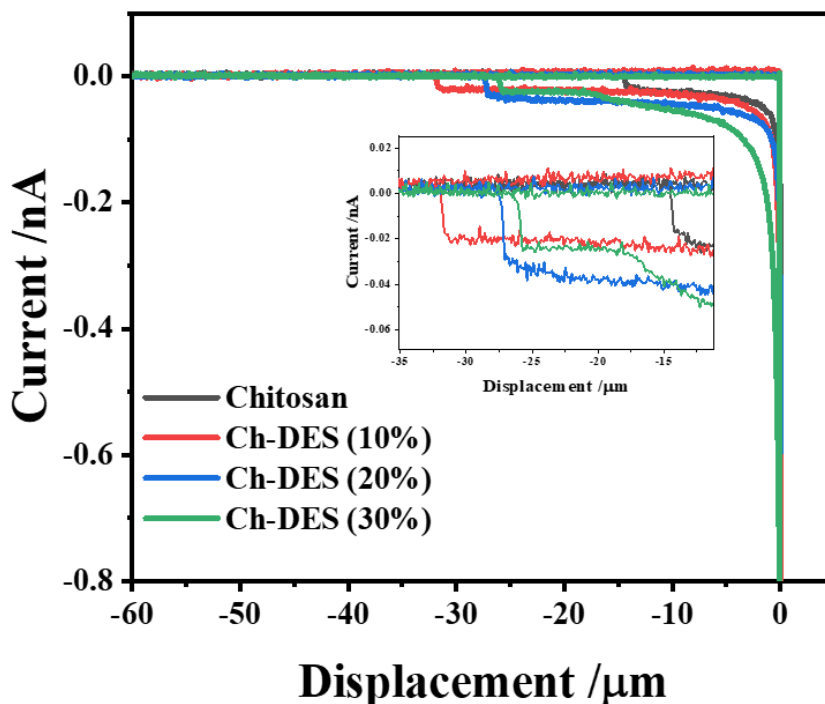


Figure 2.13 Detach and retract curves at an approach speed of $2\mu\text{m/s}$ applying a E_{probe} vs $E_{\text{sample}} = 0.5\text{V}$ and using a Pt substrate from Chitosan with 0% (A), 10% (B), 20% (C) and 30% (D) wt.% of choline chloride gel probes.

The Ch-DES gel probes were also tested performing approach and retract curves (**Figure 2.13**).

In general terms, the approach-retract behavior is similar to other chitosan-based gel probes, indicating that they could be used for SGECM measurements. Note that Ch-DES gels show an increase in the detach distance, indicating a potential change in the mechanical properties of the gel.

In general, we succeeded in obtaining new chitosan gel matrixes for gel probe fabrication by adding IL and DES to the precursor formulation. Nevertheless, results show no meaningful improvement due to its use. Further investigation is needed, trying even with new precursors.

2.6. Summary

The shape control of gel probes is a key concern in SGECM measurements. Chitosan has been proven a suitable polymer for elaborating gel probes by electrodeposition. Empirical studies

on the effect of deposition time show a way of fine-tuning the gel shape, and the results are in line with the deposition mechanism. This paves the way for co-electrodepositing chitosan with other species, for the sake of improving its mechanical strength or functionalization.

TEOS is proposed to enhance the mechanical properties of the chitosan gel probe. Its similar electrodeposition mechanism and complementary mechanical behavior to chitosan make it a good candidate for obtaining polymer-inorganic composites. Several Ch-TEOS blends were tested, showing that a 1 to 0.5 mass ratio was the optimal ratio with a *ca.* 40% detach distance diminution and a *ca.* 25% increase in the mechanical modulus. Also, different additives to enhance chitosan electrochemical behavior were tested. The results are not as evident as the improvement obtained by the addition of TEOS into the gel matrix. This work is presented in **Appendix II.**

The successful chitosan co-electrodeposition with alkoxy silanes also opens a door to gel functionalization, for example, the Ch-MPTMS co-electrodeposition towards functionalization with thiol group. A clear difference in the approach and retract curve response (compared to chitosan and Ch-TEOS gel probes) can be observed when Au-coated samples are used. Further analysis calls for a quantitative interpretation of the approach-retract curves, which shall consider the (visco)elasticity of the gel, the interaction between the gel and the sample and the deformation of the gel that changes the boundary for electrochemistry. This may allow us to understand better the information that can be derived from the approach-retract curves in the future.

Chapter III

SGECM integration with QCM for studying gel probe-sample interactions

As shown before in **Chapter II**, approach and retract curves suggest the possible existence of more than simple interactions between the gel probe and the sample surface. The current signal reflects a mixture of several factors making the analysis complicated. Therefore, QCM is introduced to provide additional information in two aspects: (1) electrolyte/liquid transfer from the probe to the sample surface, and (2) the gel-sample interactions notably on the effect of pressing. The first is a long-lasting question: does the use of a gel really prevent electrolyte leakage as SGECM claims? The former is related to the soft nature of the gel making it easily deformable under pressure. When a gel comes in contact with irregular surfaces, it will suffer from over-compression in some areas, which may lead to an increase in electrolyte remains. To achieve QCM combination with SGECM, we will focus on the sample substrate. To achieve this, we will replace the sample in the system with a coated quartz crystal to allow us to build a system resembling a QCM likely to operate in combination with SGECM experiments. A frequency is applied to the QC and recorded during the approach and retract cycles. Due to processes or modifications in the QC surface, the resonance frequency will change. Since the QCM response is non-electrochemical, it allows us to study or corroborate processes that, using only the current response, remained unsure or unclear. An example of this is the leakage of electrolyte on the sample surface. Analyzing the current approach and retract curves, the detach distance normally decreases from the first measurement until it reaches a constant value. Based on this, is safe to affirm that the gel probe goes through a stabilization process. A possible

explanation suggests that this process is due to electrolyte wetting. Fresh gel probes are fully hydrated and even with some solution remaining on the surface. It is highly probable that during gel-sample interaction, this “extra” electrolyte remains over the sample after contact, giving misleading results during the initial approach and retract cycles.

In this chapter, we integrated QCM with SGECM to study the remains of electrolyte from the gel probe upon contact with the sample surface. The results indicated that the frequency shift in QCM could qualitatively well reflect the remains of electrolyte on the sample surface, as confirmed by SEM observations. It was observed that the fresh gel probes would need several approach-retract cycles to stabilize and prevent leakage. Pressing the gel probe against the sample surface after touching may increase the electrolyte leakage due to the squeezing effect. The leakage of electrolyte is expected to be slightly more significant after soaking the gel probe in redox solution. Meanwhile, co-electrodeposition of chitosan with tetraethoxysilane (TEOS) would contribute to inhibit the leakage of gel probes. This work confirmed the advantage of gel in immobilizing electrolyte as compared with scanning droplet-based techniques. Moreover, QCM may serve as a quality control tool for gel probes before SGECM measurements.

3.1. Experimental

3.1.1. Materials and chemicals

The probes were prepared with Pt wires of 25 and 100 μm diameter (99.9% purity, Goodfellow, UK). Borosilicate glass capillaries from Sutter Instruments were used for sealing the probes and making microcapillary probes. The former took BF 150-75-10 (Outer diameter (OD): 1.5 mm, Inner diameter (ID): 0.75 mm) and the latter took B 100-75-10 (OD: 1 mm, ID: 0.75 mm). All the chemicals were used as received without further purification: chitosan (medium

molecular weight, Aldrich), tetraethoxysilane (98%, Alfa-Aesar), glycerol (99%, Sigma), NaNO_3 (99%, Fluka), ferrocenedimethanol (98%, Aldrich), KCl (Merck), chlorotrimethylsilane (98%, Acros) and polyethylene glycol (PEG 2000, Merck).

3.1.2. Fabrication of probes

The gel probes were prepared by electrodeposition of chitosan on Pt micro-disk electrode (Type I), or by “electrodeposition + pulling” on etched Pt wires (Type II). Type I gel probes were fabricated by electrodeposition on a 25 μm diameter Pt micro-disk electrode with R_g (ratio between the diameter of the insulating shield and the microelectrode) between 2 and 3, from a 1:1 (*vol.* ratio) glycerol/ H_2O solution containing 0.8 wt.% chitosan and 0.1 M NaNO_3 . For co-electrodeposition of chitosan with tetraethoxysilane (TEOS), 21.3 μL of TEOS was added in 5 mL of the solution above, reaching a TEOS concentration of 0.019 M. The electrodeposition was carried out by applying -0.95V *vs.* Ag/AgCl quasi-reference electrode (QRE) for 300 seconds. More details were reported in previous works [75,76].

Type II gel probes were prepared by “electrodeposition + pulling” following our previous work [73]. The process started with approaching an etched Pt wire (as working electrode (WE)) to the deposition solution with Ag/AgCl QRE and Pt wire counter electrode (CE). Once in contact (sensed by current feedback while applying -0.8V *vs.* Ag/AgCl QRE), the etched wire was immersed by 10 μm , held at -1 V *vs.* Ag/AgCl QRE for 1 s, and then withdrawn under the same potential at 3 $\mu\text{m}/\text{s}$ until fully detached from the solution. The deposition solution consists of 1.5 wt.% chitosan, 1 wt.% polyethylene glycol and 0.125 M NaNO_3 in 1:1 (*vol.* ratio) glycerol/ H_2O . The home-built “electrodeposition + pulling” setup consists of a potentiostat (PalmSens, The Netherlands) and a step motor (Owis, Germany) fully automated by a program written in VB.NET.

Microcapillary probes were fabricated by pulling borosilicate capillaries (OD 1.0 mm, ID 0.75 mm) on a laser puller (P-2000, Sutter Instruments). The outer walls of the pulled capillaries were silanized by immersion in chlorotrimethylsilane with nitrogen gas flowing through the orifice. After silanization, the microcapillaries were filled with 1:1 (*vol.* ratio) glycerol/H₂O containing 1 mM ferrocenedimethanol and 0.05 M KCl. A 25 μ m Pt wire was inserted in the electrolyte solution as RE/CE before electrochemical measurements. The typical images of Type I, and Type II gel probes and a microcapillary probe are shown in **Figure 3.1**.

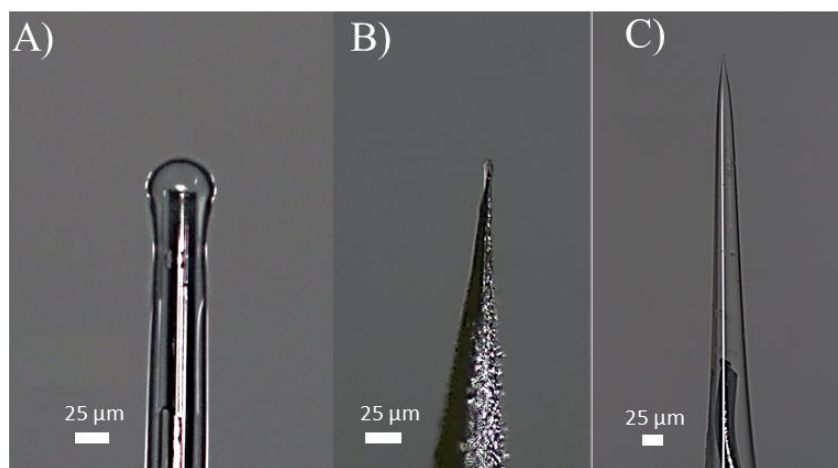


Figure 3.1 *Optical microscope images of Type I (A), Type II (B) gel probes and microcapillary probe (C).*

3.1.3. QCM coupled SGECM measurements

The QCM coupled SGECM measurements were carried out by integrating a quartz crystal analyzer (QCA 917, Princeton Applied Research) into a home-built SGECM setup as described before [75]. Standard 9 MHz AT-cut gold-coated quartz crystals of 5 mm diameter were used. The oscillator circuit is configured on a TTL-IC and with a stable oscillation function at heavy loads, offering an accuracy of 0.1 Hz and at a sample period of 0.1 s. The oscillation frequency from QCA, the current from potentiostat (PalmSens3, The Netherlands), and the piezo position from the encoder (PI, Germany) were synchronized by the same ADC data acquisition card

(PCI-2517, USA). Synchronization is of utmost importance to correlate both SGECM and QCM data. The control program was written in VB.NET.

Approach-retract curves were performed to study the leakage of electrolyte in SGECM and microcapillary-based measurements. The probes were approached toward the QC sample surface at an average speed of 2 $\mu\text{m/s}$ by current feedback at 0.4 V (E_{sample} vs. E_{probe}), as described previously [73]. After touching the sample (normalized to $z = 0$), the Type II gel probe and the microcapillary were immediately retracted at the same speed. For Type I gel probe, was also purposely pressed against the sample surface just after contact for different distances (2-10 μm range) before retraction, taking advantage of the soft nature of the gel. During the measurement, the oscillation frequency shift was recorded together with the current as a function of the vertical z position. Sequential/successive measurements were also performed to examine the stability of the probes. They were carried out by repeating the approach-retract measurements in hopping mode with a 50 μm lateral gap between adjacent sampling points.

3.1.4. Characterization of the samples

The samples after QCM-SGECM measurements were observed under optical microscope (Nikon, Japan) and they were further characterized by SEM (JEOL IT-500HR/LV, Japan). The composition of the deposited materials on the contact area (after evaporation of solvent from leaked traces) was analyzed and mapped by EDX (Oxford Instruments, UK).

3.2. QCM coupled SGECM measurements

The first step for any scanning probe technique is to approach the probe to the interaction range with the sample. For scanning electrochemical measurements with microcapillaries or gel probes, the most common and sensitive way to approach the probe is by current feedback [73,124], although other methods such as shear force were also used [69]. The concept is illustrated in **Figure 3.2A**. A voltage signal (in either DC or AC) is applied between the conductive sample and the electrode in the probe. When the probe is far from the sample, the circuit is open and only noise is recorded. Once the electrolyte in the probe touches the sample, the circuit is closed and a current spike is expected. From the instrumentation aspect, this spike is ideal for constructing closed-loop feedback. In this work, 0.4 V (E_{sample} vs. E_{probe}) DC voltage was applied for approaching all the probes. It was found to be sensitive enough, although Unwin and Koper [125] reported that AC signal could have a higher signal-to-noise ratio than DC signal for sensing the probe touching.

After touching, the probe is retracted away from the sample surface. Two scenarios are illustrated in **Figure 3.2B**. Ideally, the gel probe immobilizes the electrolyte and thus should not leave any of it on the sample surface after measurement. **Figure 3.2C** illustrates a typical approach-retract curve of a gel probe to the Au-coated QC surface, where both the current and frequency of QC are recorded in a synchronized way by potentiostat and QCM, respectively. The current response is similar to our previous work [75]. A hysteresis is observed while retracting the probe, which reflects the adhesion between the gel and the QC sample. Interestingly, the frequency response of QC follows a similar trend as the current hysteresis. It also shows a spike when the gel touches the sample, and then gradually restores to its initial value while retracting the probe. This confirms the adhesion during the retraction process.

More importantly, the good synchronization of the current and QCM frequency signals for both touching and detaching shows that QCM could be a promising tool for approaching gel probes on non-conductive surfaces. The detaching process is between a viscoelastic body (gel) and a rigid surface (QC) (**Figure 3.2B**, top). Thus, the decrease in frequency shift follows the same trend as the decrease in current, both reflecting the decrease in the contact area. After the gel probe completely detaches from the QC surface, the current reduces to noise level, and there is no significant difference in the frequency response of the QC.

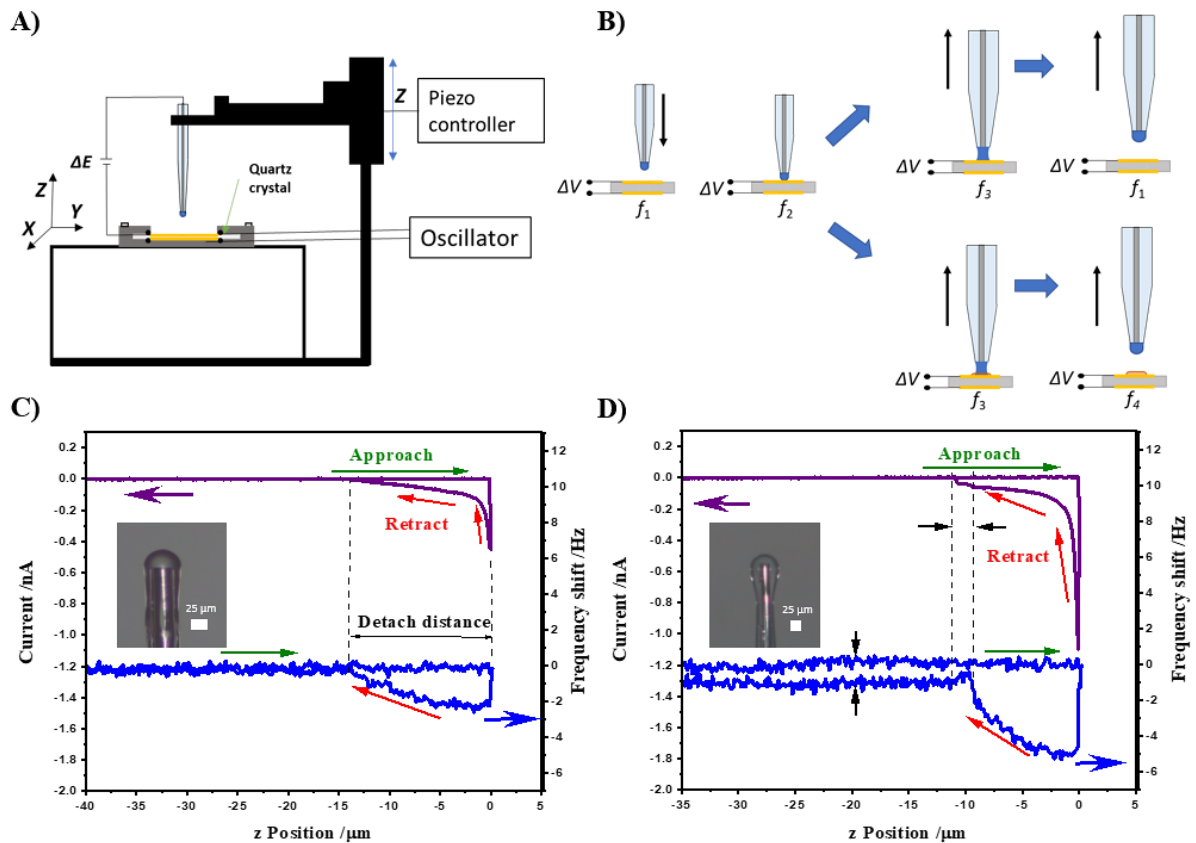


Figure 3.2 (A) Scheme of QCM-SGECM setup(A); Scheme of approaching-retracting Type I gel probe on QC surface with and without electrolyte leakage (B); Typical approach and retract curves of Type I chitosan gel probe from QCM-SGECM without (C) and with (D) leakage of electrolyte on the QC surface.

However, in reality, the immobilization of electrolyte by the gel probe may be imperfect. This might yield the electrolyte leaking and staying on the sample surface after approach-retract

measurements. Here, a purposely overgrown gel is taken to study the leakage effect, and the approach-retract curve is shown in **Figure 3.2D**. As in **Figure 3.2C**, current and frequency can sensitively detect the touching of the probe with the QC surface, and a signal hysteresis is again observed when retracting the probe. Nevertheless, the signals around the detaching position are quite different. The QCM frequency shift first decreases to almost zero, a position where the current starts to decrease from a plateau. Then, the frequency shift slightly increases to a stable value while the current decreases to zero (with noise). A hypothesis is that the detaching of the gel probe involves two steps. The first step is the detaching between viscoelastic gel and rigid QC surface, resulting in a decrease in frequency shift. However, even though the gel is already detached from QC, it may still stay in contact with the leaked electrolyte, thus the current is still measurable. During this second step of detaching between gel and the leaked electrolyte (**Figure 3.2B**, bottom) (corresponding to the positions between the two dashed lines in **Figure 3.2D**), the leaked electrolyte reshapes, which might be the reason for a slight increase in frequency shift. Meanwhile, the current decreases due to the reduction in the contact area between the gel and leaked electrolyte. This hypothesis may explain the characteristic current and frequency change in approach-retract curves. Although the transient frequency response in detaching could be highly informative, its quantification is very complicated and beyond the focus of the current work. The position where the current decreases to zero (with noise) marks the complete detaching of the gel probe from the sample. At the same time, the QCM frequency shift also becomes almost constant, yet different from the initial value. This difference may be well explained by the presence of remaining liquid electrolyte from the gel probe on the QC surface.

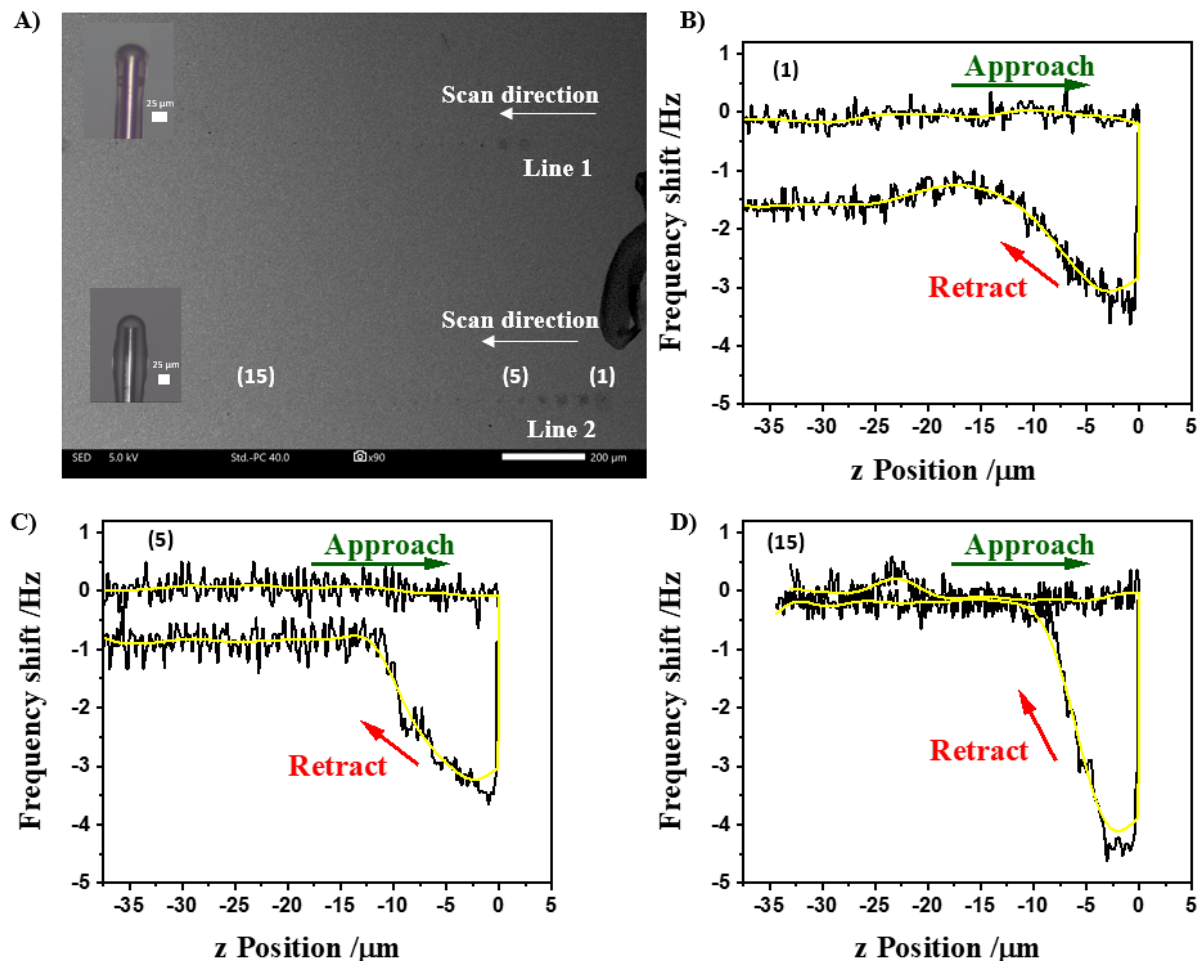


Figure 3.3 SEM image of the gold-coated QC after approach and retract measures with a Type I chitosan gel probe before (Line 1) and after (Line 2) soaking 1 mM ferrocenedimethanol solution with 0.05 M KCl and 1:1 (vol. ratio) glycerol/H₂O (inset photos) (A). Frequency shift approach-retract (black) and fast Fourier transform (FFT) smoothed (yellow) curves at 1st (B), 5th (C) and 15th (D) points in Line 2.

As reported by Unwin's group, SEM can be used to observe the leaked electrolyte after SECCM measurements to visualize the sampling points [126]. Here, the QC samples after approach-retract measurements of the gel probe are also examined by SEM after drying.

Figure 3.3A shows an SEM image of a QC sample after two line scans of measurements by fresh gel probes (respectively before (Line 1) and after (Line 2) soaking in ferrocenedimethanol). The electrolyte leakage on the sample surface is clearly visible for the first few measured spots. The spots gradually become smaller and invisible as the approach-

retract cycle number increases. The phenomenon is consistent with our previous work, where highly reproducible approach-retract curves may only be measured after stabilizing fresh gel probes with several approach-retract cycles [75]. **Figure 3.3B** represents the QCM frequency shift after the first sampling point with a gel probe freshly soaked in ferrocenedimethanol.

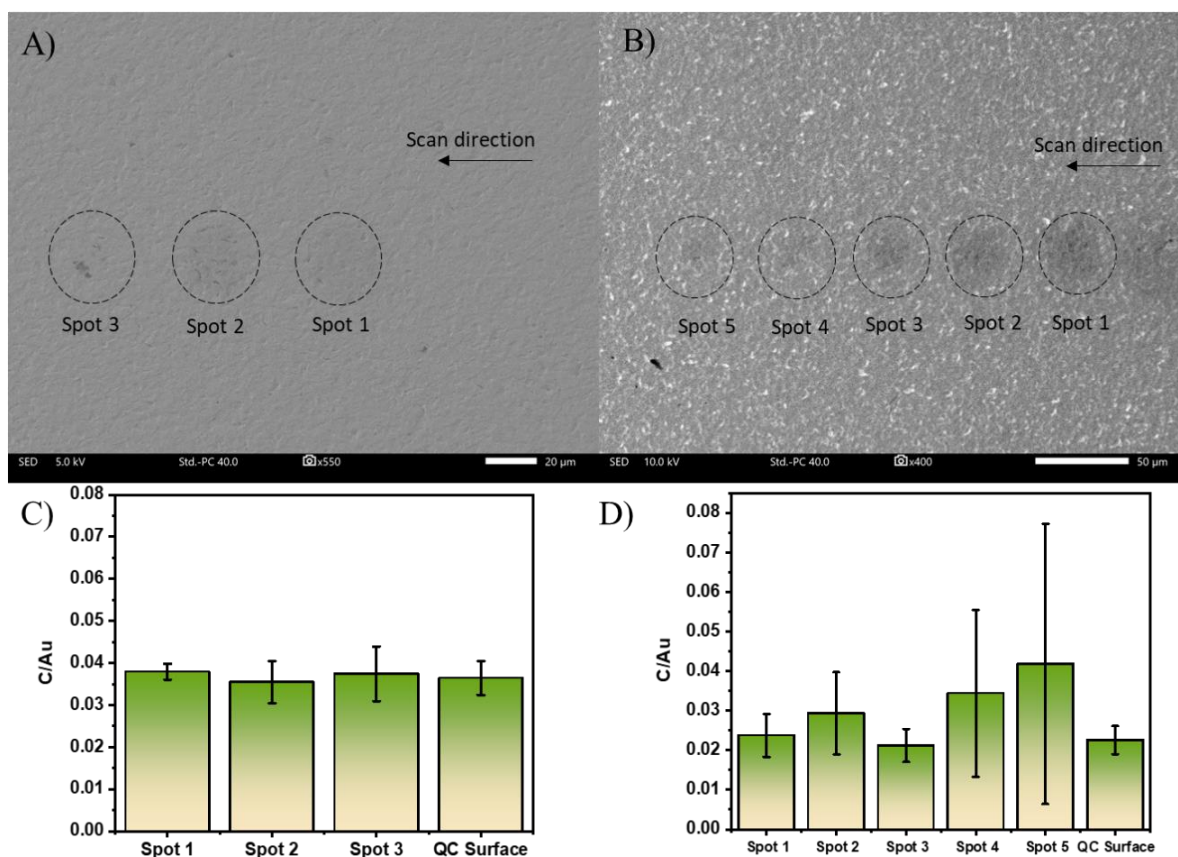


Figure 3.4 SEM images of the gold-coated quartz crystal after approach-retract curves with a Type I chitosan gel probe without (A) and with (B) soaking in 1 mM ferrocenedimethanol, 0.05 M KCl 1:1 glycerol/H₂O solution. (C) and (D): Mean C/Au ratio \pm SD ($n=3$) in EDX analysis of the recognizable points of leaked electrolyte.

A clear *ca.* 1.6 Hz frequency shift is observed, which corresponds to a large spot seen in SEM. For the fifth sampling point, the frequency shift reduces to *ca.* 0.9 Hz (**Figure 3.3C**), and the spot of the remaining electrolyte also becomes smaller. When the spot becomes invisible, the difference in the frequency shift also becomes indistinguishable (**Figure 3.3D**). The consistent results confirm the QCM frequency shift as a good indication for the remaining electrolyte on

the sample surface after approach-retract SGECM measurements. Note that EDX analysis was also attempted to characterize the spots, but there is no significant difference in the C/Au ratio even for visible spots (**Figure. 3.4** and **3.5**), perhaps due to the limited sensitivity of measurements for such ultra-thin deposits.

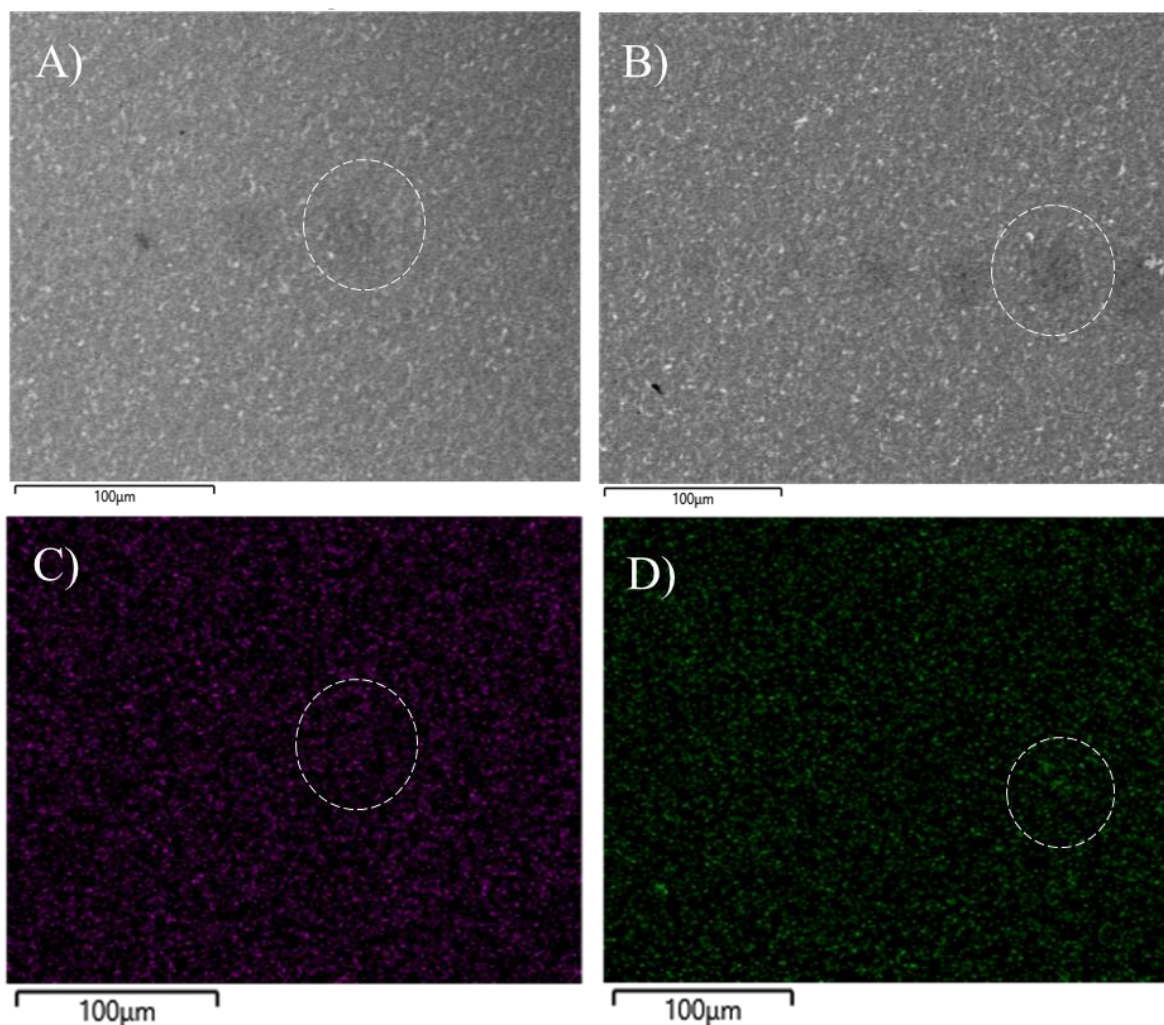


Figure 3.5 SEM images of the gold-coated quartz crystal after approach-retract curves with a Type I chitosan gel probe without (A) and with (B) soaking in 1 mM ferrocenedimethanol, 0.05 M KCl 1:1 glycerol/H₂O solution. (C) and (D): EDX mapping of C for the marked spots of leaked electrolyte.

The results above clearly indicate that QCM is a reliable tool for measuring the leakage of electrolyte from gel probes on the sample surface. Straightforward evidence is the frequency

shift of QC after detaching the gel probe, as shown in **Figure 3.3**. This is directly linked to the quantity of electrolyte left on the QC before evaporation of the solvent. Considering the shape of small droplets (as supported by SEM observations in **Figure 3.3A**), one cannot use Sauerbrey's Equation for quantitative analysis. Several reports attempted to analyze the frequency change induced by droplets in QCM based on the modification of Kanazawa's model, but their targeted droplets are much bigger in size as compared with our work [127]. Therefore, in this work, we keep using the frequency change as a measure for the extent of leakage but without over-quantification. In the following sections, the effect of stabilization and squeezing, aging of precursor, as well as soaking electrolyte on the electrolyte leakage from gel probes are systematically studied. An attempt to strengthen the gel probes by co-electrodeposition with TEOS is also demonstrated for reducing the leakage. Comparison among different types of gel probes and microcapillaries is also shown. A main advantage of QCM is that it could be integrated with SGECM and serve as a tool for real-time quality control, as approach-retract curve on a known surface is anyway a necessary check for gel probes before measuring targeted samples. QCM measurements can also provide more direct information than SEM on the leakage, as the latter must be performed after drying the leaked electrolyte.

3.3. Gel probe stabilization

Consistent with what was reported before [75], we systematically observe that the gel probes have to be stabilized by several approach-retract cycles before getting reproducible approach-retract curves. In the SEM image (**Figure 3.3A**), it is clearly seen that the gel probe leaves visible traces on the QC surface in the first 5-6 sampling points before being stabilized. Thanks to the implementation of QCM, the extent of electrolyte leakage can be measured by the

frequency shift before and after each approach-retract cycle. By repeating the cycle, the QCM frequency shift gradually reduces to zero (**Figure 3.6**), which is in good agreement with the SEM observation (**Figure 3.3A**). This confirms that the gel probes could reach a steady state without leaking any more electrolyte on the sample surface.

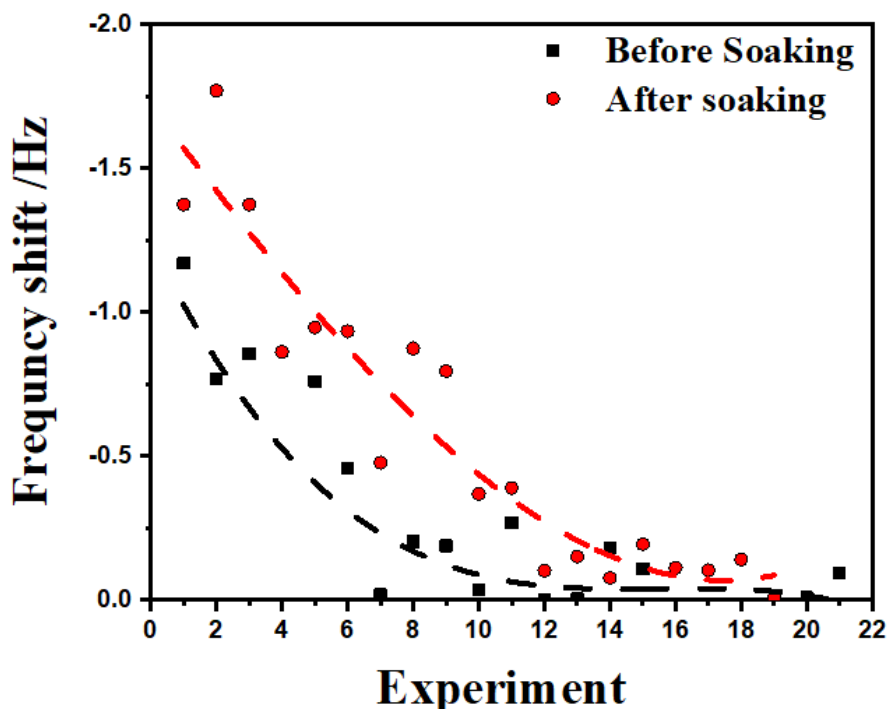


Figure 3.6. Frequency shift of gold QCM after approaching-retracting Type I chitosan gel probe before and after soaking in 1 mM ferrocenedimethanol solution with 0.05 M KCl and 1:1 (vol. ratio) glycerol/H₂O.

Soaking the gel electrode in electrolyte solution is a practical way to functionalize the probe, *e.g.*, by impregnation with redox species. However, the gel probes will swell when immersing in an electrolyte even with the same solvent and ion concentration (compare insets in **Figure 3.3A**). The freshly soaked probes would also naturally contain residue of free electrolyte. These yield much more significant leakage on the sample in the first approach-retract measurements (compare Lines 1&2 in **Figure 3.3A**). Correspondingly, the QCM frequency shift is also much higher compared with that for as-electrodeposited gel probes (**Figure 3.6**). The soaked gel probes could still be stabilized, yet it may take more approach-retract cycles.

Practically, QCM can well indicate the stabilization of the gel probes during approach-retract cycles without the need to wait for the remaining electrolyte to evaporate and to pass the sample to SEM characterizations.

Let's remind that the gel probes are prepared by electrodeposition of chitosan on micro-disk electrodes. Due to the complexity of chitosan as a natural product, it is very difficult to prepare exactly the same deposition solution in different batches. Thus, the electrodeposition conditions need to slightly vary to adapt to obtaining gel probes with well-controlled and reproducible shapes. A practical way to circumvent this limitation is to keep using the same deposition solution as long as possible. But then a question arises: Does the aging of the solution affect the properties of the gel? Comparing the inset photo of **Figure 3.7** with **Figure 3.3A**, it is seen that the aging of the solution does not visibly change the shape of electrodeposited gel under the same deposition conditions. Nevertheless, QCM frequency shift indicates that the gel probes prepared from old precursor solution (15 days) have more leakage of electrolyte in the first approach-retract cycles (**Figure 3.7**) as compared to gel probes prepared from the fresh precursor solution (**Figure 3.6**). It also takes more approach-retract cycles to stabilize the probe. The extent of leakage is similar after soaking ferrocenedimethanol. The results suggest that the gel deposited from old precursor solution is probably less condensed in structure, even though the apparent shape looks similar. This might be related to the poor stability of chitosan in solution [128,129] that increased the heterogeneity of deposits.

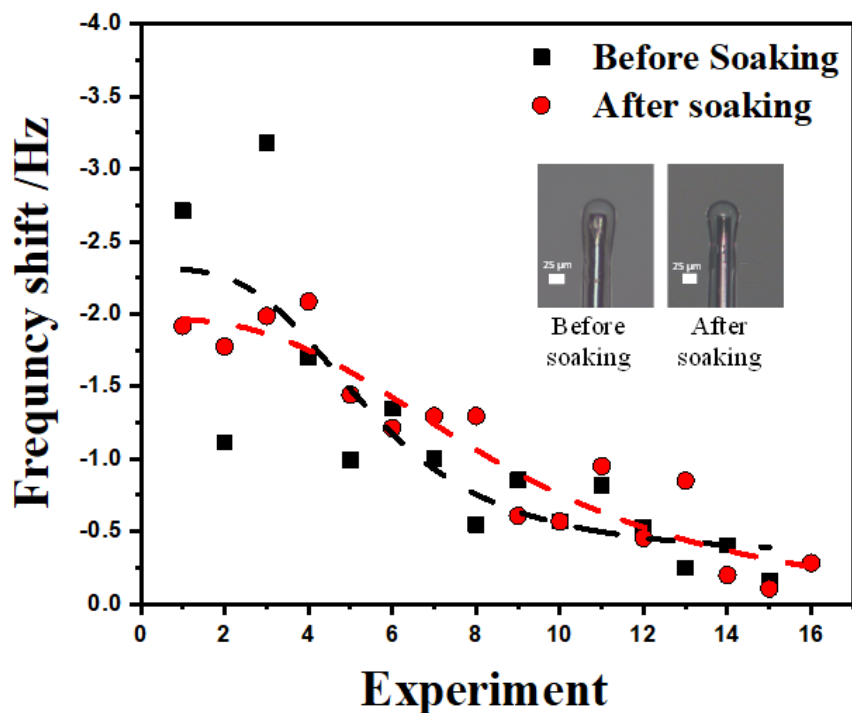


Figure 3.7 Frequency shift of gold QCM after approaching-retracting a Type I chitosan gel probe fabricated from 15 days-old precursor solution, before and after soaking in 1 mM ferrocenedimethanol solution with 0.05 M KCl and 1:1 (vol. ratio) glycerol/H₂O.

3.3. Reinforcement of the gel probe by co-electrodeposition with TEOS

It is systematically seen from the results above that freshly prepared gel probes leak electrolyte on the sample surface during the first approach-retract cycles. Apart from stabilizing it by repeating the cycles while monitoring with QCM, another strategy would be to mechanically reinforce the gel probes to reduce their swelling and thus the leakage of electrolyte solution. A common approach is to form an inorganic-organic hybrid matrix.

TEOS is a promising precursor for this purpose. It has been intensively reported that TEOS-based sol-gel-derived silica could co-deposit with chitosan, improving the mechanical properties of the obtained composite gel [104,130,131]. More importantly, TEOS could also be electrodeposited under similar conditions (yet according to a different mechanism [132]) as chitosan. In the mild acidic precursor, TEOS is in its hydrolyzed form (*i.e.*, Si(OH)₄), and by

applying a suitable cathodic potential, the local pH at the electrode increases yielding the condensation of silica precursors [103,105]. This could perfectly match the electrodeposition of chitosan, which is also based on the local modulation of pH near the cathode. Here, TEOS was added to the chitosan deposition solution and co-electrodeposition was realized as verified by the Si/C ratio from EDX (**Chapter II, Figure 2.5B**).

Figure 3.8 shows the QCM frequency shift of gel probes from co-electrodeposition of chitosan with TEOS (denoted as chitosan-TEOS probe). Only a slight shift of frequency is observed for the first two approach-retract cycles of the chitosan-TEOS probe. Afterwards, the frequency shift is negligible considering the signal drift and accuracy of QCM. This suggests a clear improvement in immobilizing electrolyte as compared with chitosan-only gel probes. Moreover, the chitosan-TEOS probe is also prepared from a 15-day aged precursor. It is clearly seen that the frequency shift becomes much higher, and it is still ineligible even after 15 approach-retract cycles (**Figure 3.8**). This is likely because TEOS is already polymerized in the aged precursor *via* condensation, which is known to be unfavorable for electrodeposition [106,133]. These results suggest that the electrolyte leakage could be reduced by reinforcing chitosan gel probes *via* co-electrodeposition with TEOS, yet the aging of precursor shall be avoided.

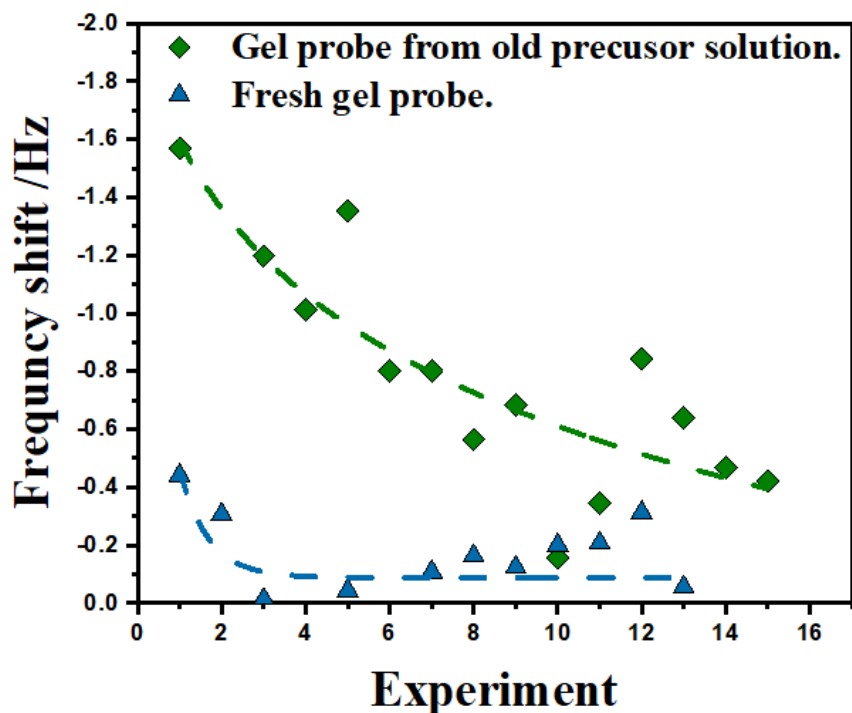


Figure 3.8 Frequency shift of gold QC after approaching-retracting chitosan-TEOS Type I gel probe fabricated from fresh and 15-day-old precursor solutions.

3.4. Squeezing effect

As discussed in our previous work [75], one major advantage of SGECEM is the soft contact between the gel probe and the sample surface, which allows the gel probe to be purposely pressed or retracted after touching the sample. This would alter the contact area and bring an important feature of flexible resolution for local electrochemical measurements. Especially, when the gel probe is pressed against the sample, a risk of squeezing the gel and leaving free electrolyte on the sample surface can be envisaged.

Figure 3.9A shows a typical frequency shift variation curve during approaching-compressing-retracting a Type I chitosan gel probe, where the gel probe is pressed for 6 μm after touching the sample. After a spike at the touching point, the frequency shift continues to increase almost linearly while the gel probe is pressed against the sample. During the retraction, the frequency

shift gradually restores until the gel probe is fully detached from the sample. Transient frequency change of QC during the compression is interesting and may suggest the mechanical properties of the gel. There is an apparent linear relation between compression and frequency shift (compression slop). Several type I gel probes were compressed from 2 to 10 μm . Transient frequency from touching point to maximum compression length is used to calculate the compression slope. Compression slopes of different gel probes using several compression lengths are displayed in **Figure 3.9B**. In almost all tested cases, compression slopes are similar for each gel probe, giving the idea of a linear relation between compression length and frequency change, and this linear relation depends on the gel in the probe. This is similar to Young experiments, where the applied force is directly proportional to the displacement (in the same direction as the force) of an object. According to these results, it may be possible to obtain gel mechanical properties using the compression slope, yet the analysis is beyond the focus of this chapter. Here, we focus on the frequency shift after a complete approach-compress-retract cycle.

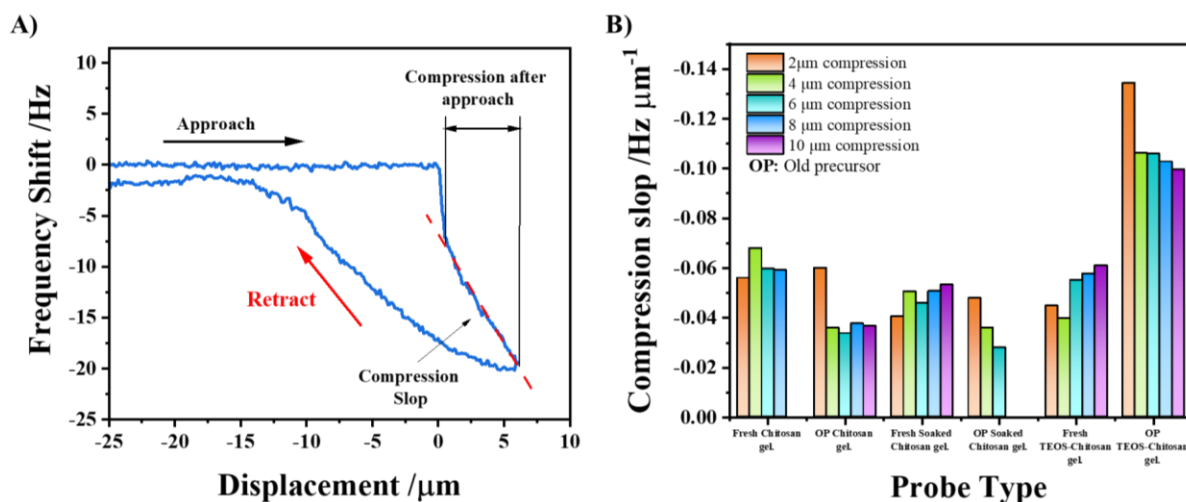


Figure 3.9 Typical frequency shift in approach-compress-retract curve of Type I chitosan gel probe from QCM-SGECM (A). Compression slopes extracted from frequency shift of gold QC curves obtained by approaching-compressing-retracting different Type I gel probes with different distances of compression after touching (B).

Figure 3.10A shows the frequency shift after retracting the stabilized probes from a vertical position where it is pressed for different distances against the QC. It is seen that for all the probes, *i.e.*, the chitosan-only probe, the chitosan probe soaked with ferrocenedimethanol, and the chitosan-TEOS probe, the frequency shift increases as the pressing distance increases. When pressing the probes “gently” for a small distance ($< 6 \mu\text{m}$), it is seen that the probe soaked with ferrocenedimethanol shows more leakage than that before soaking. This is in line with the results in **Figure 3.6**, indicating that the gel soaked in electrolyte solution is less tight.

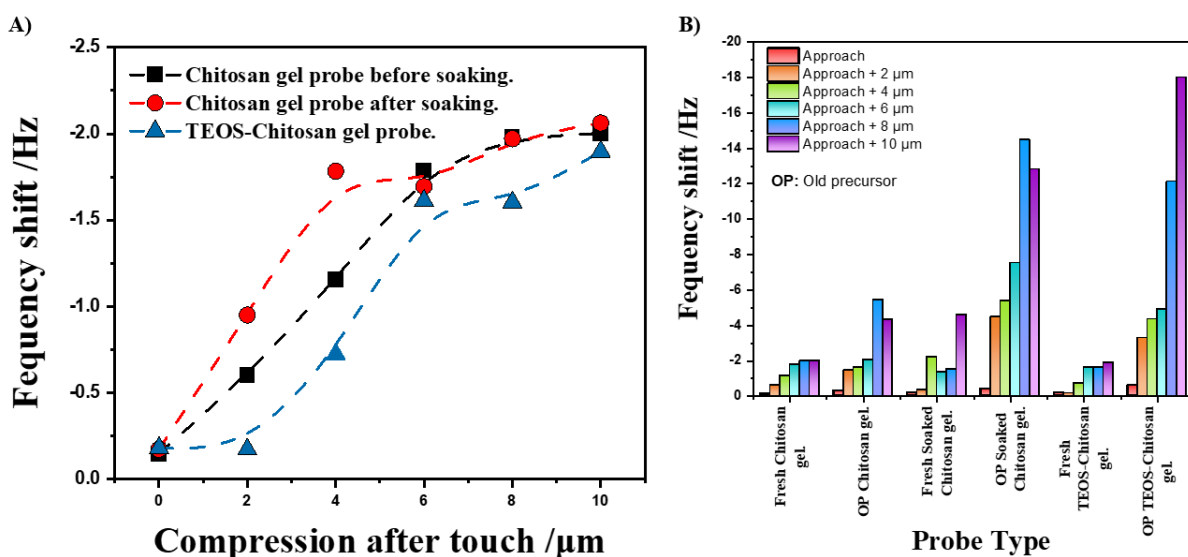


Figure 3.10 Frequency shift of gold QC after approaching-compressing-retracting Type I gel probes with different distances of compression after touching (A). Frequency shift of gold QC after approaching-compressing-retracting different Type I gel probes with different distances of compression after touching (B).

Meanwhile, co-electrodeposition with TEOS would enhance the mechanical properties of the gel and thus contribute to inhibit the wetting. The difference in frequency shift becomes minor when deeply pressing the gel up to 10 μm . Note that the height of a gel probe is usually around 30 μm . That being said, pressing for 10 μm is equivalent to squeezing the gel by *ca.* 30%, which is very harsh for the probe and rarely used in SGECM measurements. The gel probes prepared from aged precursor solutions have much more leakage upon pressing than those prepared from fresh solutions (**Figure 3.10B**). This confirms that aging of deposition solutions

is unfavorable for preparing gel probes.

3.5. Comparison among different probes

Apart from the Type I gel probe that is relatively well studied [75,76], another type of gel probe (Type II) prepared by “electrodeposition + pulling” was recently also reported for carrying out local electrochemical measurements [73]. With the established method by QCM, we compare the leakage of electrolyte using these two types of gel probes as well as classical microcapillary probes.

Figure 3.11A illustrates the frequency shift with the number of approach-retract cycles for Type I, Type II and microcapillary probes with diameter of contact *ca.* 25 μm . It is seen that both Type I and Type II gel probes have a slight frequency shift in the first experiments, but the shift gradually decreases to almost zero after 5 or 6 cycles. Meanwhile, the microcapillary with similar size of droplet has much higher frequency shift, indicating that it leaves much more electrolyte on the QC surface, as expected. Moreover, the frequency shift remains almost constant over approach-retract cycles, which is trivial as the electrolyte is not immobilized and will keep spreading on the sample surface. The leakage is also clearly visible by optical microscope (**Figure 3.12**). The results confirm the advantage of SGECM in immobilizing electrolyte and preventing leakage, which would be useful for quantitative analysis.

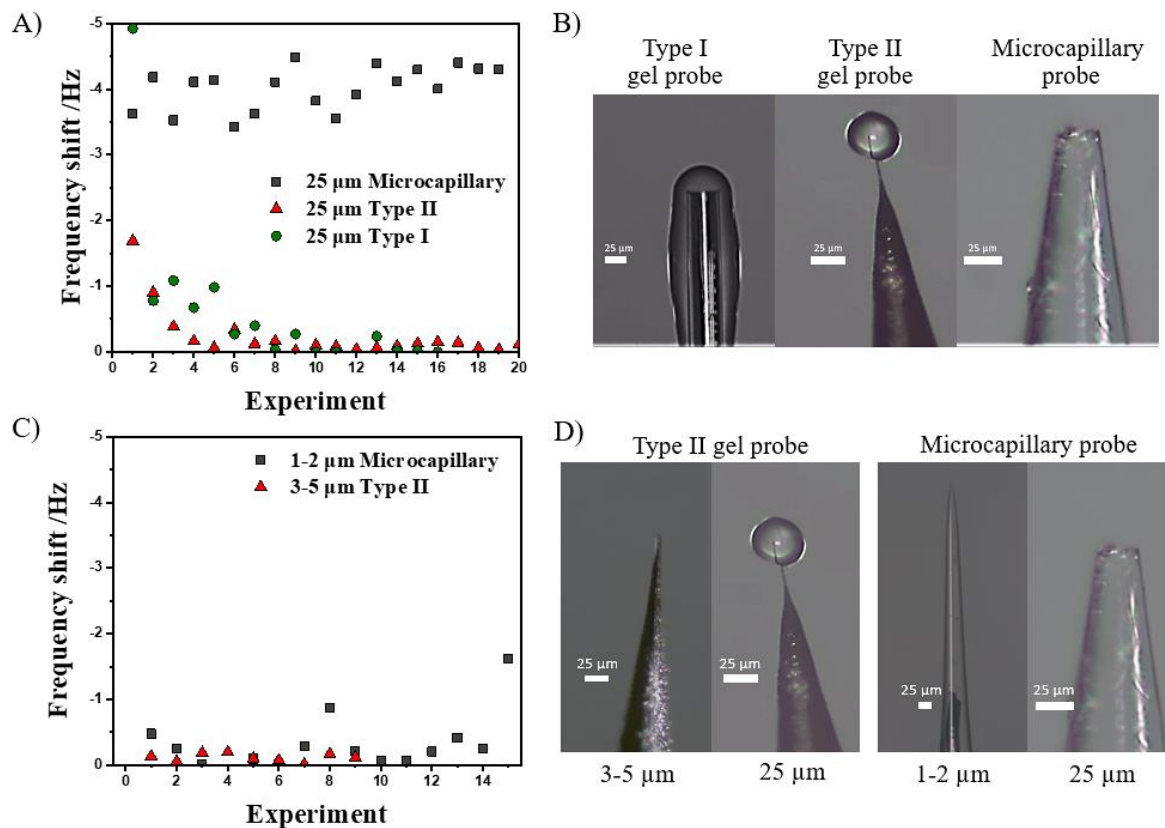


Figure 3.11 Frequency shift of gold QC after approaching-retracting Type I, Type II gel probes and microcapillary with approximately 25 μm diameter contact (A); photos of the probes used in (A) (B). Frequency shift of gold QC after approaching-retracting Type II gel probe of 3-5 μm diameter contact and microcapillary of 1-2 μm opening (C). Photos of the probes used in (C) (D).

On the other hand, it should be noted that Type II and microcapillary probes shown in **Figure 3.11B** are purposely made large for comparison. In practical applications, they can be fabricated to reach much smaller size of contact with the sample, as shown in **Figure 11D**. This could significantly improve the spatial resolution of local electrochemical measurements. **Figure 3.11C** shows that the frequency shift for Type II gel probe with a 3-5 μm diameter of contact is almost negligible even from the first experiment. The microcapillary probe of 1-2 μm opening also shows much less leakage as compared with that of 25 μm, yet the frequency shift is still visible after the experiments. The results suggest that the absolute quantity of leaked electrolyte after an approach-retract experiment can be reduced by reducing the size of

the gel or droplet for Type II or microcapillary probes, respectively. Nevertheless, one should pay attention that at small contact areas, the local electrochemical measurements are also more sensitive to leaked electrolyte.

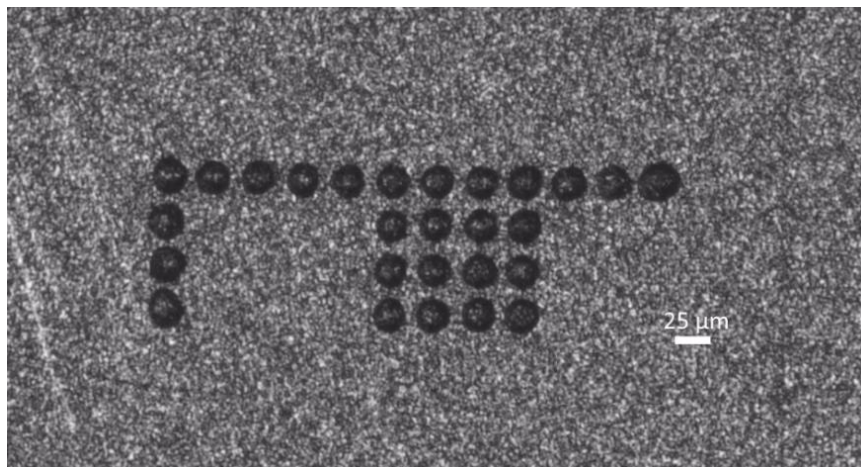


Figure 3.12 *Optical image of the gold-coated quartz crystal after approach-retract curves with a microcapillary of 25 μm diameter opening.*

3.6. Summary

In summary, the integration of QCM with SGECM setup allows tracing the frequency shift of QC samples during the approach-retract of the gel probes. The frequency shift after an approach-retract cycle indicates the absolute quantity of electrolyte remaining on the QC surface, which is confirmed by SEM observation. Taking this response, the electrolyte remaining from different gel probes is systematically studied. It is observed that the freshly prepared gel probes always have electrolyte leakage, especially after soaking redox probes, yet it can be reduced to be invisible (both from QCM frequency shift and SEM observation) after a few approach-retract cycles. This confirms that the gel probes shall be stabilized before serious SGECM measurements. Aging of chitosan precursor would deteriorate the strength of gel and thus increase the electrolyte leakage, while co-electrodeposition of chitosan with TEOS would reinforce the gel and reduce the leakage. Over-approaching the gel would slightly

induce the leakage of electrolyte due to the squeezing effect. The comparison between Type I and Type II gel probes with microcapillary probes indicates that gel probes have much less liquid remaining than microcapillaries at the same contact area with the sample, which can be explained by the immobilization of electrolyte in the gel. This work proposes a method of quality control for gel probes after preparation. Approach-retract on a QC surface can be foreseen as a standard protocol to ensure well stabilization and negligible liquid remaining of gel probes before quantitative SGECM measurements.

Chapter IV

Micro-integrated electrodes for ozone sensing

There is no doubt that SGECM can proportionate insightful results using conductive samples, as evidenced in **Chapters II** and **III**. With the current SGECM setup configuration, however, two main challenges must be addressed: (1) partially non-conductive samples that cannot be approached by current feedback control and (2) two-electrode system that complicates the analysis. The former remains a major challenge to reach quantitative analysis, but the latter could be improved by designing an appropriate configuration. Here, a concentric micro-ring electrode was added to the standard micro-disk electrode used in previous experiments. This micro-integrated electrode (MIE) presents various advantages and this will be discussed in this chapter in view of possible practical application. To achieve this goal, MIE is coated with chitosan gel and soaked in a redox probe solution. The gel-coated MIE (MIE-GC) is exposed to ozone (O_3) gas, which will react with the redox probe in the gel. Concentration ratio changes can be determined by electrochemical techniques using such concentric electrodes. Then, through the change of probe Ox/Red ratio in the gel, the presence of O_3 can be measured. Therefore, MIE-GC soaked in a redox probe is likely to act as an O_3 sensor.

Ozone, a powerful atmospheric oxidant, is of great importance environmentally and industrially [134–136]. It is also of great interest to researchers due to its applications, such as air treatment, water purification, food storage, disinfection of medical instruments, medical treatment, and deodorization [137–142]. Environmentally, the ozone layer is essential for life, protecting the earth from UV radiation. On the other hand, its presence in the lower atmosphere

is toxic (permissible exposure limit 100 ppb, OSHA 1910.1000 Table Z-1). Physicist S. Chapman formulated in 1930 the first photochemical theory for the formation and decomposition of ozone in the atmosphere [143]. Although natural photocatalytic ozone reaction is produced between 15 and 50 km from Earth, nitrogen oxides (NO_x) and volatile organic compounds (VOCs) act as precursors of ozone production in the air. Indoor, O₃ is generated by fax machines, laser printers, photocopiers, and UV disinfection lamps [144–147]. Prolonged exposure to O₃ has been linked to pathologies such as bronchitis, asthma, and cardiopulmonary issues [148–152]. Therefore, through the years, a great effort has been made to achieve an accurate and reliable ozone sensor [153–155]. Several methodologies have been reported to determine O₃, including gas chromatography, electrochemical methods or approaches based on conductivity changes of semiconductors [156–159]. Developed devices go from measuring O₃ presence on large scales [160] to miniaturized sensors operating at a laboratory scale or used to control room air quality [161]. Gas-phase chemiluminescence [162] is highly developed and most widely applied for the analysis of ozone at the lowest concentrations [163–166].

In recent years, a lot of research efforts have been invested in O₃ detection with nanostructured semiconducting thin films. Films built from metal oxides (In₂O₃ [167], SnO₂ [168], ZnO [169], WO₃ [170], etc.) and heterojunctions (V₂O₅/TiO₂ [171], ZnO/ SnO₂ [172]) are used to detect O₃ based on electrical conductivity measurements. These types of oxide films have shown highly efficient responses for ozone sensing, reaching ppm or even ppt detection levels [173]. However, optimal sensor operation condition is normally achieved at elevated temperature, typically in the range of 100–300 °C. Also, high ambient water level often notoriously affects gas sensor response, especially for those who work at low temperature. For example, an In₂O₃

sensor suffered from accuracy drops from 97% to 45% when the humidity degree rose from 0% to 85 % [167].

Besides the above conductivity sensors, there are also few reports on electrochemical (voltammetric/amperometric) methods for ozone gas determination, appearing from late 70s [174]. In most of them, O₃ gas is detected via its reduction on solid electrodes. In most electrochemical sensors, the gas has to permeate through a membrane towards the working electrode to be measured. Various electrode assemblies based on gold [175], Ag/Pt [176], and carbon [177] electrodes, have been proposed. The group of Prodromidis reported an O₃ gas sensor based on the response of polyethylene oxide (PEO)/XI/I₂ (X: Li, Rb) solid redox polymer electrolyte using a two-gold-surface electrode assembly [178]. Instead of the gas permeating through the membrane, O₃ reacts with the iodide species in the bulk electrolyte, producing triiodide species. This results in the increase of the diffusion rate of I₃ to the cathode, where I₃ is reduced to iodide [178].

In this chapter, we investigate the possible use of a micro-integrated electrode coated with chitosan (MIE-GC) and soaked with a suitable redox probe ([Fe(CN)₆]^{3-/4-} system) as ozone sensor. Due to its micrometer size and sensitivity, the gel probe can be adjusted to detect specific analytes by selecting an appropriate redox probe. This makes the gel probe highly versatile as a sensor. Moreover, with the right combination of gel coating and redox probe, the response time can also be improved. MIE-GC is first soaked in solutions containing the redox probe at different concentrations, to corroborate: (1) the possible response that can be observed with such probes, and (2) the effect of probe concentration changes on the obtained responses. Secondly, MIE-GC soaked in different concentrations of redox probe is exposed to a UV-generated ozone environment during a controlled time. Right after every exposition cycle,

cathodic and anodic currents are measured by chronoamperometry. Exposition times can be clearly correlated with the current response. As the redox probe concentration in the gel is restricted, MIE-GC re-soaking is expected to be necessary after several experiments to maintain a measurable activity, and this will be also examined here, including the possible effect of chitosan crosslinking with glutaraldehyde. Even if chitosan is not the most suitable polymer to build an ozone sensor, this work intends to show that MIE-GC can be used as such and, more importantly, that it is possible to explore oxidants or reductants present on surfaces in this way.

4.1. Experimental

4.1.1 Materials and chemicals

The probes were prepared with Pt wires of 25 and 100 μm diameter (99.9% purity, Goodfellow, UK). Borosilicate glass capillaries from Sutter Instruments were used for sealing the probes and making microcapillary probes. The former took BF 150-75-10 (Outer diameter (OD): 1.5 mm, Inner diameter (ID): 0.75 mm) and the latter took B 100-75-10 (OD: 1 mm, ID: 0.75 mm). Microelectrodes were coated using a Pt target (99.9% purity, Quorum Tech, UK).

All the chemicals were used as received without further purification: chitosan (medium molecular weight, Aldrich), glycerol (99%, Sigma), NaNO_3 (99%, Fluka), $\text{Fc}(\text{MeOH})_2$ (98%, Aldrich), KCl (Merck), $\text{K}_3[\text{Fe}(\text{CN})_6]$ and $\text{K}_4[\text{Fe}(\text{CN})_6]\cdot 3\text{H}_2\text{O}$ (>95%, PROLABO).

4.1.2. Micro-integrated electrode fabrication and characterization.

Concentric microelectrodes were built coating 25 μm Pt micro-disk electrodes. The micro-disk electrodes were prepared as described in previous works [76]. A *ca.* 2 to 3 μm Pt (**Figure 4.1A**) coating is applied by sputtering (Q150T Modular Coating Systems, Quorum Tech, UK). Then,

the electrode is gently polished until the Pt wire in the center is exposed and there is no material left connecting the external coating with it. As a result, an integrated concentric ring and a disk electrode are obtained. Optical images (Nikon, Japan) (**Figure 4.1B**), SEM (JEOL IT-500HR/LV, Japan) (**Figure 4.1C**) microscopy and EDX analysis (Oxford Instruments, UK) (**Figure 4.1C and D**) are used to monitor the electrode construction.

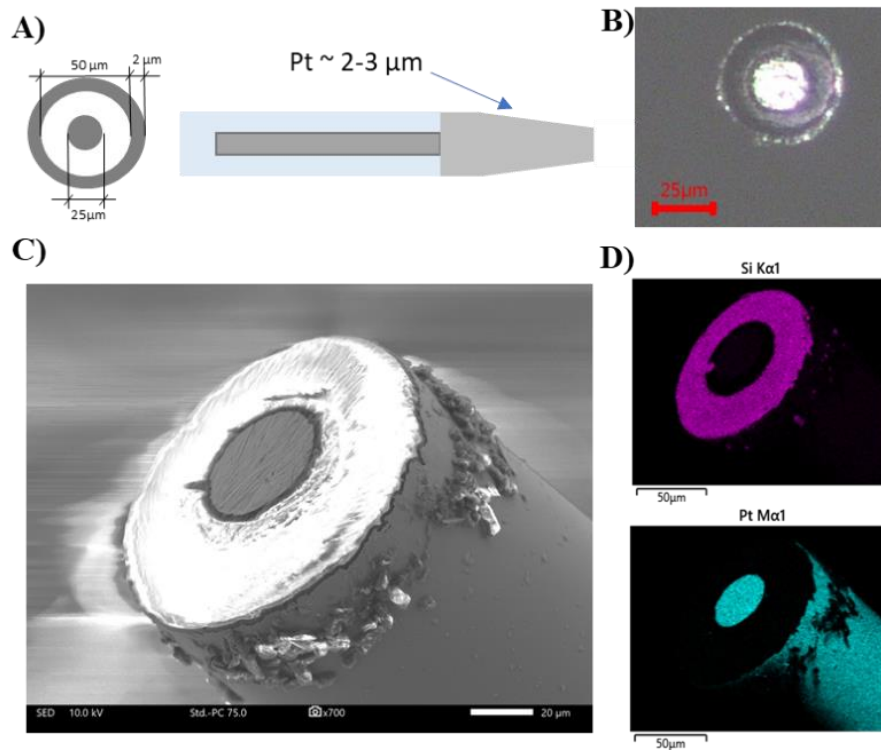


Figure 4.1 Micro-integrated electrode scheme (A), optical image (B), SEM image (C) and Pt (D) and Si (E) EDX map.

4.1.3. Electrochemical measurements.

Cyclic voltammetry and chronoamperometry experiments were performed using a potentiostat (PalmSens3, The Netherlands). Two electrochemical cell configurations were used to test the MIE. The first uses the micro-disk electrode from the MIE as working electrode (WE), platinum wire as counter electrode (CE) and Ag/AgCl as quasi reference electrode (QRE). The second uses the two electrodes from the MIE. The micro-disk electrode as WE and the

concentric Pt ring electrode as CE (with a Ag/AgCl QRE), or CE+RE. Test solutions were prepared with a concentration of 0.1 M KCl and various concentrations of $K_3[Fe(CN)_6]$ and $K_4[Fe(CN)_6]$ (from 0 up to 25 mM) using a 1:1 glycerol/H₂O mixture as solvent. Cyclic voltammeteries were performed between -0.6V and +0.6V Ag/AgCl QRE vs Pt ring electrode (depending on the experiment) at 10mV/s. Chronoamperometries were performed using the two electrodes in the MIE, the micro-disk electrode as WE and the concentric Pt ring electrode as CE+RE. For ozone sensing experiments, an ozone chamber generator by UV light was used (NOVASCAN USA).

4.2. Electrochemical behavior of micro-integrated electrodes

Micro-integrated electrodes used in this work were built in our laboratory. Their utilization as a 2-electrode and electrolyte gel-confined system is not common. Therefore, before anything, characterizing MIE electrochemical behavior is needed. With this objective, MIE was used and tested in three setups. The first one (**Figure 4.2A**) is a conventional 3-electrode setup using a MIE micro-disk electrode as WE. This configuration is normally used to test micro-disk electrode response. Here, testing the MIE using this configuration, has the objective to establish a comparison point of results with the next two configurations. In **Figure 4.2B** a 2-electrode configuration is represented, using a central micro-disk electrode as WE and external Pt coating as CE+RE. Although this setup does not have a particular application in this work, it becomes helpful to determine the viability of using Pt coating as CE+RE. The last configuration (**Figure 4.2C**) is, again, a 2-electrode arrangement (as in the previous configuration). With the electrolyte confined at the tip of the probe, the external Pt coating is only partially exposed to the electrolyte, acting as micro-ring electrode in this configuration.

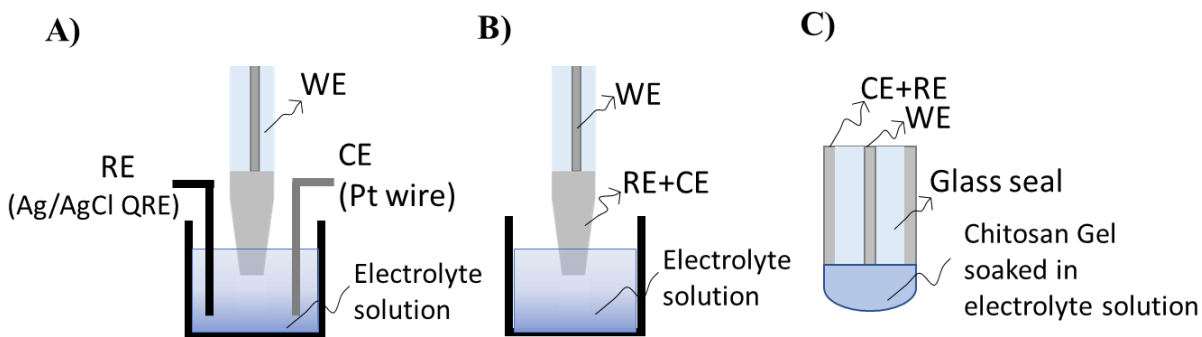


Figure 4.2 Scheme of micro-integrate electrode tested setup 3-electrode (A), 2-electrode (B) and 2-electrode with electrolyte confined in gel form (C).

As was mentioned before, 3- (**Figure 4.2A**) and 2-electrode (**Figure 4.2B**) configurations aim to determine the effects of replacing Ag/AgCl QRE plus Pt wire by the Pt coating as CE and RE. They were first characterized using ferrocenedimethanol ($\text{Fc}(\text{MeOH})_2$) as a model redox probe. The test was carried out using these two setups to record CV from 0V to 0.35V in 25mM $\text{Fc}(\text{MeOH})_2$, 0.1M KCl, 1:1 glycerol/ H_2O solution (**Figure 4.3**). Later, the experiment was repeated with the third configuration, where the external Pt coating conforms a ring electrode used as CE+RE. For both, 3- and 2-electrode configurations, cyclic voltammograms recorded in bulk solution (under the same conditions) are similar. This response matches micro-disk electrode behavior, widely studied in the past [31,86,179]. Where the current is given by **equation 5.1** [21]

$$I_{T,\infty} = 4nFC^*Da \quad \text{equation 5.1}$$

where n is the number of electrons exchanged in the redox reaction, F is the Faraday constant, D is the diffusion coefficient of the redox species in solution, C^* is the concentration in solution and a is the radius of the electroactive surface of the electrode.

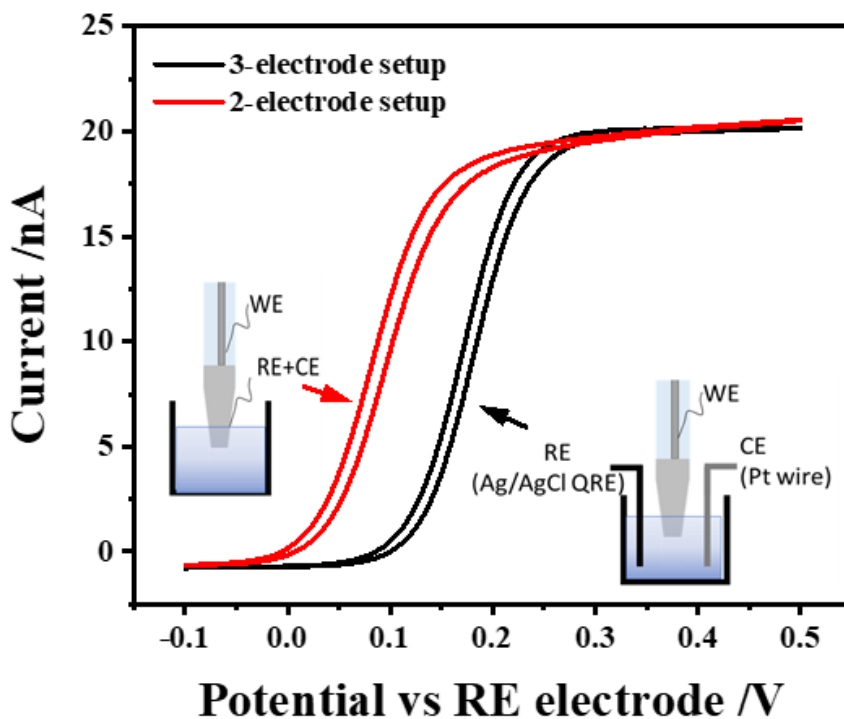


Figure 4.3 Cyclic voltammograms recorded using MIE 3- and 2-electrode configurations in 25 mM $Fc(MeOH)_2$, 0.1M KCl 1-1 glycerol/ H_2O solution at 50 mV/s.

Even if **Figure 4.3** is considered just as a quality control of the MIE, it also adds highly important information. General microelectrodes theory is based on a 3-electrode configuration, and, as a result, the counter electrode (CE) does not interfere either in the current distribution or in the diffusion of redox species. There is a high risk that could happen when CE is placed near the WE (WE and CE+RE are separated *ca.* 13 μ m in the MIE 2-electrode configuration). WE response indicates that, in bulk solution, the small separation between CE and WE does not affect its behavior. Later, in this work, we will analyze what happens when the electrolyte is confined to a small volume.

Due to differences in the nature of the REs, CV presents a shift in the mid-wave potential but is still characterized by the same limiting current values. No effect of the short distance between WE and CE in a 2-electrode configuration can be spotted. However, when the experiment is performed in a reduced volume (instead of bulk solution) we will have a different

response. This matter will be further discussed below.

Figure 4.4A shows the cyclic voltammograms obtained at various concentration ratios of redox probes in bulk solution using a MIE. The central micro-disk electrode acts as working electrode, while the external coating as counter and reference electrode. As shown, MIE response in bulk solution is consistent with a micro-disk electrode used in a standard 3-electrode electrochemical set-up. Several $[\text{Fe}(\text{CN})_6]^{3-}/[\text{Fe}(\text{CN})_6]^{4-}$ (redox probes) ratios were tested, confirming the correlation between the redox probes concentrations and their limiting currents recorded in bulk solution. A list of redox probe and electrolyte concentrations can be found in **Table 4.1**.

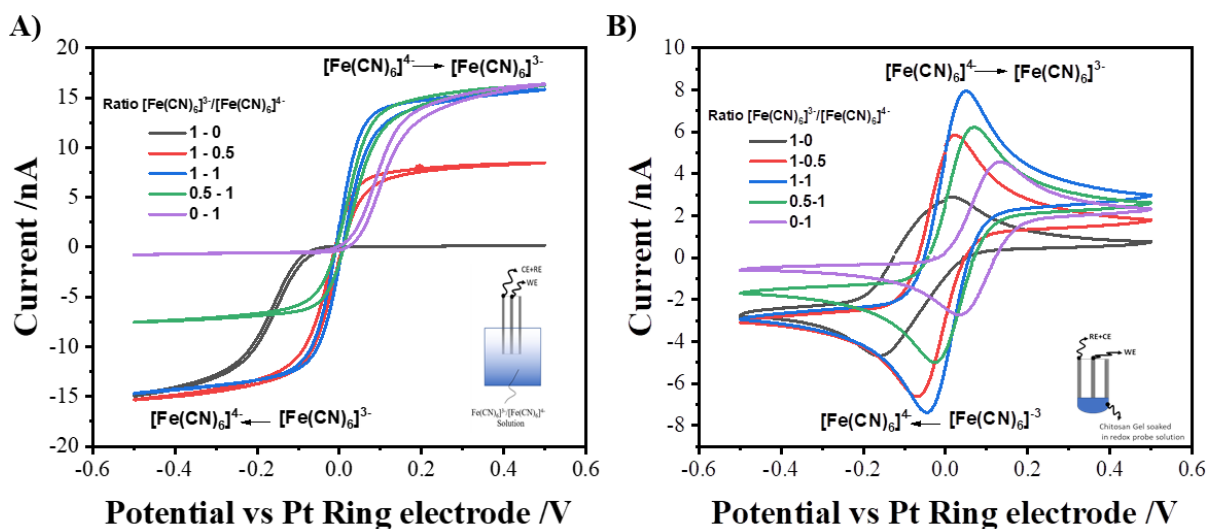


Figure 4.4 Cyclic voltammetry recorded at 10 mV/s using several $[\text{Fe}(\text{CN})_6]^{3-}/[\text{Fe}(\text{CN})_6]^{4-}$ concentration ratios, 0.1M KCl, 1:1 glycerol/ H_2O solution of MIE in bulk solution at 50 mV/s (A) and MIE-GC at 10 mV/s (B).

Table 4.1. Composition of solutions prepared to get results of **Figure 4.4**.

Solution	Volume /mL			Concentration/mM	
	[Fe(CN) ₆] ³⁻ *	[Fe(CN) ₆] ⁴⁻ *	KCl **	[Fe(CN) ₆] ³⁻ *	[Fe(CN) ₆] ⁴⁻ *
A	0.750	0.000	0.750	25	0
B	0.750	0.375	0.375	25	12.5
C	0.750	0.750	0.000	25	25
D	0.375	0.750	0.375	12.5	25
E	0.000	0.750	0.750	0	25

*with 0.1 M KCl in 1-1 Gly-water ** 0.1 M in 1-1 Gly-water

Cathodic and anodic limiting currents reach their maximum (absolute) values according to the respective concentrations of reduced and oxidized species in the solution. At a concentration of 25 mM ferrocyanide and 0 mM ferricyanide (respectively, maximum and minimum concentrations used in the experiment) the curve 0-1 $[\text{Fe}(\text{CN})_6]^{3-}/[\text{Fe}(\text{CN})_6]^{4-}$ is obtained, with an anodic current of *ca.* 15 nA and no noticeable cathodic current. Current values from the various redox probe concentration ratios vary in this interval depending on the concentration of each of them. MIE thus offers a good configuration for determining redox probe concentration ratios. A similar experiment was carried out by fixing one redox probe concentration while the other was slightly modified (**Figure 4.5**). The results and general behavior match well with those obtained in the experiment described above, confirming the successful use of MIE to evidence red/ox concentration variations when operating with the disk as WE and the ring as RE+CE.

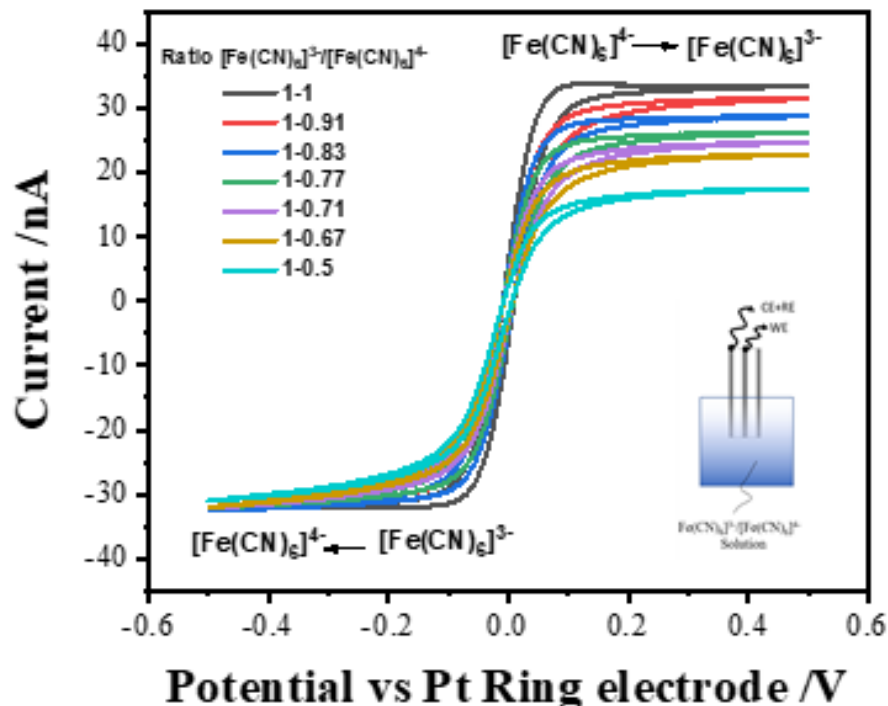


Figure 4.5 Cyclic voltammetry recorded at 10 mV/s using several $[\text{Fe}(\text{CN})_6]^{3-}/[\text{Fe}(\text{CN})_6]^{4-}$ concentration ratios, 0.1M KCl, 1:1 glycerol/H₂O solution of MIE in bulk solution at 50 mV/s

To build a micro-sized electrochemical cell using MIE without solution, the electrode was now coated with chitosan polymer by electrodeposition. To control as much as possible the area of both electrodes, only the tip is coated. Using the micro-disk platinum electrode in the tip as cathode, chitosan is polymerized from a precursor solution at constant potential. Condensation can be controlled to obtain a semispherical form that covers only the tip. The gel can be (with some limitations depending on the gel of choice) further soaked in electrolyte solutions if needed. As a result, the gel-coated micro-integrated electrode (MIE-GC) becomes a micrometer-sized 2-electrode electrochemical cell, where the electrolyte is confined in a gel form in contact with a micro-ring and a micro-disk electrode (**Figure 4.2C**).

MIE-GC was soaked in solutions containing the redox probes at various concentration ratios of $[\text{Fe}(\text{CN})_6]^{3-}/[\text{Fe}(\text{CN})_6]^{4-}$, and it was kept in the atmospheric conditions before recording CV curves. Results are shown in **Figure 4.4B**. As in **Figure 4.4A**, CV response shows a






dependency with the $[\text{Fe}(\text{CN})_6]^{3-}/[\text{Fe}(\text{CN})_6]^{4-}$ concentration ratios soaked in the MIE-GC. Even though, visually, the shape of the cyclic voltammograms obtained using the MIE-GC set-up recalls a more classical CV shape from 3-electrode systems; its analysis cannot be carried out as if they were such. CVs obtained with the MIE-G present, in all the cases, two peaks, an anodic and a cathodic one.

The peak currents have been measured from their baseline and values varied in function of the redox probe concentration ratios, but no correlation between peak current values and these ratios can be found. For example, the most obvious case is the apparition of a peak (either cathodic or anodic) when the concentration of one of the redox probes soaked in the MIE-GC is zero. Such peak should not exist. Then, one can deduce that the presence of this peak and its current value are not related to the concentration ratios of redox probes in the gel. It is more likely related to the confined 2-electrode system used to perform the measurements. Normally, in a 3-electrode system, one does not pay attention to CE reactions, but 2-electrode configurations demand the analysis of the CE. During CV, not only WE potential is changing, but CE potential does it too. In a micrometer-sized system, this can lead to responses that are not totally accurate. At least using a technique where the potential is in constant change and diffusion layer thickness [72] is so close to the dimensions of the system.

Although a deep analysis is still ongoing, one can still obtain useful information from soaked MIE-GC cyclic voltammetry experiments. By comparison of the results obtained in the bulk and confined systems (**Figure 4.4A and B**), a similar behavior/shape can be spotted at high overpotentials. As the overpotential increases or decreases during the potential scan, there is a tendency in the confined system to achieve a pseudo-limiting current. Pseudo cathodic limiting current ($I_{L,c}$) and pseudo anodic limiting current ($I_{L,a}$) from CV of confined MIE-GC soaked in

different redox probes concentration ratios are given in **Table 2**. Measured $I_{L,c}$ and $I_{L,a}$ shows a better correlation with redox probes ratios than the corresponding peak currents. The analysis of similar devices can help to explain this and indicate if CV is the correct technique to use in such device.

Table 4.2 Pseudo-cathodic and anodic limiting current values obtained from MIE and MIE-GC based on cyclic voltammograms recorded (**Figure 4.4**) from solutions as in **Table 4.1**.

Ratio	MIE CV in bulk solution (scan rate 50 mV/s)			Soaked MIE-GP CV (scan rate 10 mV/s)		
	$I_{L,a}/nA$	$I_{L,c}/nA$	$ I_{L,a}/I_{L,c} $	$I_{L,a}/nA$	$I_{L,c}/nA$	$ I_{L,a}/I_{L,c} $
 1-0	0.08	-18.94	0.0	0.27	-1.287	0.2
 1-0.5	9.803	-18.55	0.5	0.79	-1.224	0.6
 1-1	16.6	-17.01	1.0	1.47	-1.429	1.0
 0.5-1	18.1	-8.47	2.1	1.41	-0.76	1.9
 0-1	16.91	-0.5	$\rightarrow\infty$	1.31	-0.093	$\rightarrow\infty$

Some similarities can be found between MIE-GC configuration and interdigitated electrode arrays (IDA). Its theory has been studied by Aoki *et al.* and Compton *et al.* although they investigated 4-electrode configurations. IDA analysis can be partially applied to the MIE-GC. Studies were focused on the analysis of generator–collector mode, emphasizing how the distance between the electrodes affects the response. While Aoki described the stationary state chronoamperometry response, Compton focused on the cyclic voltammetry response of ring-interdigitated electrodes. AS in the systems studied by Aoki and Compton groups, the current sampled at a two concentric microelectrodes system is influenced by the migration of electrogenerated species from the WE to the CE. In 4-electrode configurations, electrochemical reactions at the CE are considered fast enough not to influence those carried out on the WE. This is different when working in a 2-electrode configuration. CE reactions may interfere with the WE response. Aoki demonstrated that a steady state can be reached in an interdigitated band array electrode [180] and Compton extends this theory [181] to concentric ring

electrodes. Based on these results, we can assume that chronoamperometry will correspond to the stationary MIE-GC stationary state. Therefore, chronoamperometry is a more suitable tool to use for the analysis of variation of redox probes concentration ratios at MIE-GC.

4.3. Chronoamperometry using gel coated micro-integrated electrodes

As aforementioned, chronoamperometry could be a suitable tool for performing analysis with MIE-GC. For this, one should determine the most suitable constant potential to apply and how long. Early CV experiments, shown at the beginning of this work, have been of great help for this. From MIE in bulk solution and soaked MIE-GC, cyclic voltammograms recorded using diverse redox probes concentration ratios indicated that one can reach steady current values below -0.5 V and above 0.5 V *vs.* Pt ring electrode (**Figure 4.4B**). Thus, chronoamperometries have been performed by applying -0.5 V and +0.5 V *vs.* Pt ring electrode for 30 s. It was empirically observed that this time is enough to reach a steady current value. Working with this methodology also gives us a common point of current comparison between cyclic voltammetry and chronoamperometry. In chronoamperometry, we denoted I_c to the steady cathodic current values obtained by applying -0.5 V *vs.* for 30s and, analogously, I_a when the applied potential was 0.5 V, both potentials being given *vs.* Pt ring electrode. Here, steady-state currents I_c and I_a will be evaluated to analyze their correlation with the concentration of redox probes in the MIE-GC.

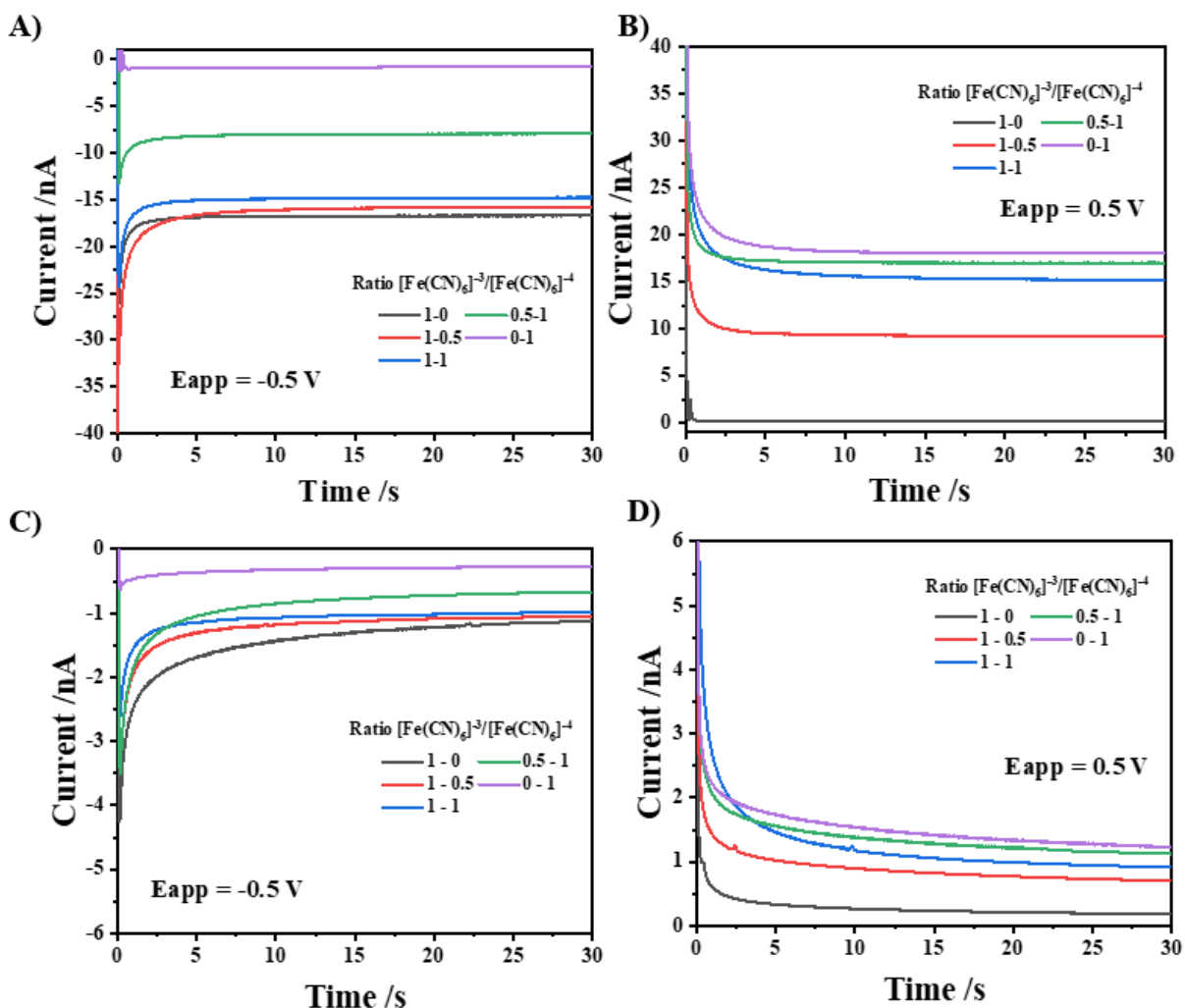


Figure 4.6 Chronoamperometry using several $[\text{Fe}(\text{CN})_6]^{3-}/[\text{Fe}(\text{CN})_6]^{4-}$ concentration ratios, 0.1M KCl 1-1 glycerol/ H_2O solution of MIE in bulk solution (A-B) and MIE-GC (C-D).

Figure 4.6 shows chronoamperometry data obtained from media (solutions or gels) containing the $[\text{Fe}(\text{CN})_6]^{3-}/[\text{Fe}(\text{CN})_6]^{4-}$ redox probes at distinct concentration ratios using two kinds of electrodes: (1) MIE while immersed in the solution and applying -0.5 V (**Figure 4.6A**) or 0.5 V (**Figure 4.6B**); (2) MIE-GC previously soaked in solution but kept in ambient conditions while measuring currents upon applying -0.5 V (**Figure 4.6C**) or 0.5 V (**Figure 4.6D**). In each case, steady state current was named I_c and I_a as it was explained before. The composition of redox probes solutions used in this experiment can be found in **Table 1**.

I_c and I_a values can be well correlated to $[\text{Fe}(\text{CN})_6]^{3-}/[\text{Fe}(\text{CN})_6]^{4-}$ (redox probes concentration

ratios). Going from a maximum I_c current when the redox probes ratio is 1 to 0 (*i.e.*, only $[\text{Fe}(\text{CN})_6]^{3-}$) and a maximum I_a when 0 to 1 (*i.e.*, only $[\text{Fe}(\text{CN})_6]^{4-}$). Nevertheless, as expected, I_c and I_a values recorded from MIE and MIE-GC systems are not equal, whereas I_c/I_a ratios from both configurations are very similar and directly related to redox probes concentration ratios. Thus, one could use chronoamperometry in these experimental conditions as a tool to follow changes in $[\text{Fe}(\text{CN})_6]^{3-}/[\text{Fe}(\text{CN})_6]^{4-}$ concentration ratios in the MIE-GC.

The current response obtained by chronoamperometry from MIE in bulk solution differs at least by one order of magnitude from when the solution is soaked in the gel of a MIE-GC. There is a clear impact of the electrolyte confinement in the recorded current. A possible factor that influences this response is the distance between electrodes. Confinement of the electrolyte could provoke an overlapping of the diffusion layers, interfering with each other. Compton et al. [173] have shown the effect of diffusion layer interference in the total current using microelectrodes arrays. Recording cyclic voltammeteries at different distances between the microelectrodes in the array. As the distance between them decreased, the total current did it as well. The work was carried out using a 3-electrode system. Therefore, the diffusion layer interference analysis in microelectrode arrays cannot be directly compared to the effect of electrolyte confinement in a MIE-GC. Yet the principle, of total current diminution due to the overlapping of diffusion layers, could help to explain the results obtained when the electrolyte is confined in a MIE-GC. Another factor that affects the total current value is the CE area. While in MIE-GC the CE and WE areas are similar (*ca.* $2 \times 10^{-9} \text{ m}^2$), it is not the case in bulk solution experiments as there the CE is much bigger than WE. Even if geometrical areas are equal, electrochemical areas may not. This is a critical aspect to consider in MIE fabrication. One must always ensure that the CE area is bigger than the area of the WE. This way, one can

be sure that the results obtained with the MIE-GC are not affected by the CE area. Lastly, if we compare I_c with $I_{L,c}$ and I_a with $I_{L,a}$, the values are similar. So, the use of CV should not be completely discarded as a MIE-GC analysis technique. In particular, for the system proposed in this work, using CV requires (as mentioned before) more investigation. And the information that we are looking for can be obtained easily using chronoamperometry. Yet, when electrochemical reactions in MIE-GC may have higher complexity than those addressed in this work, a deeper understanding of micro-sized 2-electrode configuration setups will be needed.

4.4. Ozone detection by integrated electrodes.

Until here, $[\text{Fe}(\text{CN})_6]^{3-}/[\text{Fe}(\text{CN})_6]^{4-}$ concentration ratio in MIE-GC was controlled by soaking. With this methodology, we were able to demonstrate that this configuration can measure changes in the redox probe concentration ratios, using CV (yet requiring further analysis) or chronoamperometry. A logical next step would be to study the MIE-GC response when the redox probes concentration ratio is changed due to an electrochemical interaction with a substance (in solution or onto a surface). For this, we took advantage of the well-known oxidant power of ozone gas. Ozone can be generated by UV radiation (ozone generation chambers are used for material sterilization, for instance).

MIE-GC is firstly soaked in a 25 mM $\text{K}_4[\text{Fe}(\text{CN})_6]$ and 0.1M KCl solution (1-1 glycerol/ H_2O), then placed inside the ozone chamber (**Figure 4.7A**). The gel probe is then exposed to an ozone atmosphere generated by UV radiation. O_3 gas, surrounding the gel surface, will react with $[\text{Fe}(\text{CN})_6]^{4-}$ ions in the gel (by oxidizing them). After a defined time in the chamber, MIE-GC is immediately removed to perform electrochemical analyses in ambient conditions. As some $[\text{Fe}(\text{CN})_6]^{4-}$ ions are expected to have been oxidized into $[\text{Fe}(\text{CN})_6]^{3-}$ by the strong oxidant ozone, the $[\text{Fe}(\text{CN})_6]^{3-}/[\text{Fe}(\text{CN})_6]^{4-}$ concentration ratio in the gel probe has changed, and it

should be determined by chronoamperometry or CV. As was shown earlier (**Figure 4.4B**), CV response dependency from redox probes concentrations ratios can be observed, particularly, in what was previously denoted as $I_{L,a}$ and $I_{L,c}$. Both currents show a straightforward relation with the ozone exposition time. The same results have been obtained from chronoamperometry measurements. **Figure 4.7A** and **B** presents I_c and I_a obtained by chronoamperometry using either MIE in solution or the probe-soaked MIE-GC electrode (respectively) using several $[\text{Fe}(\text{CN})_6]^{3-}/[\text{Fe}(\text{CN})_6]^{4-}$ concentration ratios. They show clearly that chronoamperometry is a good tool to analyze the change in redox probe concentration ratios induced by reaction with ozone.

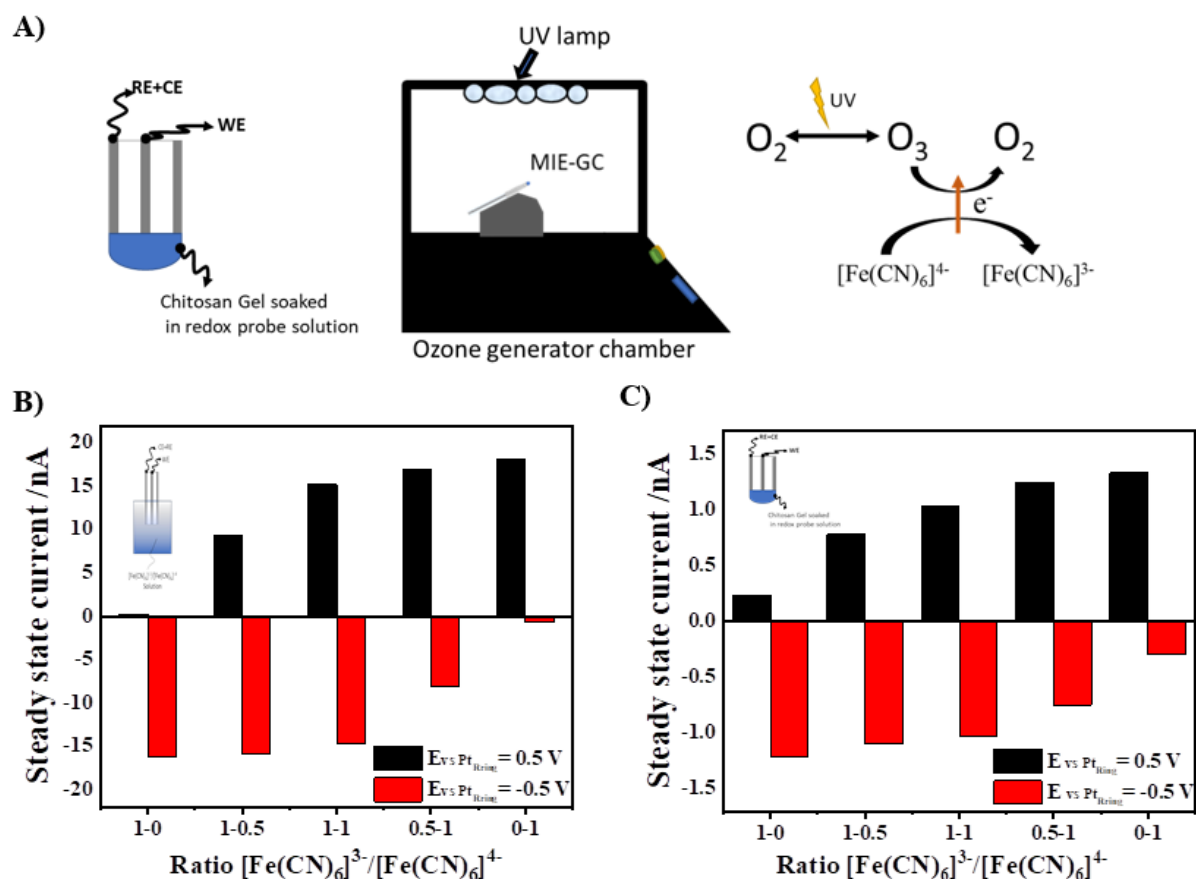


Figure 4.7 MIE-GC ozone application and reaction scheme (A), I_c and I_a obtained by chronoamperometry using several $[\text{Fe}(\text{CN})_6]^{3-}/[\text{Fe}(\text{CN})_6]^{4-}$ concentration ratios, 0.1M KCl 1-1 glycerol/H₂O solution of MIE in bulk solution (B) and MIE-GC (C).

Figure 4.8 shows the obtained I_a and I_c values recorded by chronoamperometry at applied potentials of 0.5 V (**Figure 4.8A**) and -0.5 V (**Figure 4.8B**), using MIE-GC soaked in $[\text{Fe}(\text{CN})_6]^{4-}$ solution, before and after consecutive ozone exposition cycles in the O_3 chamber. As the $[\text{Fe}(\text{CN})_6]^{4-}$ is converting into $[\text{Fe}(\text{CN})_6]^{3-}$, I_c values increased while I_a decreased. This behavior can be more clearly observed in **Figure 4.8C**.

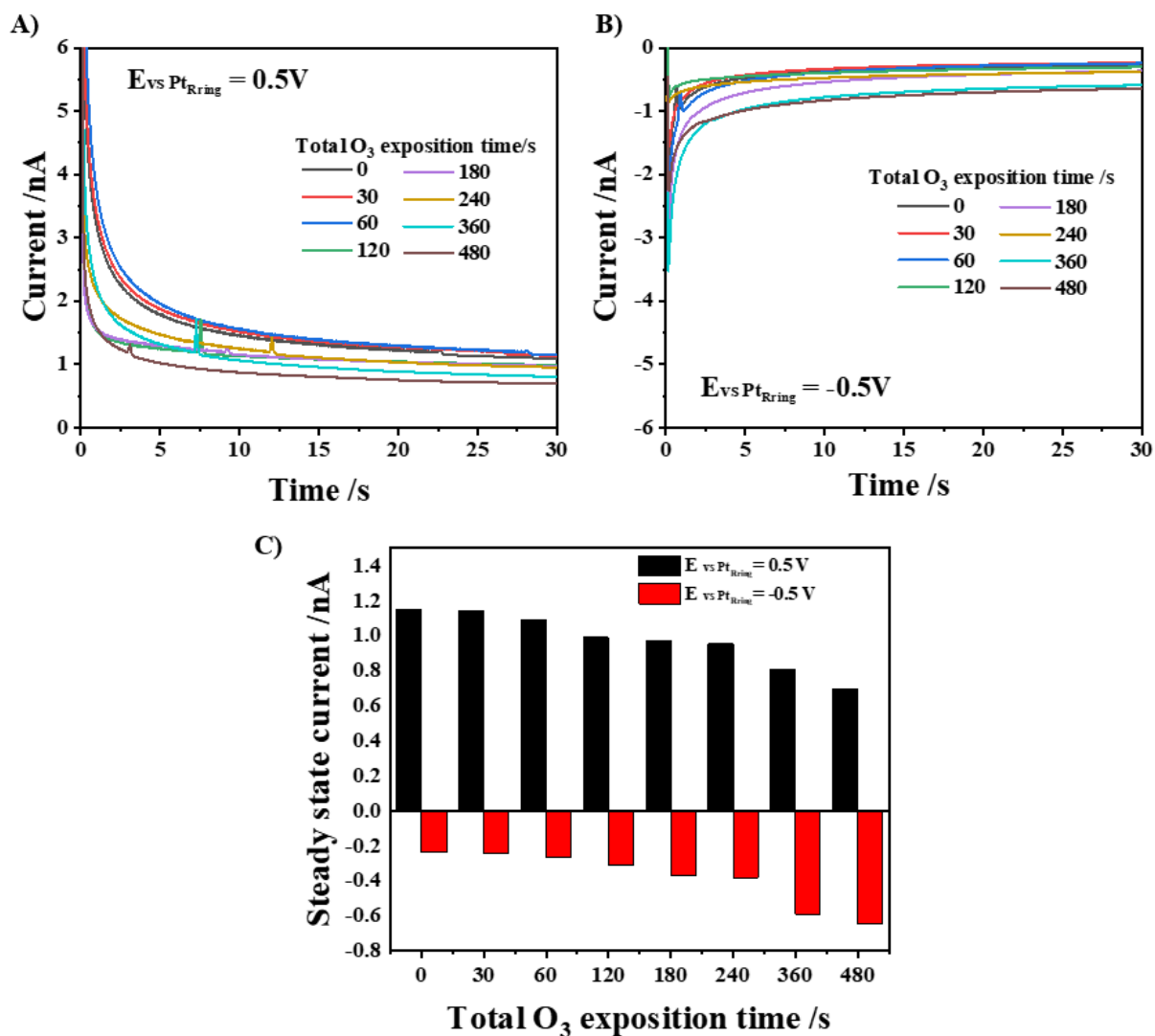


Figure 4.8 MIE-GC chronoamperometries of a soaked MIE-GC in $[\text{Fe}(\text{CN})_6]^{4-}$ at different periods of ozone exposition, as recorded at applied potentials (E_{app}) of respectively 0.5V (**A**) and -0.5V (**B**); corresponding variation of I_a and I_c with ozone exposition time (**C**).

There is no doubt that through chronoamperometry, one can follow the effect of ozone over the CME-GP using a redox probe immobilized in the gel electrode. Furthermore, because of the MIE-GC nature and size and selecting the adequate hydrogel-redox probe, this methodology could be used to study redox-active surfaces by scanning gel electrochemical microscopy [69].

Two undesirable effects may result from placing the MIE-GC inside the O₃ generator chamber: (1) side reactions that may affect the gel due to direct exposition to UV light, and (2) ozone could be soaked in the gel. The first will be addressed in the next section of this chapter. To study the latter, the MIE-GC was kept inside the chamber between ozone exposure cycles, and chronoamperometries measurements were performed without removing the gel probe from the chamber. The results (**Figure 4.9**) indicate that with an increase in the number of exposure cycles, the increase in I_c is several times greater than the decrease in I_a . It seems like the I_c value is not solely a consequence of the reduction of the oxidized redox probe concentration in the gel anymore. It is highly likely that O₃ gas was dissolved in the gel and diffused towards the electrode surface, leading to an increase in I_c beyond what would be expected by observing I_a reduction.

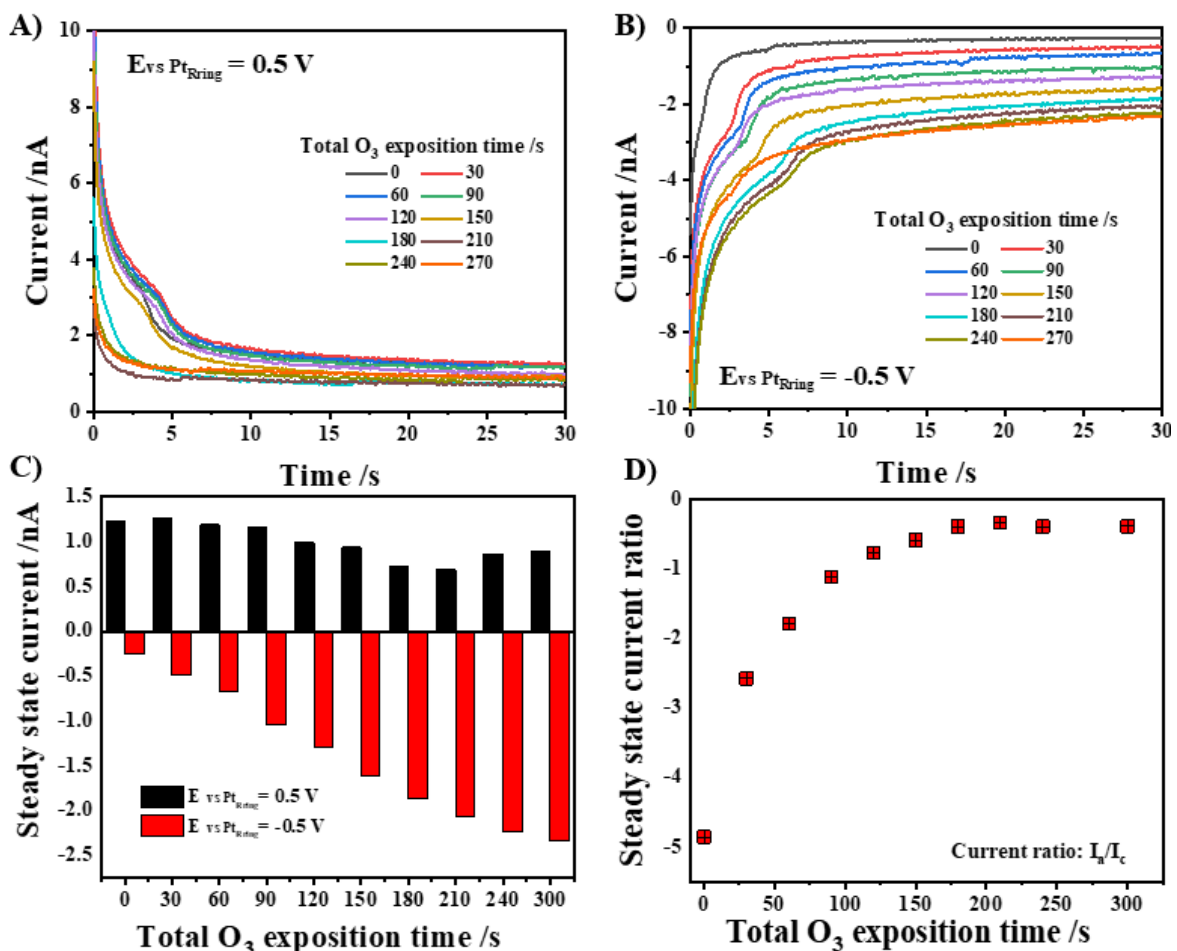


Figure 4.9 MIE-GC chronoamperometry data obtained without removing the electrode from the ozone chamber, for a $[Fe(CN)_6]^{4-}$ -soaked MIE-GC undergoing different periods of ozone exposition; measurements have been performed at applied potentials of respectively 0.5V (A) and -0.5V (B), and corresponding I_a and I_c values (C) and their relative ratios (D).

4.5. Improving the durability of integrated electrodes

4.5.1. MIE-GC ozone exposition with UV protection

Using an ozone generator chamber has plenty of advantages: easy to use, high ozone concentration atmosphere and no need for special adaptation or device for placing the MIE-GC inside the chamber. However, is possible that UV radiation may affect the gel coating. It is well known that a combination of ozone and UV radiation is a powerful tool for water and surface disinfection. So, it is easy to think that chitosan, a natural organic polymer, would be affected as well by the UV radiation. If this is as such, two scenarios are possible: (1) polymer

-affected or not by UV radiation- does not produce any additional electroactive species, and (2) electroactive species are produced. The first one, would not interfere with the electrochemical response of the device, thus it will not be considered as a problem. Mechanical properties may be affected, but such investigation is beyond the scope of this work. The former is the most harmful. Here, one indeed realized that the electrochemical response is affected by UV radiations (**Figure 4.10**), and therefore another ozone source needs to be found.

To test UV radiation's influence over the experiment, a cage for the MIE-GC was built. This “UV protection” was designed to block the direct incidence of the UV lamp while ozone can flow freely through the whole chamber volume. So, the atmosphere surrounding the electrode is similar to the previous experiments in this work. Experiments were performed as before, cycles of leaving MIE-GC in the ozone chamber (now with and without UV protection) for a selected time and performing chronoamperometry afterward.

As shown in **Figure 4.10A**, there is a change of behavior in the MIE-GC response right after taking UV protection. It is highly noticeable that I_c and I_a variation (ΔI_c and ΔI_a) between O_3 exposition cycles (**Figure 4.10B**) is modified by the presence of the UV protection system. This response can have, at least, two explanations: (1) indeed, the UV radiation affects chitosan gel by creating electrochemically active species or (2) UV protection affects the ozone flow inside the chamber, decreasing the amount of ozone that effectively interacts with the MIE-GC. The setup used to perform this experiment does not allow us to clearly evaluate which effect has more impact on the anodic or cathodic current variation. The O_3 generator chamber is a practical device to test MIE-GC proof-of-concept. Yet a deeper analysis, testing other devices to protect the MIE-GC from UV radiation, must be performed to reach a stronger conclusion.

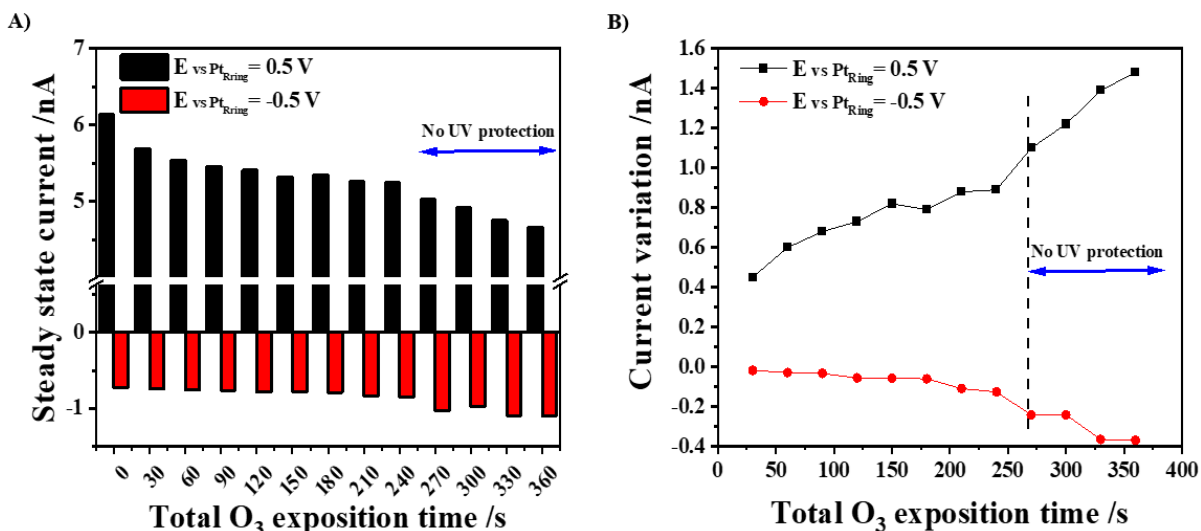


Figure 4.10 MIE-GC soaked in $[Fe(CN)_6]^{4-}$ I_a and I_c after different periods of exposition to an ozone atmosphere with and without UV protection (A). current variation before and after every O₃ exposition (B).

4.5.2. MIE-GC regeneration

As it has been proved, exposing the MIE-GC to an ozone atmosphere modifies the ratio of the redox probes soaked in the gel. In the system proposed in this work, the concentration of the redox probe in its reduced form will, after several consecutive measurements, reach its minimum value, disabling MIE-GC to perform more experiments. Therefore, to carry out the measurements, out is necessary to regenerate the gel probe. MIE-GC reset is achieved by re-soaking the gel probe in the redox probe solution. MIE-GP stability and integrity are key parameters to its long-term use and re-soaking may affect them. Therefore, it must be studied. Two types of gel will be investigated to this end: a 'simple' chitosan one and a crosslinked chitosan.

To study chitosan MIE-GC regeneration, the same gel probe was (1) exposed to ozone atmosphere for 60 s, (2) extracted from the chamber to perform a 30 s chronoamperometry at +0.5V and other at -0.5V and (3) immediately re-soaked in the redox probe solution after performing the chronoamperometries. This cycle was repeated five times, increasing ozone

exposition time and evaluating optically the gel probe size after every cycle.

Obtained currents are presented in **Figure 4.11**. After re-soaking the MIE-GC for a fourth time, initial I_c cannot be reached and, after a fifth regeneration, neither I_c nor I_a can. Afterward, while re-soaking the MIE-GC for a sixth time, gel volume decreased substantially, forcing us to stop the experiment.

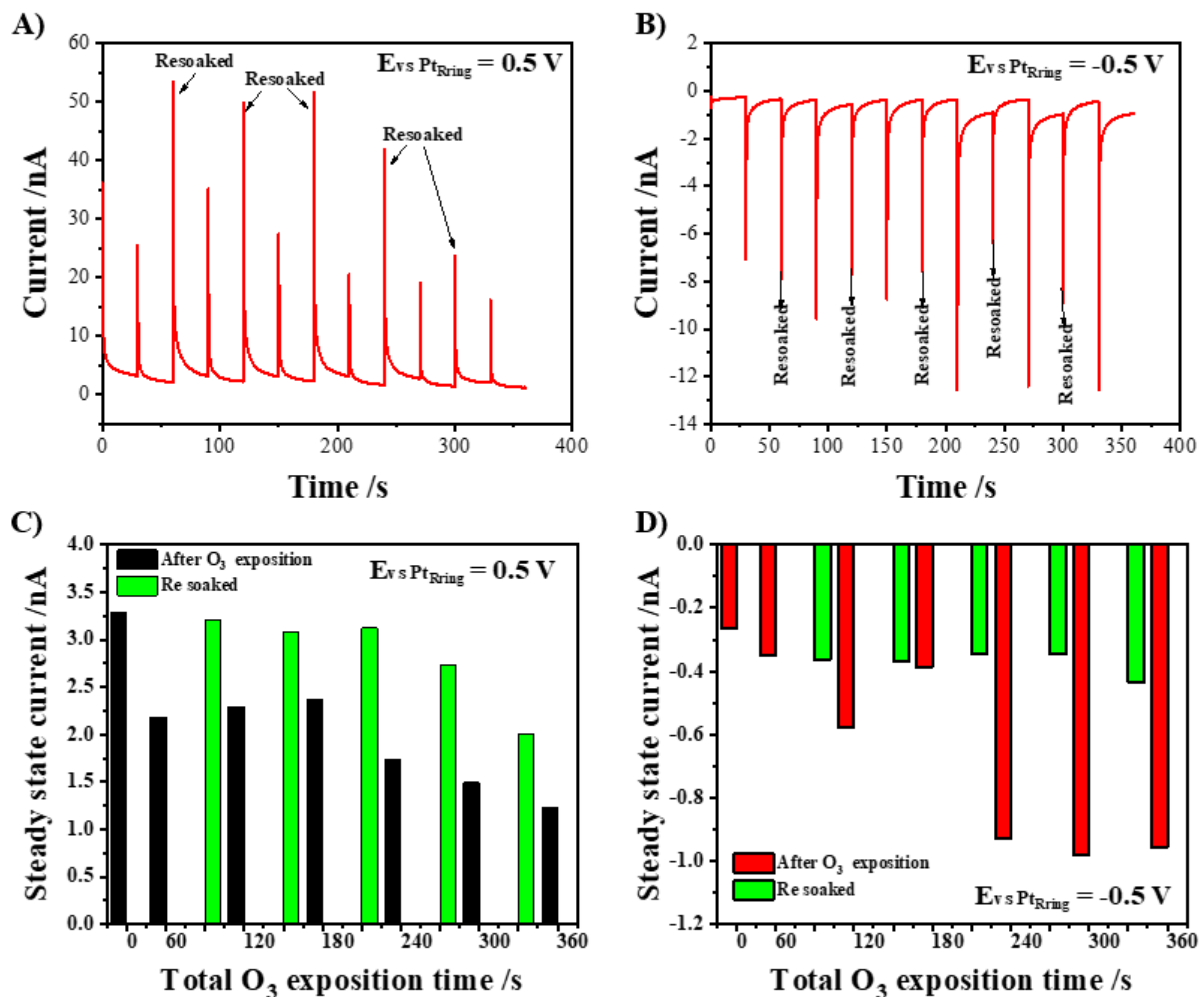


Figure 4.11 MIE-GC chitosan chronoamperometries of a soaked and regenerated MIE-GC in 25 mM $[Fe(CN)_6]^{4-}$ at different periods of exposition to an ozone atmosphere at 0.5 V (A) and -0.5 V (B). I_a (C) and I_c (D) values obtained from (A) and (B) as a function of the resoaking cycles.

Chemical crosslinking with glutaraldehyde is a well-known procedure applied to improve the mechanical properties of chitosan hydrogel. Crosslinked chitosan gel probe has been achieved

by soaking the MIE-GC for 2.5 hours in a 0.25% glutaraldehyde solution (1-1 glycerol/ H_2O). A crosslinked MIE-GC was then used to repeat the regeneration tests, aiming at increasing the number of possible MIE-GC resoaking cycles and, therefore, its durability. Unfortunately, almost similar results as with non-crosslinked chitosan were achieved (**Figure 4.12**). Although it was possible to perform one more cycle before irreversible damaging the MIE-GC, problems with regenerating the electrode started from the third cycle.

Many works discuss chitosan's advantages and disadvantages [76,182,183] as natural polymer. It is commonly accepted that its mechanical properties could be improved, but its poor performance in this experiment may not be entirely linked to this. MIE-GC is not only resoaked in these experiments, it is also exposed to UV radiation every cycle. While immersing the MIE-GC in redox probe solution, a small amount of chitosan could dissolve spontaneously due to the concentration gradient, this amount can increase if chitosan polymer chains are damaged upon continuous exposition to UV radiation.

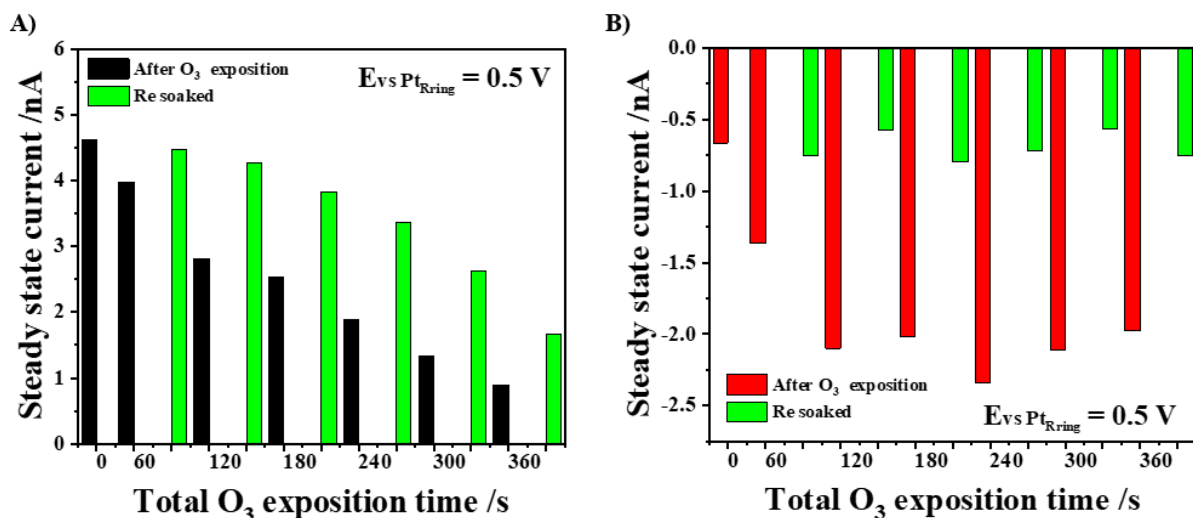


Figure 4.12 Crosslinked chitosan MIE-GC I_a (A) and I_c (B) after several a soaked, exposition to an ozone atmosphere, and regeneration cycles using a 25 mM $[Fe(CN)_6]^{4-}$ solution.

4.6. Summary

The micro-integrated electrode coated with chitosan gel (MIE-GC) soaked with a redox probe has been proven a promising tool to measure, through electrochemistry, highly oxidant substances such as ozone. Chronoamperometry was chosen as the preferred method, due to its relatively fast response and easy analysis. First, the MIE-GC was soaked in solutions with different $[\text{Fe}(\text{CN})_6]^{3-}/[\text{Fe}(\text{CN})_6]^{4-}$ ratios. Chronoamperometries were performed at 0.5V and -0.5 V vs Pt micro-ring electrode for 30 s. A straightforward relation between the steady currents and redox probes concentration ratios was obtained. To test the feasibility of the MIE-GC as device to identify highly oxidant or reductant substances, a MIE-GC soaked in $[\text{Fe}(\text{CN})_6]^{4-}$ was exposed to an O_3 atmosphere. Soaked MIE-GC was placed inside an ozone generator chamber at a controlled time. Chronoamperometries were performed right after every exposition. Exposition time was successfully correlated with the chronoamperometry response of the probe. Chitosan and crosslinked Chitosan MIE-GC integrity was also tested. Both probes were exposed to an O_3 atmosphere and then resoaked in $[\text{Fe}(\text{CN})_6]^{4-}$ solution. Chronoamperometries were performed after every step. Results indicate that neither chitosan nor crosslinked chitosan MIE-GC remains after a few exposition-resoaking cycles.

The impact in the MIE-GC of the direct UV radiation of the lamp inside the chamber was also studied. MIE-GC soaked in $[\text{Fe}(\text{CN})_6]^{4-}$ was placed inside the O_3 generator chamber with and without a UV radiation protection device. The gel probe was exposed for consecutive fixed time periods. Chronoamperometries were performed after each period. Results showed an increment of the current variation after removing the UV protection device. Suggesting a possible effect of the direct UV radiation in the gel probe.

Overall, we demonstrated that there is a good relation between O_3 exposition and the current

response obtained by chronoamperometry. Confirming MIE-GC as a suitable option to identify the presence of this substance. Furthermore, MIE-GC is a promising configuration to characterize redox-active surfaces by scanning gel electrochemical microscopy in the future.

Chapter V

General conclusion and perspectives

There is no doubt of the power of Scanning Electrochemical Probe techniques (SEPM) in local electrochemical analysis. To expand the SEPM family and extend its applications, Scanning Gel Electrochemical Microscopy (SGECM) was recently developed. The concept is based on a gel probe that is in soft contact with the sample surface, allowing local electrochemical measurements to be performed at the gel/sample interface with the confined gel electrolyte. That being said, the heart of the technique is the gel probe. This thesis addresses gel probe issues and limitations, aiming to support the further development and applications of SGECM. A systematic study of chitosan electrodeposition is presented in **Chapter II**, exposing the complexity of gel probe fabrication. Yet, reliable and reproducible chitosan gel probes can be obtained. Successful co-electrodeposition of chitosan with alkoxysilane unlocked a wide range of possibilities for the gel probe. Chitosan co-electrodeposition with TEOS exhibited an important enhancement of the gel mechanical properties, while chitosan-MPTMS blend co-electrodeposition became a promising method for chitosan functionalization. Less productive attempts to improve the chitosan gel probe were made using DES and IL. But even then, we succeeded in obtaining gel probes that are suitable for SGECM measurements. All gel probes were characterized using, mainly, approach and retract curves. Although its quantitative interpretation is not fully developed, it still offers a lot of valuable information about gel probe-surface interaction, making it a very useful tool for gel probe characterization.

SGECM immobilizes the electrolyte in gel form at the tip of the electrode. For measuring, the

gel probe physically contacts the sample, so there is a real risk of leaving an amount of electrolyte on the sample surface. **In Chapter III**, electrolyte leakage was successfully studied integrating SGECM with a quartz crystal microbalance (QCM). Quartz crystal (QC) frequency shift was recorded along with the current signal. Results showed a high QC sensitivity to the interaction with the gel probe. When leakage occurs, a variation in the QC frequency is spotted. This frequency shift has been used to study the electrolyte leakage of several probes. Results showed that freshly prepared gel probes have electrolyte leakage, especially after soaking redox probes, yet it can be reduced to be invisible after a few approach-retract cycles, confirming the necessity of stabilizing the gel probe before SGECM measurements. Co-electrodeposition of chitosan with TEOS showed a decrease in the electrolyte leakage and cycles needed to stabilize the probe. Moreover, the QC frequency response when the gel probe is over-approach revealed a linear relation with the compression distance. This may open the possibilities for using SGECM-QCM as a method to characterize micro-sized hydrogel mechanical properties.

Micro-integrated electrode coated with chitosan gel (MIE-GC) introduced in **Chapter IV** showed promising results in electrochemical sensing of oxidant species such as O_3 when soaked in a redox probe solution. Currents obtained by chronoamperometry can be satisfactorily correlated to MIE-GC time of exposition to an O_3 gas atmosphere, confirming the relation between the variation of redox probes concentration in the gel probe with the exposition to an oxidizing agent. Furthermore, the stability of chitosan MIE-GC was tested by resoaking the electrode in redox probe solution after periods of O_3 exposition. Results showed that MIE-GC is stable only for a few cycles, assuming that chitosan may not be the best option to build MIE-GC. The same test was performed by crosslinking the chitosan gel with

glutaraldehyde, results were similar to those obtained using only chitosan. Even if chitosan may not be the best choice to build MIE-GC, the use of integrated electrodes presents interesting applications, being a great option to expand SGECM applications.

At the end of this thesis, it is clear that the many efforts to expand our gel probe knowledge and SGECM applications were fructiferous. Yet, there are some issues that we need to overcome. Perhaps the most important subject that needs to be addressed, is the quantification of the approach and retract curve. Even if a qualitative analysis was reached, offering insightful information about gel probe-sample interaction, a deeper quantitative analysis of the approach and retract curves is needed to fully interpret SGECM results. Current response is composed of different mechanical and electrochemical processes, so approach and retract curve quantification is no easy task. In this direction, attempts to model the gel probe approach and retract cycle using COMSOL and Matlab have been made [184]. Although good partial results were successfully obtained, further analysis is needed.

As mentioned above, gel mechanical properties also influence the approach and retract curve. Viscoelastic systems, such as chitosan hydrogel, mechanical modeling is a widely studied subject. However, current mechanical models present some difficulties in interpreting highly elastic systems, especially micro-sized hydrogels such as those used for SGECM. In **Chapter III**, it was shown how the QC frequency can be related to the compression of the gel probe against the QC surface, suggesting gel mechanical properties could be obtained using this method. Further development of the SEGM-QCM setup may extend its application to mechanical characterization of micro-sized. Continuing with the gel compression studies initiated in the abovementioned chapter. Studying SGECM gel probes mechanical properties is fundamental to achieving a quantitative modelization of its current response. As was

discussed earlier in this work, gel deformation plays a key role in the diffusion analysis of the redox species. Also, to study gel probe mechanical properties, an inverted microscope is in its initial phase of being coupled with the SGECM setup. Use of transparent samples may allow us an accurate measurement of contact area, a value of high importance for the interpretation of the current response.

In **Chapter IV**, a micro-integrated electrode (MIE) was introduced. But, due to a time limitation, we were not able to explore all its possible applications. We demonstrated that concentration changes of redox probe in the gel probe (MIE-GC) can be followed by chronoamperometry using the electrodes from the MIE-GC. The possibility of using this method to detect the remains of oxidant or reductant substances on surfaces using SGECM is yet to be tested. But also, a MIE with an external micro-ring Ag/AgCl QRE was fabricated and not tested yet in the SGECM setup. This electrode configuration would allow us to form if the sample is conductive, a 3-electrode system. Opening the possibilities to introduce, for example, a QRE into the gel probe SGECM to control WE potential. Some initial efforts were made to test a new way to approach the gel probe in SGECM using the recently developed MIE-GC. A voltage is applied between the two electrodes in the MIE-GC and approaches the surface while the current is continually measured. When the MIE-GC reaches the sample, the perturbation in the system could be reflected by the current, signal that may be used as feedback to stop the approach of the probe. Early tests indicated that the MIE-GC could be approached using this method, method that would be incredibly helpful when working with non-conductive samples. But, once more, further analysis is required before claiming this as a valid MIE-GC approach method.

Chitosan has been proven a great ally to build gel probes. Either using micro-disk electrodes,

etched metal wires or micro-integrated electrodes, we always succeeded in obtaining a chitosan gel probe. But, as it was mentioned a few times in this work, is not suitable to use under severe conditions. So, even if we have positive results working with chitosan co-electrodeposition with TEOS, new hydrogels must be explored. Fabrication of gel probes using *e.g.*, polyacrylic acid (PAA) or low molecular weight polymers (–COOH terminus) is yet to be tested.

As a final remark, is fair to say, that after conquering the above-mentioned challenges, SGECM has the chance to become a widely applied technique for the study of local electrochemical properties in complex surfaces. The use of relatively easy-to-build probes, an accurate approach feedback, the possibility to modify the electrolyte and functionalize the gel according to the system one wants to study and the possibility to minimize the electrolyte infiltration on the sample, are some of the advantages brought by SGECM. Advantages that, with the ongoing system modeling for results quantification, will establish SGECM as the powerful technique that we have envisioned.

References

- [1] A. Yoshino, The Birth of the Lithium-Ion Battery, *Angew. Chemie - Int. Ed.* 51 (2012) 5798–5800. <https://doi.org/10.1002/anie.201105006>.
- [2] J. Yan, B.R. Saunders, Third-Generation Solar Cells: A Review and Comparison of Polymer: fullerene, Hybrid Polymer and Perovskite Solar Cells, *RSC Adv.* 4 (2014) 43286–43314. <https://doi.org/10.1039/c4ra07064j>.
- [3] S. Mekhilef, R. Saidur, A. Safari, Comparative Study of Different Fuel Cell Technologies, *Renew. Sustain. Energy Rev.* 16 (2012) 981–989. <https://doi.org/10.1016/j.rser.2011.09.020>.
- [4] S.A. Grigoriev, V.N. Fateev, D.G. Bessarabov, P. Millet, Current Status, Research Trends, and Challenges in Water Electrolysis science and Technology, *Int. J. Hydrogen Energy.* 45 (2020) 26036–26058. <https://doi.org/10.1016/j.ijhydene.2020.03.109>.
- [5] G. Binnig, H. Rohrer, Scanning Tunneling Microscopy., *IBM J. Res. Dev.* 30 (1986) 355–369. <https://doi.org/10.2320/materia1962.25.821>.
- [6] G. Binnig, C.F. Quate, Atomic Force Microscopy, *Phys. Rev. Lett.* 56 (1986) 51–59. <https://doi.org/10.1201/9781420075250>.
- [7] A.N. Patel, C. Kranz, (Multi)functional Atomic Force Microscopy Imaging, *Annu. Rev. Anal. Chem.* 11 (2018) 329–350. <https://doi.org/10.1146/annurev-anchem-061417-125716>.
- [8] H.Y. Liu, F.R.F. Fan, C.W. Lin, A.J. Bard, Scanning Electrochemical and Tunneling Ultramicroelectrode Microscope for High-Resolution Examination of Electrode Surfaces in Solution, *J. Am. Chem. Soc.* 108 (1986) 3838–3839.

- <https://doi.org/10.1021/ja00273a054>.
- [9] D. Kolb, Reconstruction phenomena at metal-electrolyte interfaces, *Prog. Surf. Sci.* 51 (1996) 109–173. [https://doi.org/10.1016/0079-6816\(96\)00002-0](https://doi.org/10.1016/0079-6816(96)00002-0).
- [10] O.M. Magnussen, Ordered Anion Adlayers on Metal Electrode Surfaces, *Chem. Rev.* 102 (2002) 679–725. <https://doi.org/10.1021/cr000069p>.
- [11] T. Wandlowski, Phase Transitions in Two-dimensional Adlayers at Electrode Surfaces: Thermodynamics, Kinetics, and Structural Aspects, *Encycl. Electrochem.* (2002). <https://doi.org/10.1002/9783527610426.bard010303>.
- [12] B. Han, Z. Li, C. Li, I. Pobelov, G. Su, R. Aguilar-Sanchez, T. Wandlowski, From Self-Assembly to Charge Transport With Single Molecules - An Electrochemical Approach, *Top. Curr. Chem.* 287 (2009) 181–255. https://doi.org/10.1007/128_2008_152.
- [13] N. Batina, T. Will, D.M. Kolb, Study of the Initial Stages of Copper Deposition by In Situ Scanning Tunnelling Microscopy, *Faraday Discuss.* 94 (1992) 93–106. <https://doi.org/10.1039/FD9929400093>.
- [14] M. Lunardon, T. Kosmala, C. Durante, S. Agnoli, G. Granozzi, Atom-by-Atom Identification of Catalytic Active Sites in Operando Conditions by Quantitative Noise Detection, *Joule.* 6 (2022) 617–635. <https://doi.org/10.1016/j.joule.2022.02.010>.
- [15] J. Meier, K.A. Friedrich, U. Stimming, Novel Method for the Investigation of Single Nanoparticle Reactivity, *Faraday Discuss.* 121 (2002) 365–372. <https://doi.org/10.1039/b200014h>.
- [16] I. Díez-Pérez, F. Sanz, P. Gorostiza, In Situ Studies of Metal Passive Films, *Curr. Opin. Solid State Mater. Sci.* 10 (2006) 144–152. <https://doi.org/10.1016/j.cossms.2007.01.002>.

- [17] F.P. Zamborini, R.M. Crooks, Corrosion Passivation of Gold by N-Alkanethiol Self-Assembled Monolayers: Effect of Chain Length and End Group, *Langmuir*. 14 (1998) 3279–3286. <https://doi.org/10.1021/la971121o>.
- [18] A. Thie, *Encyclopedia of Nanotechnology*, 2012. <https://doi.org/10.1007/978-90-481-9751-4>.
- [19] A. Lagunas, A. Guerra-Castellano, A. Nin-Hill, I. Díaz-Moreno, M.A. De la Rosa, J. Samitier, C. Rovira, P. Gorostiza, Long Distance Electron Transfer Through the Aqueous Solution Between Redox Partner Proteins, *Nat. Commun.* 9 (2018) 3–9. <https://doi.org/10.1038/s41467-018-07499-x>.
- [20] A.J. Bard, F.R.F. Fan, J. Kwak, O. Lev, Scanning Electrochemical Microscopy. Introduction and Principles, *Anal. Chem.* 61 (1989) 132–138. <https://doi.org/10.1021/ac00177a011>.
- [21] D. Polcari, P. Dauphin-Ducharme, J. Mauzeroll, Scanning Electrochemical Microscopy: A Comprehensive Review of Experimental Parameters from 1989 to 2015, *Chem. Rev.* 116 (2016) 13234–13278. <https://doi.org/10.1021/acs.chemrev.6b00067>.
- [22] G.A. Anshebo, A.A. Gebreyohanes, B.G. Difer, T.A. Anshebo, Scanning Electrochemical Microscope Studies of Charge Transfer Kinetics at the Interface of the Perovskite/Hole Transport Layer, *J. Nanotechnol.* 2023 (2023) 13–16. <https://doi.org/10.1155/2023/1844719>.
- [23] Y.F. Yang, G. Denuault, Scanning Electrochemical Microscopy (SECM): Study of the Adsorption and Desorption of Hydrogen on Platinum Electrodes in Na₂SO₄ Solution (pH = 7), *J. Electroanal. Chem.* 418 (1996) 99–107. [https://doi.org/10.1016/S0022-0728\(96\)04768-7](https://doi.org/10.1016/S0022-0728(96)04768-7).

- [24] H. Qian, D. Xu, C. Du, D. Zhang, X. Li, L. Huang, L. Deng, Y. Tu, J.M.C. Mol, H.A. Terry, Dual-Action Smart Coatings With a Self-Healing Superhydrophobic Surface and Anti-Corrosion Properties, *J. Mater. Chem. A.* 5 (2017) 2355–2364. <https://doi.org/10.1039/c6ta10903a>.
- [25] S. De Zio, M. Beconi, A. Soldà, M. Malferrari, A. Lesch, S. Rapino, Glucose Micro-Biosensor for Scanning Electrochemical Microscopy Characterization of Cellular Metabolism in Hypoxic Microenvironments, *Bioelectrochemistry.* 150 (2023). <https://doi.org/10.1016/j.bioelechem.2022.108343>.
- [26] S. Park, S. Kumar, C.S. Maier, J. Kreth, D. Koley, Simultaneous Chemical Mapping of Live Biofilm Microenvironmental pH and Hydrogen Peroxide in Real Time with a Triple Scanning Electrochemical Microscopy Tip, *Anal. Chem.* (2022) 2–10. <https://doi.org/10.1021/acs.analchem.2c05258>.
- [27] R. Zhu, S.M. Macfie, Z. Ding, Effects of Cadmium on Photosynthetic Oxygen Evolution from Single Stomata in *Brassica Juncea* (L.) Czern, *Langmuir.* 24 (2008) 14261–14268. <https://doi.org/10.1021/la8018875>.
- [28] E. Malel, J. Colleran, D. Mandler, Studying the Localized Deposition of Ag Nanoparticles on Self-Assembled Monolayers by Scanning Electrochemical Microscopy (SECM), *Electrochim. Acta.* 56 (2011) 6954–6961. <https://doi.org/10.1016/j.electacta.2011.06.017>.
- [29] R.G. Fedorov, D. Mandler, Local Deposition of Anisotropic Nanoparticles Using Scanning Electrochemical Microscopy (SECM), *Phys. Chem. Chem. Phys.* 15 (2013) 2725–2732. <https://doi.org/10.1039/c2cp42823g>.
- [30] J. Tang, J.J. Zheng, Y.T. Yu, L. Chen, N. Zhang, Z. Tian, Selective Etching of ZnO

- Films on an ITO Substrate Using a Scanning Electrochemical Microscope, *Electrochim. Acta.* 83 (2012) 247–252. <https://doi.org/10.1016/j.electacta.2012.07.106>.
- [31] A.J. Bard, P.R. Unwin, D.O. Wipf, F. Zhou, *Scanning Electrochemical Microscopy*, 235 (2008) 235–247. <https://doi.org/10.1063/1.41416>.
- [32] P.K. Hansma, B. Drake, S.A. C Gould, C.B. Prater, *The Scanning Ion-Conductance Microscope*, *Earth Plan. Sci. Lett.* 3 (1966) 1389. <https://doi.org/10.1126/science.2464851>.
- [33] J. Rheinlaender, N.A. Geisse, R. Proksch, T.E. Schäffer, *Comparison of Scanning Ion Conductance Microscopy With Atomic Force Microscopy for Cell Imaging*, *Langmuir.* 27 (2011) 697–704. <https://doi.org/10.1021/la103275y>.
- [34] Y.E. Korchev, M. Milovanovic, C.L. Bashford, D.C. Bennett, E. V. Sviderskaya, I. Vodyanoy, M.J. Lab, *Specialized Scanning Ion-Conductance Microscope for Imaging of Living Cells*, *J. Microsc.* 188 (1997) 17–23. <https://doi.org/10.1046/j.1365-2818.1997.2430801.x>.
- [35] Y.E. Korchev, J. Gorelik, M.J. Lab, E. V. Sviderskaya, C.L. Johnston, C.R. Coombes, I. Vodyanoy, C.R.W. Edwards, *Cell volume measurement Using Scanning Ion Conductance Microscopy*, *Biophys. J.* 78 (2000) 451–457. [https://doi.org/10.1016/S0006-3495\(00\)76607-0](https://doi.org/10.1016/S0006-3495(00)76607-0).
- [36] X. Gong, X. Fan, Y. Huang, Y. Du, X. Wang, X. Liu, Z. He, *Applications of Scanning Ion Conductance Microscope in Biomedical Fields*, *MedComm – Biomater. Appl.* 2 (2023). <https://doi.org/10.1002/mba2.26>.
- [37] B.P. Nadappuram, K. McKelvey, R. Al Botros, A.W. Colburn, P.R. Unwin, *Fabrication and Characterization of Dual Function Nanoscale pH-Scanning Ion Conductance*

- Microscopy (SICM) Probes for High Resolution pH Mapping, *Anal. Chem.* 85 (2013) 8070–8074. <https://doi.org/10.1021/ac401883n>.
- [38] D.J. Comstock, J.W. Elam, M.J. Pellin, M.C. Hersam, Integrated Ultramicroelectrode-Nanopipet Probe for Concurrent Scanning Electrochemical Microscopy and Scanning Ion Conductance Microscopy, *Anal. Chem.* 82 (2010) 1270–1276. <https://doi.org/10.1021/ac902224q>.
- [39] C.G. Williams, M.A. Edwards, A.L. Colley, J. V. Macpherson, P.R. Unwin, Scanning Micropipet Contact Method for High-Resolution Imaging of Electrode Surface Redox Activity, *Anal. Chem.* 81 (2009) 2486–2495. <https://doi.org/10.1021/ac802114r>.
- [40] C. Santana Santos, B.N. Jaato, I. Sanjuán, W. Schuhmann, C. Andronesco, Operando Scanning Electrochemical Probe Microscopy during Electrocatalysis, *Chem. Rev.* 123 (2023) 4972–5019. <https://doi.org/10.1021/acs.chemrev.2c00766>.
- [41] B. Tao, P.R. Unwin, C.L. Bentley, Nanoscale Variations in the Electrocatalytic Activity of Layered Transition-Metal Dichalcogenides, *J. Phys. Chem. C.* 124 (2020) 789–798. <https://doi.org/10.1021/acs.jpcc.9b10279>.
- [42] A.G. Güell, A.S. Cuharuc, Y.R. Kim, G. Zhang, S.Y. Tan, N. Ebejer, P.R. Unwin, Redox-Dependent Spatially Resolved Electrochemistry at Graphene and Graphite Step Edges, *ACS Nano.* 9 (2015) 3558–3571. <https://doi.org/10.1021/acsnano.5b00550>.
- [43] A.G. Güell, N. Ebejer, M.E. Snowden, J. V. MacPherson, P.R. Unwin, Structural Correlations in Heterogeneous Electron Transfer at Monolayer and Multilayer Graphene Electrodes, *J. Am. Chem. Soc.* 134 (2012) 7258–7261. <https://doi.org/10.1021/ja3014902>.
- [44] E.P. Sharel, Y.R. Kim, D. Perry, C.L. Bentley, P.R. Unwin, Nanoscale Electrocatalysis

- of Hydrazine Electro-Oxidation at Blistered Graphite Electrodes, *ACS Appl. Mater. Interfaces*. 8 (2016) 30458–30466. <https://doi.org/10.1021/acsami.6b10940>.
- [45] G. Zhang, P.M. Kirkman, A.N. Patel, A.S. Cuharuc, K. McKelvey, P.R. Unwin, Molecular Functionalization of Graphite Surfaces: Basal Plane Versus Step Edge Electrochemical Activity, *J. Am. Chem. Soc.* 136 (2014) 11444–11451. <https://doi.org/10.1021/ja505266d>.
- [46] P.M. Kirkman, A.G. Güell, A.S. Cuharuc, P.R. Unwin, Spatial and Temporal Control of the Diazonium Modification of sp² Carbon Surfaces, *J. Am. Chem. Soc.* 136 (2014) 36–39. <https://doi.org/10.1021/ja410467e>.
- [47] Y. Takahashi, T. Yamashita, D. Takamatsu, A. Kumatani, T. Fukuma, Nanoscale Kinetic Imaging of Lithium Ion Secondary Battery Materials Using Scanning Electrochemical Cell Microscopy, *Chem. Commun.* 56 (2020) 9324–9327. <https://doi.org/10.1039/d0cc02865g>.
- [48] Y. Takahashi, Y. Kobayashi, Z. Wang, Y. Ito, M. Ota, H. Ida, A. Kumatani, K. Miyazawa, T. Fujita, H. Shiku, Y.E. Korchev, Y. Miyata, T. Fukuma, M. Chen, T. Matsue, High-Resolution Electrochemical Mapping of the Hydrogen Evolution Reaction on Transition-Metal Dichalcogenide Nanosheets, *Angew. Chemie - Int. Ed.* 59 (2020) 3601–3608. <https://doi.org/10.1002/anie.201912863>.
- [49] A. Kumatani, Y. Takahashi, C. Miura, H. Ida, H. Inomata, H. Shiku, H. Munakata, K. Kanamura, T. Matsue, Scanning Electrochemical Cell Microscopy for Visualization and Local Electrochemical Activities of Lithium-ion (de) Intercalation Process in Lithium-Ion Batteries Electrodes, *Surf. Interface Anal.* 51 (2019) 27–30. <https://doi.org/10.1002/sia.6538>.

- [50] D. Martín-Yerga, A. Costa-García, P.R. Unwin, Correlative Voltammetric Microscopy: Structure-Activity Relationships in the Microscopic Electrochemical Behavior of Screen Printed Carbon Electrodes, *ACS Sensors*. 4 (2019) 2173–2180. <https://doi.org/10.1021/acssensors.9b01021>.
- [51] B.D.B. Aaronson, J. Garoz-Ruiz, J.C. Byers, A. Colina, P.R. Unwin, Electrodeposition and Screening of Photoelectrochemical Activity in Conjugated Polymers Using Scanning Electrochemical Cell Microscopy, *Langmuir*. 31 (2015) 12814–12822. <https://doi.org/10.1021/acs.langmuir.5b03316>.
- [52] C.L. Bentley, R. Agoston, B. Tao, M. Walker, X. Xu, A.P. O’Mullane, P.R. Unwin, Correlating the Local Electrocatalytic Activity of Amorphous Molybdenum Sulfide Thin Films with Microscopic Composition, Structure, and Porosity, *ACS Appl. Mater. Interfaces*. 12 (2020) 44307–44316. <https://doi.org/10.1021/acsami.0c11759>.
- [53] C.L. Bentley, D. Perry, P.R. Unwin, Stability and Placement of Ag/AgCl Quasi-Reference Counter Electrodes in Confined Electrochemical Cells, *Anal. Chem*. 90 (2018) 7700–7707. <https://doi.org/10.1021/acs.analchem.8b01588>.
- [54] E.E. Oseland, Z.J. Ayres, A. Basile, D.M. Haddleton, P. Wilson, P.R. Unwin, Surface Patterning of Polyacrylamide Gel Using Scanning Electrochemical Cell Microscopy (SECCM), *Chem. Commun.* 52 (2016) 9929–9932. <https://doi.org/10.1039/c6cc05153g>.
- [55] B.D.B. Aaronson, C.H. Chen, H. Li, M.T.M. Koper, S.C.S. Lai, P.R. Unwin, Pseudo-Single-Crystal Electrochemistry on Polycrystalline Electrodes: Visualizing Activity at Grains and Grain Boundaries on Platinum for the Fe²⁺/Fe³⁺ Redox Reaction, *J. Am. Chem. Soc.* 135 (2013) 3873–3880. <https://doi.org/10.1021/ja310632k>.

- [56] B.D.B. Aaronson, S.C.S. Lai, P.R. Unwin, Spatially Resolved Electrochemistry in Ionic Liquids: Surface Structure Effects on Triiodide Reduction at Platinum Electrodes, *Langmuir*. 30 (2014) 1915–1919. <https://doi.org/10.1021/la500271f>.
- [57] T. Yamamoto, T. Ando, Y. Kawabe, T. Fukuma, H. Enomoto, Y. Nishijima, Y. Matsui, K. Kanamura, Y. Takahashi, Characterization of the Depth of Discharge-Dependent Charge Transfer Resistance of a Single LiFePO₄ Particle, *Anal. Chem.* 93 (2021) 14448–14453. <https://doi.org/10.1021/acs.analchem.1c02851>.
- [58] M. V. Makarova, F. Amano, S. Nomura, C. Tateishi, T. Fukuma, Y. Takahashi, Y.E. Korchev, Direct Electrochemical Visualization of the Orthogonal Charge Separation in Anatase Nanotube Photoanodes for Water Splitting, *ACS Catal.* 12 (2022) 1201–1208. <https://doi.org/10.1021/acscatal.1c04910>.
- [59] T. Tsujiguchi, Y. Kawabe, S. Jeong, T. Ohto, S. Kukunuri, H. Kuramochi, Y. Takahashi, T. Nishiuchi, H. Masuda, M. Wakisaka, K. Hu, G. Elumalai, J.I. Fujita, Y. Ito, Acceleration of Electrochemical CO₂ Reduction to Formate at the Sn/ Reduced Graphene Oxide Interface, *ACS Catal.* 11 (2021) 3310–3318. <https://doi.org/10.1021/acscatal.0c04887>.
- [60] T. Ando, K. Asai, J. Macpherson, Y. Einaga, T. Fukuma, Y. Takahashi, Nanoscale Reactivity Mapping of a Single-Crystal Boron-Doped Diamond Particle, *Anal. Chem.* 93 (2021) 5831–5838. <https://doi.org/10.1021/acs.analchem.1c00053>.
- [61] T. Quast, S. Varhade, S. Saddeler, Y.T. Chen, C. Andronescu, S. Schulz, W. Schuhmann, Single Particle Nanoelectrochemistry Reveals the Catalytic Oxygen Evolution Reaction Activity of Co₃O₄ Nanocubes, *Angew. Chemie - Int. Ed.* 60 (2021) 23444–23450. <https://doi.org/10.1002/anie.202109201>.

- [62] T. Tarnev, H.B. Aiyappa, A. Botz, T. Erichsen, A. Ernst, C. Andronesu, W. Schuhmann, Scanning Electrochemical Cell Microscopy Investigation of Single ZIF-Derived Nanocomposite Particles as Electrocatalysts for Oxygen Evolution in Alkaline Media, *Angew. Chemie - Int. Ed.* 58 (2019) 14265–14269. <https://doi.org/10.1002/anie.201908021>.
- [63] C.L. Bentley, C. Andronesu, M. Smialkowski, M. Kang, T. Tarnev, B. Marler, P.R. Unwin, U.P. Apfel, W. Schuhmann, Local Surface Structure and Composition Control the Hydrogen Evolution Reaction on Iron Nickel Sulfides, *Angew. Chemie - Int. Ed.* 57 (2018) 4093–4097. <https://doi.org/10.1002/anie.201712679>.
- [64] T. Tarnev, S. Cychy, C. Andronesu, M. Muhler, W. Schuhmann, Y.T. Chen, A Universal Nano-capillary Based Method of Catalyst Immobilization for Liquid-Cell Transmission Electron Microscopy, *Angew. Chemie - Int. Ed.* 59 (2020) 5586–5590. <https://doi.org/10.1002/anie.201916419>.
- [65] C.H. Chen, K.E. Meadows, A. Cuharuc, S.C.S. Lai, P.R. Unwin, High Resolution Mapping of Oxygen Reduction Reaction Kinetics at Polycrystalline Platinum Electrodes, *Phys. Chem. Chem. Phys.* 16 (2014) 18545–18552. <https://doi.org/10.1039/c4cp01511h>.
- [66] D. Valavanis, P. Ciocci, G.N. Meloni, P. Morris, J.-F. Lemineur, I.J. McPherson, F. Kanoufi, P.R. Unwin, Hybrid Scanning Electrochemical Cell Microscopy-Interference Reflection Microscopy (SECCM-IRM): Tracking Phase Formation on Surfaces in Small Volumes, *Faraday Discuss.* 233 (2022) 122–148. <https://doi.org/10.1039/d1fd00063b>.
- [67] Y. Li, A. Morel, D. Gallant, J. Mauzeroll, Oil-Immersed Scanning Micropipette Contact

- Method Enabling Long-term Corrosion Mapping, *Anal. Chem.* 92 (2020) 12415–12422.
<https://doi.org/10.1021/acs.analchem.0c02177>.
- [68] Y. Li, A. Morel, D. Gallant, J. Mauzeroll, Correlating Corrosion to Surface Grain Orientations of Polycrystalline Aluminum Alloy by Scanning Electrochemical Cell Microscopy, *ACS Appl. Mater. Interfaces.* 14 (2022) 47230–47236.
<https://doi.org/10.1021/acsami.2c12813>.
- [69] L. Liu, M. Etienne, A. Walcarius, Scanning Gel Electrochemical Microscopy for Topography and Electrochemical Imaging, *Anal. Chem.* 90 (2018) 8889–8895.
<https://doi.org/10.1021/acs.analchem.8b01011>.
- [70] J. Hui, Z.T. Gossage, D. Sarbapalli, K. Hernández-Burgos, J. Rodríguez-López, Advanced Electrochemical Analysis for Energy Storage Interfaces, *Anal. Chem.* 91 (2019) 60–83. <https://doi.org/10.1021/acs.analchem.8b05115>.
- [71] Q. Zheng, J. Zhuang, T. Wang, X. Liao, L. Cheng, S. Gu, Investigating the Effects of Solution Viscosity on the stability and success Rate of SECCM Imaging, *Ultramicroscopy.* 254 (2023) 113843. <https://doi.org/10.1016/j.ultramic.2023.113843>.
- [72] N. Dang. Developments of scanning gel electrochemical microscopy. *Analytical chemistry*. Ph.D. dissertation Université de Lorraine, Nancy, 2020. Available: <https://theses.hal.science/tel-03272273/>
- [73] M.A. Brites Helú, L. Liu, Rational Shaping of Hydrogel by Electrodeposition Under Fluid Mechanics for Electrochemical Writing on Complex Shaped Surfaces at Microscale, *Chem. Eng. J.* 416 (2021) 129029.
<https://doi.org/10.1016/j.cej.2021.129029>.
- [74] M. Etienne, E.C. Anderson, S.R. Evans, W. Schuhmann, I. Fritsch, Feedback-

- Independent Pt Nanoelectrodes for Shear Force-Based Constant-Distance Mode Scanning Electrochemical Microscopy, *Anal. Chem.* 78 (2006) 7317–7324. <https://doi.org/10.1021/ac061310o>.
- [75] N. Dang, M. Etienne, A. Walcarius, L. Liu, Scanning Gel Electrochemical Microscopy (SGECM): Lateral Physical Resolution by Current and Shear Force Feedback, *Anal. Chem.* 92 (2020) 6415–6422. <https://doi.org/10.1021/acs.analchem.9b05538>.
- [76] N. Dang, M. Etienne, A. Walcarius, L. Liu, Scanning Gel Electrochemical Microscopy (SGECM): The Potentiometric Measurements, *Electrochem. Commun.* 97 (2018) 64–67. <https://doi.org/10.1016/j.elecom.2018.10.020>.
- [77] A. Arnau, D. Soares, Fundamentals on Piezoelectricity, *Piezoelectric Transducers Appl.* (2004) 1–37. https://doi.org/10.1007/978-3-662-05361-4_1.
- [78] J. Curie, P. Curie, Développement par Compression de l'Électricité Polaire dans les Cristaux Héliédres à Faces Inclinées, *Bull. La Société Minéralogique Fr.* 3 (1880) 90–93.
- [79] M.D. Ward, D.A. Buttry, In Situ Interfacial Mass Detection With Piezoelectric Transducers, *Science* (80-.). 249 (1990) 1000–1007. <https://doi.org/10.1126/science.249.4972.1000>.
- [80] C. Stambaugh, H. Shakeel, M. Litorja, J.M. Pomeroy, Linking Mass Measured by the Quartz Crystal Microbalance to the SI, *Metrologia.* 57 (2020). <https://doi.org/10.1088/1681-7575/ab54a5>.
- [81] G. Sauerbrey, Verwendung von Schwingquarzen zur Wägung Dünner Schichten und zur Mikrowägung, *Zeitschrift Für Phys.* 155 (1959) 206–222. <https://doi.org/10.1007/BF01337937>.

- [82] K.K. Kanazawa, J.G. Gordon, Frequency of a Quartz Microbalance in Contact with Liquid, *Anal. Chem.* 57 (1985) 1770–1771. <https://doi.org/10.1021/ac00285a062>.
- [83] L. Sziráki, Z. Pilbáth, K. Papp, E. Kálmán, Studies of Copper Corrosion Inhibition Using Electrochemical Quartz Crystal Nanobalance and Quartz Crystal Immittance Techniques, *Electrochim. Acta.* 46 (2001) 3801–3815. [https://doi.org/10.1016/S0013-4686\(01\)00667-3](https://doi.org/10.1016/S0013-4686(01)00667-3).
- [84] S. Sigalov, M.D. Levi, L. Daikhin, G. Salitra, D. Aurbach, Electrochemical Quartz Crystal Admittance Studies of Ion Adsorption on Nanoporous Composite Carbon Electrodes in Aprotic Solutions, *J. Solid State Electrochem.* 18 (2014) 1335–1344. <https://doi.org/10.1007/s10008-013-2171-7>.
- [85] D. Aurbach, M. Moshkovich, Y. Cohen, A. Schechter, Study of Surface Film Formation on Noble-Metal Electrodes in Alkyl Carbonates/Li Salt Solutions, Using Simultaneous In Situ AFM, EQCM, FTIR, and EIS, *Langmuir.* 15 (1999) 2947–2960. <https://doi.org/10.1021/la981275j>.
- [86] D.E. Cliffel, A.J. Bard, Scanning Electrochemical Microscopy. 36. A Combined Scanning Electrochemical Microscope-Quartz Crystal Microbalance Instrument for Studying Thin Films, *Anal. Chem.* 70 (1998) 1993–1998. <https://doi.org/10.1021/ac971217n>.
- [87] L.R. Pace, Z.L. Harrison, M.N. Brown, W.O. Haggard, J.A. Jennings, Characterization and Antibiofilm Activity of Mannitol–Chitosan-Blended Paste for Local Antibiotic Delivery System, *Mar. Drugs.* 17 (2019) 517. <https://doi.org/10.3390/md17090517>.
- [88] M. Liu, Y. Zhou, Y. Zhang, C. Yu, S. Cao, Preparation and Structural Analysis of Chitosan Films With and Without Sorbitol, *Food Hydrocoll.* 33 (2013) 186–191.

- <https://doi.org/10.1016/j.foodhyd.2013.03.003>.
- [89] P. Pereira, S.S. Pedrosa, A. Correia, C.F. Lima, M.P. Olmedo, Á. González-Fernández, M. Vilanova, F.M. Gama, Biocompatibility of a Self-Assembled Glycol Chitosan Nanogel, *Toxicol. Vitro*. 29 (2015) 638–646. <https://doi.org/10.1016/j.tiv.2014.11.004>.
- [90] K.C. Gupta, F.H. Jabrail, Glutaraldehyde and Glyoxal Cross-Linked Chitosan Microspheres for Controlled Delivery of Centchroman, *Carbohydr. Res.* 341 (2006) 744–756. <https://doi.org/10.1016/j.carres.2006.02.003>.
- [91] T. Baran, A. Menteş, Highly Efficient Suzuki Cross-Coupling Reaction of Biomaterial Supported Catalyst Derived from Glyoxal and Chitosan, *J. Organomet. Chem.* 803 (2016) 30–38. <https://doi.org/10.1016/j.jorganchem.2015.12.011>.
- [92] F.-L. Mi, S.-S. Shyu, S.-T. Lee, T.-B. Wong, Kinetic Study of Chitosan-Tripolyphosphate Complex Reaction and Acid-Resistive Properties of the Chitosan-Tripolyphosphate Gel Beads Prepared by In-Liquid Curing Method, (n.d.) 14. [http://files/119/Mi et al. - Kinetic study of chitosan-tripolyphosphate complex.pdf](http://files/119/Mi%20et%20al.%20-%20Kinetic%20study%20of%20chitosan-tripolyphosphate%20complex.pdf).
- [93] L. Lv, Y. Xie, G. Liu, G. Liu, J. Yu, Removal of Perchlorate from Aqueous Solution by Cross-Linked Fe(III)-Chitosan Complex, *J. Environ. Sci.* 26 (2014) 792–800. [https://doi.org/10.1016/S1001-0742\(13\)60519-7](https://doi.org/10.1016/S1001-0742(13)60519-7).
- [94] M. Hasegawa, A. Isogai, F. Onabe, M. Usuda, R.H. Atalla, Characterization of Cellulose–Chitosan Blend Films, *J. Appl. Polym. Sci.* 45 (1992) 1873–1879. <https://doi.org/10.1002/app.1992.070451101>.
- [95] Y.X. Xu, K.M. Kim, M.A. Hanna, D. Nag, Chitosan–Starch Composite Film: Preparation and Characterization, *Ind. Crops Prod.* 21 (2005) 185–192. <https://doi.org/10.1016/j.indcrop.2004.03.002>.

- [96] E.A. El-Hefian, M.M. Nasef, A.H. Yahaya, Preparation and Characterization of Chitosan/Polyvinyl Alcohol Blends-A Rheological Study, *E-Journal Chem.* 7 (2010) S349–S357. <https://doi.org/10.1155/2010/275135>.
- [97] M.J. Calvo, P. Remuñán-López, C. Vila-Jato, J. L. Alonso, Novel Hydrophilic Chitosan-Polyethylene Oxide Nanoparticles as Protein Carriers, *J. Appl. Polym. Sci.* 63 (1997) 125–1328. [https://doi.org/10.1002/\(SICI\)1097-4628\(19970103\)63:1<125::AID-APP13>3.0.CO;2-4](https://doi.org/10.1002/(SICI)1097-4628(19970103)63:1<125::AID-APP13>3.0.CO;2-4).
- [98] B. Smitha, S. Sridhar, A.A. Khan, Chitosan–Poly(Vinyl Pyrrolidone) Blends as Membranes for Direct Methanol Fuel Cell Applications, *J. Power Sources.* 159 (2006) 846–854. <https://doi.org/10.1016/j.jpowsour.2005.12.032>.
- [99] A.J. Al-Manhel, A.R.S. Al-Hilphy, A.K. Niamah, Extraction of Chitosan, Characterisation and its Use for Water Purification, *J. Saudi Soc. Agric. Sci.* 17 (2018) 186–190. <https://doi.org/10.1016/j.jssas.2016.04.001>.
- [100] I.N. Sneddon, Boussinesq’s Problem for a Rigid Cone, *Math. Proc. Cambridge Philos. Soc.* 44 (1948) 492–507. <https://doi.org/10.1017/S0305004100024518>.
- [101] R.A. Zangmeister, J.J. Park, G.W. Rubloff, M.J. Tarlov, Electrochemical Study of Chitosan Films Deposited from Solution at Reducing Potentials, *Electrochim. Acta.* 51 (2006) 5324–5333. <https://doi.org/10.1016/j.electacta.2006.02.003>.
- [102] D. Avnir, J. Blum, Z. Nairoukh, Better Catalysis with Organically Modified Sol-Gel Materials, *Sol-Gel Handb.* 2–3 (2015) 963–986. <https://doi.org/10.1002/9783527670819.ch31>.
- [103] L. Liu, A. Walcarius, Kinetics of the Electrochemically-Assisted Deposition of Sol-Gel Films, *Phys. Chem. Chem. Phys.* 19 (2017) 14972–14983.

<https://doi.org/10.1039/c7cp01775h>.

- [104] N.A. Sulaiman, N.Z. Kassim Shaari, N. Abdul Rahman, A Study on Anti – Fouling Behaviour and Mechanical Properties of PVA/Chitosan/TEOS Hybrid Membrane in the Treatment of Copper Solution, *IOP Conf. Ser. Mater. Sci. Eng.* 358 (2018). <https://doi.org/10.1088/1757-899X/358/1/012055>.
- [105] A. Walcarius, D. Mandler, J.A. Cox, M. Collinson, O. Lev, Exciting New Directions in the Intersection of Functionalized Sol-Gel Materials with Electrochemistry, *J. Mater. Chem.* 15 (2005) 3663–3689. <https://doi.org/10.1039/b504839g>.
- [106] T.Y.A. Essel, A. Koomson, M.P.O. Seniagya, G.P. Cobbold, S.K. Kwofie, B.O. Asimeng, P.K. Arthur, G. Awandare, E.K. Tiburu, Chitosan Composites Synthesized Using Acetic Acid and Tetraethylorthosilicate Respond Differently to Methylene Blue Adsorption, *Polymers (Basel)*. 10 (2018). <https://doi.org/10.3390/polym10050466>.
- [107] H. Häkkinen, The Gold–Sulfur Interface at the Nanoscale, *Nat. Chem.* 4 (2012) 443–455. <https://doi.org/10.1038/nchem.1352>.
- [108] J.C. Love, L.A. Estroff, J.K. Kriebel, R.G. Nuzzo, G.M. Whitesides, Self-Assembled Monolayers of Thiolates on Metals as a Form of Nanotechnology, *Chem. Rev.* 105 (2005) 1103–1170. <https://doi.org/10.1021/cr0300789>.
- [109] F. Schreiber, Self-Assembled Monolayers: from Simple Model Systems to Biofunctionalized Interfaces, *J. Phys. Condens. Matter.* 16 (2004) R881–R900. <https://doi.org/10.1088/0953-8984/16/28/R01>.
- [110] F. Schreiber, Structure and Growth of Self-Assembling Monolayers, *Prog. Surf. Sci.* 65 (2000) 151–257. [https://doi.org/10.1016/S0079-6816\(00\)00024-1](https://doi.org/10.1016/S0079-6816(00)00024-1).
- [111] Y. Wang, Q. Chi, N.S. Hush, J.R. Reimers, J. Zhang, J. Ulstrup, Scanning Tunneling

- Microscopic Observation of Adatom-Mediated Motifs on Gold–Thiol Self-Assembled Monolayers at High Coverage, *J. Phys. Chem. C.* 113 (2009) 19601–19608. <https://doi.org/10.1021/jp906216k>.
- [112] C.M. Kim, J. Bechhoefer, Conductive Probe AFM Study of Pt-Thiol and Au-Thiol Contacts in Metal-Molecule-Metal Systems, *J. Chem. Phys.* 138 (2013) 14707. <https://doi.org/10.1063/1.4773436>.
- [113] C. Zhang, D. Lu, P. Jiang, J. Li, Y. Leng, Thiol Functionalized Cross-Linked Chitosan Polymer Supporting Palladium for Oxidative Heck Reaction and Reduction of p-Nitrophenol, *Catal. Letters.* 147 (2017) 2534–2541. <https://doi.org/10.1007/s10562-017-2174-6>.
- [114] P. Sharma, M. Mourya, D. Choudhary, M. Goswami, I. Kundu, M.P. Dobhal, C.S.P. Tripathi, D. Guin, Thiol Terminated Chitosan Capped Silver Nanoparticles for Sensitive and Selective Detection of Mercury (II) Ions in Water, *Sensors Actuators B Chem.* 268 (2018) 310–318. <https://doi.org/10.1016/j.snb.2018.04.121>.
- [115] S. Pokhrel, P.N. Yadav, Functionalization of Chitosan Polymer and Their Applications, *J. Macromol. Sci. Part A.* 0 (2019) 1–26. <https://doi.org/10.1080/10601325.2019.1581576>.
- [116] T. Ling, J. Lin, J. Tu, S. Liu, W. Weng, K. Cheng, H. Wang, P. Du, G. Han, Mineralized Collagen Coatings Formed by Electrochemical Deposition, *J. Mater. Sci. Mater. Med.* 24 (2013) 2709–2718. <https://doi.org/10.1007/s10856-013-5028-9>.
- [117] L. Dolgov, O. Yaroshchuk, L. Qiu, SEM Investigations of the Polymer Morphology in the Liquid Crystal-Polymer Composites With Different Polymer Contents, *Mol. Cryst. Liq. Cryst.* 468 (2007) 335/[687]-344/[696].

<https://doi.org/10.1080/15421400701231780>.

- [118] F. Altal, J. Gao, High Resolution Scanning Optical Imaging of a Frozen Polymer P-N Junction, *J. Appl. Phys.* 120 (2016). <https://doi.org/10.1063/1.4962720>.
- [119] B. Kirchner, *Ionic Liquids*, Springer Berlin Heidelberg, Berlin, Heidelberg, 2010. <https://doi.org/10.1007/978-3-642-01780-3>.
- [120] K. Lewandowska, Effect of an Ionic Liquid on the Physicochemical Properties of Chitosan/Poly(Vinyl Alcohol) Mixtures, *Int. J. Biol. Macromol.* 147 (2020) 1156–1163. <https://doi.org/10.1016/j.ijbiomac.2019.10.084>.
- [121] M. Chen, T. Runge, L. Wang, R. Li, J. Feng, X.L. Shu, Q.S. Shi, Hydrogen Bonding Impact on Chitosan Plasticization, *Carbohydr. Polym.* 200 (2018) 115–121. <https://doi.org/10.1016/j.carbpol.2018.07.062>.
- [122] C.A. Nkuku, R.J. LeSuer, Electrochemistry in Deep eutectic Solvents, *J. Phys. Chem. B.* 111 (2007) 13271–13277. <https://doi.org/10.1021/jp075794j>.
- [123] K.A. Omar, R. Sadeghi, Physicochemical Properties of Deep Eutectic Solvents: A Review, *J. Mol. Liq.* 360 (2022) 119524. <https://doi.org/10.1016/j.molliq.2022.119524>.
- [124] M.E. Snowden, A.G. Güell, S.C.S. Lai, K. McKelvey, N. Ebejer, M.A. Oconnell, A.W. Colburn, P.R. Unwin, Scanning Electrochemical Cell Microscopy: Theory and Experiment for Quantitative High Resolution Spatially-Resolved Voltammetry and Simultaneous Ion-Conductance Measurements, *Anal. Chem.* 84 (2012) 2483–2491. <https://doi.org/10.1021/ac203195h>.
- [125] C.H. Chen, L. Jacobse, K. McKelvey, S.C.S. Lai, M.T.M. Koper, P.R. Unwin, Voltammetric Scanning Electrochemical Cell Microscopy: Dynamic Imaging of Hydrazine Electro-Oxidation on Platinum Electrodes, *Anal. Chem.* 87 (2015) 5782–

5789. <https://doi.org/10.1021/acs.analchem.5b00988>.
- [126] L.C. Yule, V. Shkirskiy, J. Aarons, G. West, B.A. Shollock, C.L. Bentley, P.R. Unwin, Nanoscale Electrochemical Visualization of Grain-Dependent Anodic Iron Dissolution from Low Carbon Steel, *Electrochim. Acta.* 332 (2020) 135267. <https://doi.org/10.1016/j.electacta.2019.135267>.
- [127] Q. Bai, X. Huang, Effective Mass Layer of a Single Drop of Liquid Located on a Quartz Crystal Microbalance, *Sensors Mater.* 29 (2017) 539–544. <https://doi.org/10.18494/SAM.2017.1434>.
- [128] E. Szymańska, K. Winnicka, Stability of Chitosan - A Challenge for Pharmaceutical and Biomedical Applications, *Mar. Drugs.* 13 (2015) 1819–1846. <https://doi.org/10.3390/md13041819>.
- [129] T.T.B. Nguyen, S. Hein, C.-H. Ng, W.F. Stevens, Molecular Stability of Chitosan in Acid Solutions Stored at Various Conditions, *J. Appl. Polym. Sci.* 107 (2008) 2588–2593. <https://doi.org/https://doi.org/10.1002/app.27376>.
- [130] T.E. Lin, A. Lesch, C.L. Li, H.H. Girault, Mapping the Antioxidant Activity of Apple Peels with Soft Probe Scanning Electrochemical Microscopy, *J. Electroanal. Chem.* 786 (2017) 120–128. <https://doi.org/10.1016/j.jelechem.2017.01.015>.
- [131] H. Kang, S. Hwang, J. Kwak, Hydrogel Pen for Electrochemical Reaction and Its Applications for 3D Printing, *Nanoscale.* 7 (2015) 994–1001. <https://doi.org/10.1039/c4nr06041e>.
- [132] E. Sibottier, S. Sayen, F. Gaboriaud, A. Walcarius, Factors affecting the preparation and properties of electrodeposited silica thin films functionalized with amine or thiol groups, *Langmuir.* 22 (2006) 8366–8373. <https://doi.org/10.1021/la060984r>.

- [133] G.J. Copello, M.E. Villanueva, J.A. González, S. López Egües, L.E. Diaz, TEOS as an Improved Alternative for Chitosan Beads Cross-Linking: A Comparative Adsorption Study, *J. Appl. Polym. Sci.* 131 (2014) 1–8. <https://doi.org/10.1002/app.41005>.
- [134] D.B. Miklos, C. Remy, M. Jekel, K.G. Linden, J.E. Drewes, U. Hübner, Evaluation of Advanced Oxidation Processes for Water and Wastewater Treatment – A Critical Review, *Water Res.* 139 (2018) 118–131. <https://doi.org/10.1016/j.watres.2018.03.042>.
- [135] L. Varga, J. Szigeti, Use of Ozone in the Dairy Industry: A Review, *Int. J. Dairy Technol.* 69 (2016) 157–168. <https://doi.org/10.1111/1471-0307.12302>.
- [136] Z.B. Guzel-Seydim, A.K. Greene, A.C. Seydim, Use of ozone in the food industry, *Lwt.* 37 (2004) 453–460. <https://doi.org/10.1016/j.lwt.2003.10.014>.
- [137] M.A. Khadre, A.E. Yousef, J.G. Kim, Microbiological Aspects of Ozone Applications in Food: A Review, *J. Food Sci.* 66 (2001) 1242–1252. <https://doi.org/10.1111/j.1365-2621.2001.tb15196.x>.
- [138] C.O. Donnell, P.J. Cullen, *Ozone in Food Processing* Edited by Colm O'Donnell, B.K. Tiwari, P.J. Cullen, rip G. Rice, 2012.
- [139] A.J. Brodowska, A. Nowak, K. Śmigielski, Ozone in the Food Industry: Principles of Ozone Treatment, Mechanisms of Action, and Applications: An overview, *Crit. Rev. Food Sci. Nutr.* 58 (2018) 2176–2201. <https://doi.org/10.1080/10408398.2017.1308313>.
- [140] S. Lim, J.L. Shi, U. von Gunten, D.L. McCurry, Ozonation of Organic Compounds in Water and Wastewater: A Critical Review, *Water Res.* 213 (2022) 118053. <https://doi.org/10.1016/j.watres.2022.118053>.
- [141] M.F. Boeniger, Use of Ozone Generating Devices to Improve Indoor Air Quality, *Am.*

- Ind. Hyg. Assoc. J. 56 (1995) 590–598. <https://doi.org/10.1080/15428119591016827>.
- [142] S.T. Oyama, Chemical and Catalytic Properties of Ozone, *Catal. Rev. - Sci. Eng.* 42 (2000) 279–322. <https://doi.org/10.1081/CR-100100263>.
- [143] S. Chapman, Some Phenomena of the Upper Atmosphere, *Proc. Phys. Soc. Sect. B.* 64 (1951) 833–844. <https://doi.org/10.1088/0370-1301/64/10/301>.
- [144] R. Vingarzan, A Review of Surface Ozone Background Levels and Trends, *Atmos. Environ.* 38 (2004) 3431–3442. <https://doi.org/10.1016/j.atmosenv.2004.03.030>.
- [145] H. Claus, Ozone Generation by Ultraviolet Lamps†, *Photochem. Photobiol.* 97 (2021) 471–476. <https://doi.org/10.1111/php.13391>.
- [146] A. Ordnance, C. Engineering, Ozone Formation in Photochemical Oxidation of Organic Substan, 45 (1951).
- [147] M.S. Jaakkola, L. Yang, A. Jeronimon, J.J.K. Jaakkola, Office Work, SBS and Respiratory and Sick Building Syndrome Symptoms, *Occup. Environ. Med.* 64 (2007) 178–184. <https://doi.org/10.1136/oem.2005.024596>.
- [148] C.S. Kim, N.E. Alexis, A.G. Rappold, H. Kehrl, M.J. Hazucha, J.C. Lay, M.T. Schmitt, M. Case, R.B. Devlin, D.B. Peden, D. Diaz-Sanchez, Lung Function and Inflammatory Responses in Healthy Young Adults Exposed to 0.06 ppm Ozone for 6.6 Hours, *Am. J. Respir. Crit. Care Med.* 183 (2011) 1215–1221. <https://doi.org/10.1164/rccm.201011-1813OC>.
- [149] C.J. Weschler, Ozone’s Impact on Public Health: Contributions from Indoor Exposures to Ozone and Products of Ozone-Initiated Chemistry, *Environ. Health Perspect.* 114 (2006) 1489–1496. <https://doi.org/10.1289/ehp.9256>.
- [150] S. Liu, Y. Zhang, R. Ma, X. Liu, J. Liang, H. Lin, P. Shen, J. Zhang, P. Lu, X. Tang, T.

- Li, P. Gao, Long-Term Exposure to Ozone and Cardiovascular Mortality in a Large Chinese Cohort, *Environ. Int.* 165 (2022) 107280. <https://doi.org/10.1016/j.envint.2022.107280>.
- [151] M. Jerrett, R.T. Burnett, C.A. Pope, K. Ito, G. Thurston, D. Krewski, Y. Shi, E. Calle, M. Thun, Long-Term Ozone Exposure and Mortality, *N. Engl. J. Med.* 360 (2009) 1085–1095. <https://doi.org/10.1056/nejmoa0803894>.
- [152] N. Zhao, L. Pinault, O. Toyib, J. Vanos, M. Tjepkema, S. Cakmak, Long-term Ozone Exposure and Mortality from Neurological Diseases in Canada, *Environ. Int.* 157 (2021) 106817. <https://doi.org/10.1016/j.envint.2021.106817>.
- [153] R. Knake, P.C. Hauser, Sensitive Electrochemical Detection of Ozone, *Anal. Chim. Acta.* 459 (2002) 199–207. [https://doi.org/10.1016/S0003-2670\(02\)00121-6](https://doi.org/10.1016/S0003-2670(02)00121-6).
- [154] N. Bao, J.I. Gold, T. Szilvási, H. Yu, R.J. Twieg, M. Mavrikakis, N.L. Abbott, Designing Chemically Selective Liquid Crystalline Materials that Respond to Oxidizing Gases, *J. Mater. Chem. C.* 9 (2021) 6507–6517. <https://doi.org/10.1039/d1tc00544h>.
- [155] T. Doll, J. Lechner, I. Eisele, K.D. Schierbaum, W. Göpel, Ozone Detection in the ppb Range with Work Function Sensors Operating at Room Temperature, *Sensors Actuators, B Chem.* 34 (1996) 506–510. [https://doi.org/10.1016/S0925-4005\(96\)01941-7](https://doi.org/10.1016/S0925-4005(96)01941-7).
- [156] M. Belaqziz, M. Amjoud, A. Gaddari, B. Rhouta, D. Mezzane, Enhanced Room Temperature Ozone Response of SnO₂ thin Film Sensor, *Superlattices Microstruct.* 71 (2014) 185–189. <https://doi.org/10.1016/j.spmi.2014.03.040>.
- [157] Z. Zhu, J.L. Chang, R.J. Wu, Fast Ozone Detection by Using a Core-Shell Au@TiO₂ Sensor at Room Temperature, *Sensors Actuators, B Chem.* 214 (2015) 56–62.

<https://doi.org/10.1016/j.snb.2015.03.017>.

- [158] A. Bejaoui, J. Guerin, J.A. Zapien, K. Aguir, Theoretical and Experimental Study of the Response of CuO Gas Sensor Under Ozone, *Sensors Actuators, B Chem.* 190 (2014) 8–15. <https://doi.org/10.1016/j.snb.2013.06.084>.
- [159] J. Ollitrault, N. Martin, J. Rauch, J. Sanchez, F. Berger, J. Ollitrault, N. Martin, J. Rauch, J. Sanchez, F. Berger, Improvement of Ozone Detection with WO₃ Oriented Films, (2020). <https://doi.org/10.1016/j.snb.2013.06.084>.
- [160] P.F. Levelt, G.H.J. Van Den Oord, M.R. Dobber, A. Mälkki, H. Visser, J. De Vries, P. Stammes, J.O.V. Lundell, H. Saari, The Ozone Monitoring Instrument, *IEEE Trans. Geosci. Remote Sens.* 44 (2006) 1093–1100. <https://doi.org/10.1109/TGRS.2006.872333>.
- [161] X. Pang, M.D. Shaw, A.C. Lewis, L.J. Carpenter, T. Batchellier, Electrochemical Ozone Sensors: A Miniaturised Alternative for Ozone Measurements in Laboratory Experiments and Air-Quality Monitoring, *Sensors Actuators, B Chem.* 240 (2017) 829–837. <https://doi.org/10.1016/j.snb.2016.09.020>.
- [162] S.K. Manna, D. Kuilya, A. Adhikary, A. Maiti, S. Mondal, A Minireview of Recent Developments in Ozone Detection Using Optical Chemodosimeters, *Analyst.* 148 (2023) 954–965. <https://doi.org/10.1039/d2an01971j>.
- [163] D. Bersis, E. Vassiliou, A Chemiluminescence Method for Determining Ozone, *Analyst.* (1966) 499–505. <https://doi.org/10.1039/AN9669100499>.
- [164] U. Isacson, G. Wettermark, Chemiluminescence in Analytical Chemistry, *Anal. Chim. Acta.* 68 (1974) 339–362. [https://doi.org/10.1016/S0003-2670\(01\)82590-3](https://doi.org/10.1016/S0003-2670(01)82590-3).
- [165] A. Roda, M. Guardigli, P. Pasini, M. Mirasoli, E. Michelini, M. Musiani, Bio- and

- Chemiluminescence Imaging in Analytical Chemistry, *Anal. Chim. Acta.* 541 (2005) 25–35. <https://doi.org/10.1016/j.aca.2004.11.083>.
- [166] E.S. Massima Mouele, O.O. Fatoba, O. Babajide, K.O. Badmus, L.F. Petrik, Review of the Methods for Determination of Reactive Oxygen Species and Suggestion for their Application in Advanced Oxidation Induced by Dielectric Barrier Discharges, *Environ. Sci. Pollut. Res.* 25 (2018) 9265–9282. <https://doi.org/10.1007/s11356-018-1392-9>.
- [167] N. Sui, P. Zhang, T. Zhou, T. Zhang, Selective ppb-Level Ozone Gas Sensor Based on Hierarchical Branch-Like In₂O₃ Nanostructure, *Sensors Actuators, B Chem.* 336 (2021) 129612. <https://doi.org/10.1016/j.snb.2021.129612>.
- [168] G. Korotcenkov, V. Brinzari, B.K. Cho, In₂O₃- and SnO₂-Based Thin Film Ozone Sensors: Fundamentals, *J. Sensors.* 2016 (2016). <https://doi.org/10.1155/2016/3816094>.
- [169] Y.N. Colmenares, W. Correr, B.S. Lima, V.R. Mastelaro, The Effect of Morphology on the Ozone-Gas Sensing Properties of Zinc Oxide Sputtered Films, *Thin Solid Films.* 703 (2020). <https://doi.org/10.1016/j.tsf.2020.137975>.
- [170] X. Xu, M. Arab Pour Yazdi, J.B. Sanchez, A. Billard, F. Berger, N. Martin, Exploiting the Dodecane and Ozone Sensing Capabilities of Nanostructured Tungsten Oxide Films, *Sensors Actuators, B Chem.* 266 (2018) 773–783. <https://doi.org/10.1016/j.snb.2018.03.190>.
- [171] W. Avansi, A.C. Catto, L.F. Da Silva, T. Fiorido, S. Bernardini, V.R. Mastelaro, K. Aguir, R. Arenal, One-Dimensional V₂O₅/TiO₂ Heterostructures for Chemiresistive Ozone Sensors, *ACS Appl. Nano Mater.* 2 (2019) 4756–4764. <https://doi.org/10.1021/acsanm.9b00578>.
- [172] L.F. da Silva, M.A. Lucchini, J.-C. M’Peko, S. Bernardini, K. Aguir, C. Ribeiro, E.

- Longo, M. Niederberger, ZnO/SnO₂ Heterojunctions Sensors with UV-Enhanced Gas-Sensing Properties at Room Temperature, (2017) 418. <https://doi.org/10.3390/proceedings1040418>.
- [173] B.S. de Lima, A.A. Komorizono, W.A.S. Silva, A.L. Ndiaye, J. Brunet, M.I.B. Bernardi, V.R. Mastelaro, Ozone Detection in the ppt-Level with rGO-ZnO Based Sensor, *Sensors Actuators, B Chem.* 338 (2021) 129779. <https://doi.org/10.1016/j.snb.2021.129779>.
- [174] R.B. Smart, R. Dormond-Herrera, K.H. Mancy, In Situ Voltammetric Membrane Ozone Electrode, *Anal. Chem.* 51 (1979) 2315–2319. <https://doi.org/10.1021/ac50050a006>.
- [175] G. Schiavon, G. Zotti, Amperometric Monitoring of Ozone in Gaseous Media by Gold Electrodes Supported on Ion Exchange Membranes (Solid Polymer Electrolytes), *Anal. Chem.* (1990) 293–298.
- [176] S. Suzuki, K. Nagashima, A galvanic Solid-State Sensor for Monitoring Ozone and Nitrogen Dioxide, *Anal. Chim. Acta.* 144 (1982) 261–266.
- [177] S. Uchiyama, T. Ikarugi, M. Mori, K. Kasama, Y. Ishikawa, M. Kaneko, A. Umezawa, Highly Sensitive Electrochemical Sensor for Ozone in Water Using Porous Carbon Felt Electrode, *Electroanalysis.* 5 (1993) 121–124. <https://doi.org/10.1002/elan.1140050205>.
- [178] D. V. Stergiou, T. Stergiopoulos, P. Falaras, M.I. Prodromidis, Solid Redox Polymer Electrolyte-Based Amperometric Sensors for the Direct Monitoring of Ozone in Gas Phase, *Electrochem. Commun.* 11 (2009) 2113–2116. <https://doi.org/10.1016/j.elecom.2009.09.007>.
- [179] P.R. Unwin, A.J. Bard, Scanning electrochemical Microscopy 9. Theory and Application of the Feedback Mode to the Measurement of Following Chemical Reaction

- Rates in Electrode Processes, *J. Phys. Chem.* 95 (1991) 7814–7824.
<https://doi.org/10.1021/j100173a049>.
- [180] K. Aoki, M. Tanaka, Time-Dependence of Diffusion-Controlled Currents of a Soluble Redox Couple at Interdigitated Microarray Electrodes, *J. Electroanal. Chem.* 266 (1989) 11–20. [https://doi.org/10.1016/0022-0728\(89\)80211-6](https://doi.org/10.1016/0022-0728(89)80211-6).
- [181] R.C. E. Barnes, A Fernandez-la-Villa, D. Pozo-Ayuso, M. Castanio-Alvarez, F. Marken, Interdigitated Ring Electrodes: Theory and Experiment, *J. Electroanal. Chem.* 709 (2013) 57–64. <https://doi.org/http://dx.doi.org/10.1016/j.elechem.2013.10.009>.
- [182] K. Kim, J. Cheng, Q. Liu, X.Y. Wu, Y. Sun, Investigation of Mechanical Properties of Soft Hydrogel Microcapsules in Relation to Protein Delivery Using a MEMS Force Sensor, *J. Biomed. Mater. Res. - Part A.* 92 (2010) 103–113.
<https://doi.org/10.1002/jbm.a.32338>.
- [183] G.A.F. Roberts, Chemical Behaviour of Chitin and Chitosan, *Chitin Chem.* (1992) 203–273. https://doi.org/10.1007/978-1-349-11545-7_5.
- [184] L. Liu, Scanning Gel Electrochemical Microscopy: On the Way to the Quantitative Analysis. Presented at 74th Annual Meeting International Society of Electrochemistry, Lyon, France, 3-8 September, 2023.

Appendix I

Gel Probe characterization.

Gels obtained in **Chapter II** were characterized with poor results by FT-IR and Raman spectroscopy. Chitosan, Ch-TEOS and Ch-MPTMS were prepared as described in **Chapter II**. Samples for Raman spectroscopy (Spectrometer Raman Renishaw inVia Qontor, UK) were made by electrodeposition using a Pt micro-disk electrode as WE at 0.95V 300s. For FT-IR (Spectrometer FT-IR (Bruker Tensor 27, Germany) characterization, same precursor/s solution was used. As WE electrode clean bare ITO was used. Electrodeposition was carried out by applying 1.05V for 300s. For both techniques, a Pt wire was used as CE and Ag/AgCl QRE as RE. Samples were dried at 60 °C overnight.

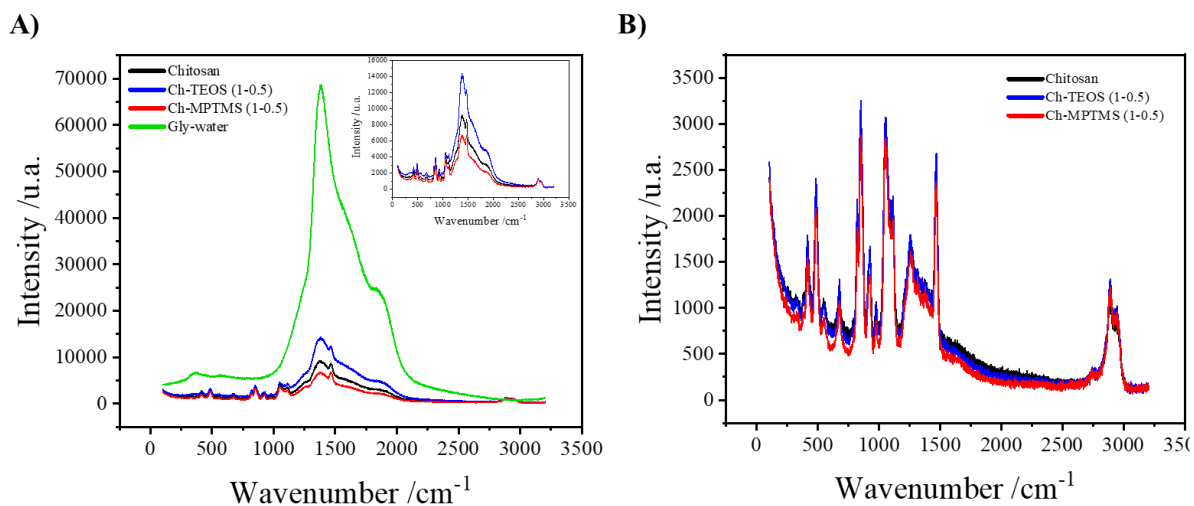


Figure A1.1 Raman spectrum of chitosan, Ch-TEOS (1-0.5) and Ch-MPTMOS (1-0.5) dried precursor abluptions and solvent (1:1 glycerol/H₂O) (A) and dried electrodeposited gels (B)

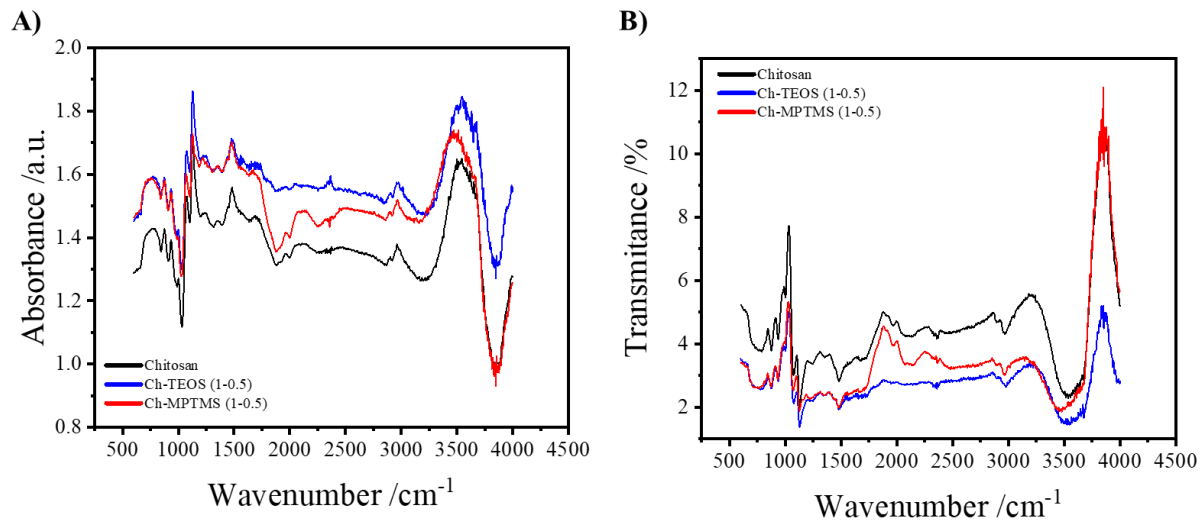


Figure A1.2 FT-IR spectrum of chitosan, Ch-TEOS (1-0.5) and Ch-MPTMOS dried electrodeposited gels, as absorbance (A) and transmittance % (B).

Although no meaningful information can be extracted from the previous spectrums, chitosan Raman spectrum is in line with those that can be found in the bibliography. As well as FT-IR results. Nevertheless, efforts to use them to characterize chitosan blends gave poor results.

Appendix II

Chitosan gel probe 3-MPA functionalization.

Chapter II explores and exposes the results of using co-electrodeposition as method to functionalize chitosan gel probe. As this is not the only approach to this task, we tried first to functionalize the gel probe after chitosan electrodeposition. A chitosan gel probe was made as described in Chapter II: then, it was immersed in a 0,25% (V/V) 3-mercaptopropionic acid (3-MPA) 1:1 glycerol/ H_2O solution. 3-MPA bound to chitosan through aldehyde groups, which reacts with the primary amine groups of chitosan (Schiff-base reaction). Leaving a thiol substituent free to interact with the sample (**Figure A2.1**)

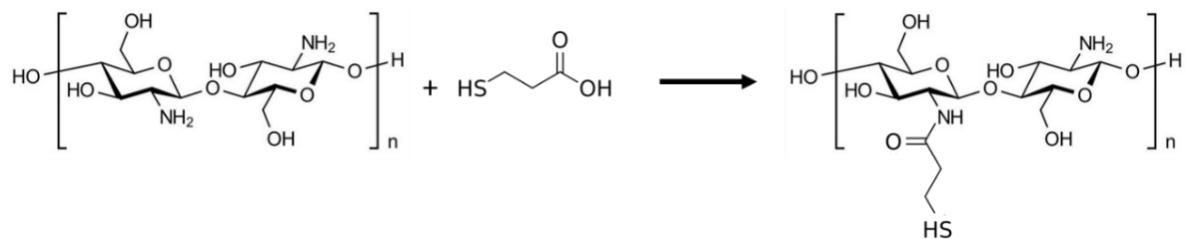


Figure A2.1 Chitosan and 3-mercaptopropionic acid reaction.

To evaluate the electrochemical behavior of the gel probe, $Fc(MeOH)_2$ is added to the chitosan solution. In previous SGECM experiments, the gel probe was soaked in $Fc(MeOH)_2$ solution after the gel electrodeposition. But this procedure can produce the loose of the thiol substituents due to the reversibility of the Schiff-base reaction, therefore is avoided.

Using a gold-coated substrate, a different response is expected when a thiol functionalized gel is used instead of a just chitosan gel probe. Moreover, if a difference can be identified, is this difference related to the type of gold sample used in the analysis?

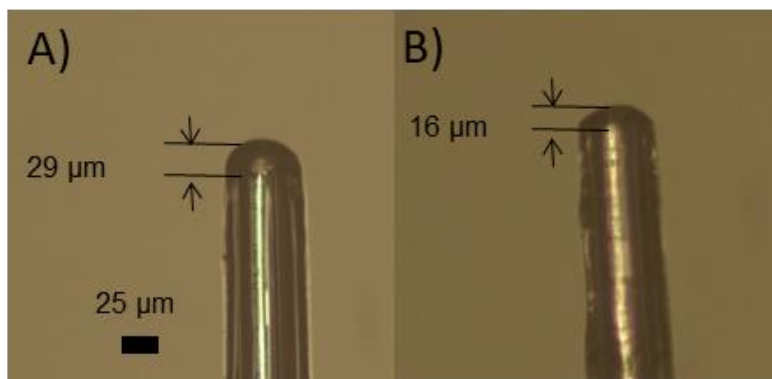


Figure A2.2 Chitosan electrodeposited gel before (A) and after (B) functionalization with 3-mercaptopropanoic acid.

In **Figure A2.2** we can observe the resulting probe after immersing it three minutes in the functionalization solution. Due to this process, the gel reduces its size considerably. While the gel probe is immersed in the functionalization solution, a gradient of concentration between the gel and the solution drives chitosan from the gel to the solution. Thus, the final gel probe size is hard to control. A pathway to avoid this problem is to obtain an already functionalized gel via *in situ* functionalization during electrodeposition. To achieve this, we add 0,25% (V/V) 3-MPA to the chitosan solution formulation. After analysis, no inconvenience was found to proceed with the modification of the original chitosan solution. In general, we can add components to the electrodeposition formulation as long solution's pH stays between 6 and 5,5 (to avoid chitosan condensation).

Chitosan and factionalized (by posttreatment and *by addition of 3-MPA in the electrodeposition solution formulation*) gel probes were tested over a platinum surface. Performing approach and retract curves to evaluate gel behavior after functionalization. Taken distance of gel to detach the surface during gel probe retraction after touching the sample (detach distance) was used as comparison parameter. As it was discussed in Chapter II, this value is highly useful for comparing gel probes and their mechanical performance. Obtained

approach and retract curves are shown in **Figure A2.3**. Both functionalized chitosan gel probes show an increasing detach distance in comparison to just chitosan gel probes. 1.3 times bigger using posttreatment functionalization and 6 times bigger with *in situ* functionalization. The latter is problematic, extremely elastic gels are not adequate to perform SGECEM measurements. Functionalization rate is probably higher using this method, mainly because is not only the surface that is in contact with the functionalization reagent. The first one, presents the problem of gel size control, making the fabrication of the gel probe difficult.

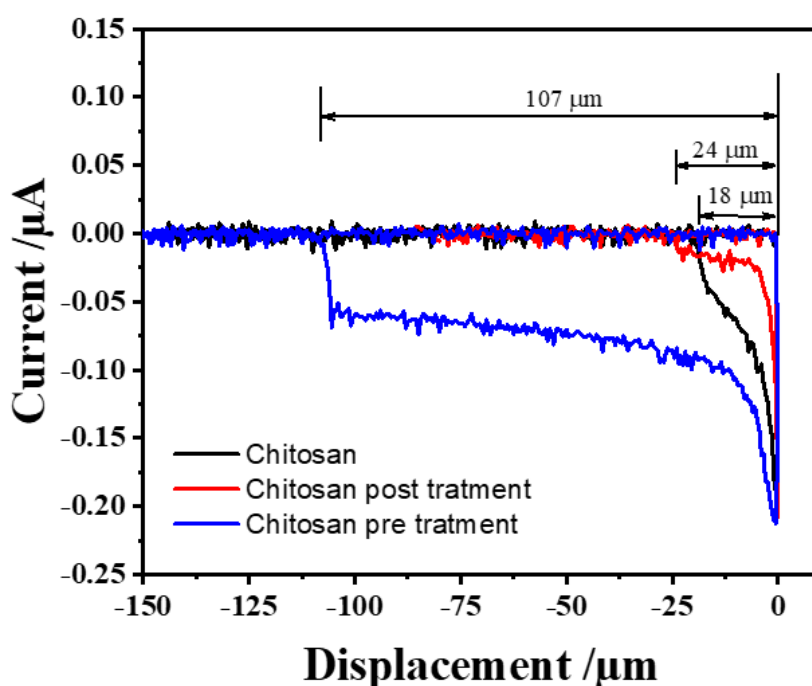


Figure A2.3 Approach and retract curves from chitosan gel probe, without functionalization, chitosan functionalized with 3-MPA before electrodeposition and chitosan functionalized with 3-MPA before electrodeposition applying a E_{probe} vs $E_{sample} = 0.4V$ and approach speed of $2\mu m/s$ using a Pt plate as sample

Even if our goal is to functionalize chitosan gel, we should not forget that this probe must be suitable; also, to be used for SGECEM. Both functionalization methods tested using 3-MPA, fail to produce a reliable functional gel probe for SGECEM. This pushed us to try new mechanisms, such as the use of chitosan blends with other polymers.